

## Magnetocaloric effect in M5XB2 family compounds

Mutu, H.

**DOI**

[10.4233/uuid:7974f26d-00e7-4b4b-9123-21dec4c6570](https://doi.org/10.4233/uuid:7974f26d-00e7-4b4b-9123-21dec4c6570)

**Publication date**

2023

**Document Version**

Final published version

**Citation (APA)**

Mutu, H. (2023). *Magnetocaloric effect in M5XB2 family compounds*. [Dissertation (TU Delft), Delft University of Technology]. <https://doi.org/10.4233/uuid:7974f26d-00e7-4b4b-9123-21dec4c6570>

**Important note**

To cite this publication, please use the final published version (if applicable).  
Please check the document version above.

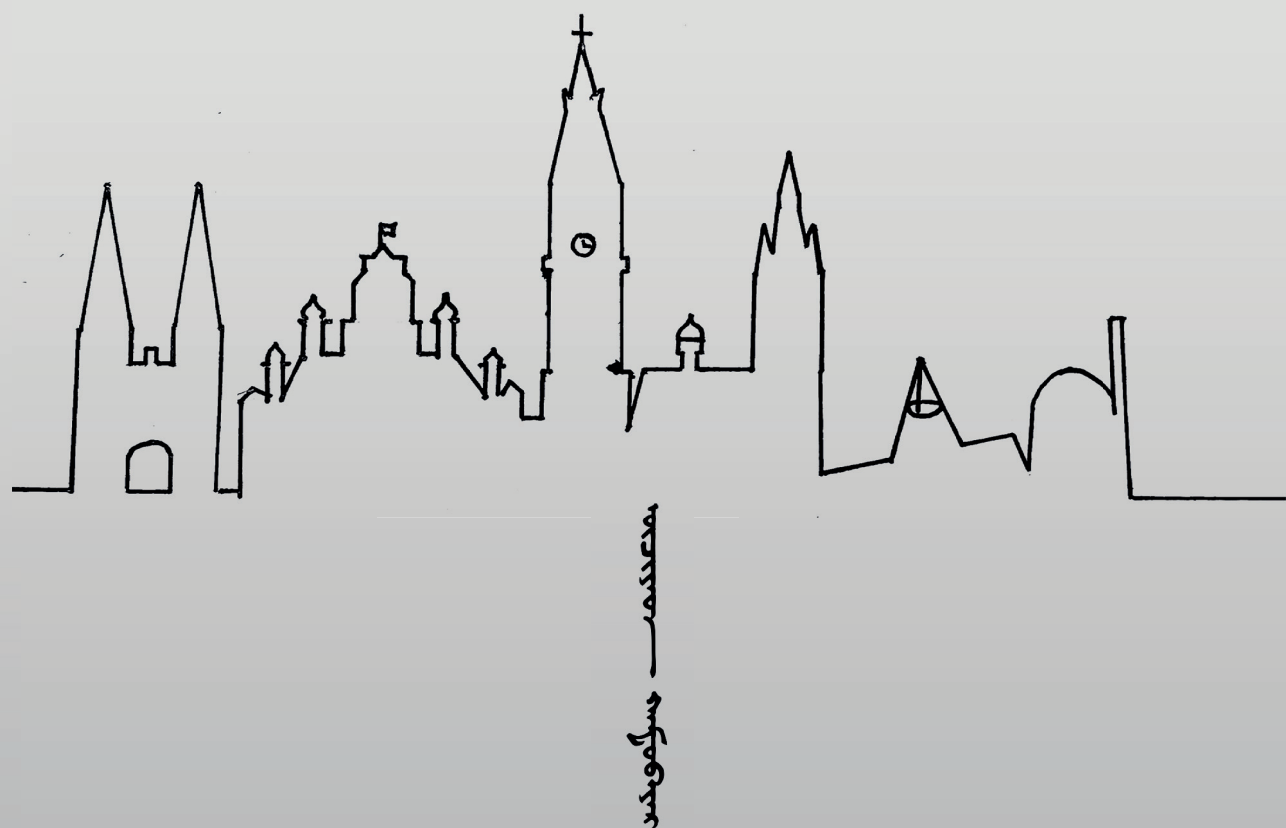
**Copyright**

Other than for strictly personal use, it is not permitted to download, forward or distribute the text or part of it, without the consent of the author(s) and/or copyright holder(s), unless the work is under an open content license such as Creative Commons.

**Takedown policy**

Please contact us and provide details if you believe this document breaches copyrights.  
We will remove access to the work immediately and investigate your claim.

# Magnetocaloric effect in $M_5XB_2$ family compounds



Hamutu



# Magnetocaloric effect in $M_5XB_2$ family compounds



# Magnetocaloric effect in $M_5XB_2$ family compounds

## **Dissertation**

for the purpose of obtaining the degree of doctor at Delft University of Technology by  
the authority of the Rector Magnificoes prof.dr.ir. T.H.J.J. van der Hagen, chair of the

Board for Doctorates

to be defended publicly on

Monday 8 January 2024 at 15:00 o'clock

by

**HAMUTU**

Master of Science in Condensed Matter Physics,

Inner Mongolia Normal University, China

born in Inner Mongolia, China

This dissertation has been approved by the promotor.

Composition of the doctoral committee:

Rector Magnificus  
Prof. dr. E. H. Brück  
Dr. ir. N.H. van Dijk

Chairperson  
Technische Universiteit Delft, promotor  
Technische Universiteit Delft, promotor

Independent members

Prof. dr. C. Pappas  
Prof. dr. P.J. Vardon  
Prof. dr. J. Aarts  
Prof. dr. B. Koopmans  
Prof. dr. Tegusi

Technische Universiteit Delft  
Technische Universiteit Delft  
Rijksuniversiteit Leiden  
Technische Universiteit Eindhoven  
Inner Mongolia Normal University,  
China

The work presented in this PhD thesis was carried out in the section of Fundamental Aspects of Materials and Energy (FAME) at the Faculty of Applied Sciences, Delft University of Technology. The project received financial support from NWO, Swiss Blue Energy and RSP Technology in the framework of Industrial Partnership Programmes IP 680-91-013.



**Keywords:** Magnetocaloric materials; Magnetocaloric effect; Second-order phase transition; Magnetocaloric energy harvesting;  $\text{Mn}_5(\text{Si,P})\text{B}_2$  compounds.

Printed by Proefschrift specialist

Copyright © 2023 by Hamutu

**ISBN 978-94-6384-522-9**

An electronic version of this dissertation is available at <http://repository.tudelft.nl/>.

*Dedicated to my parents, my sisters, my niece and Uyinga*



## Contents

<b>Chapter 1 Introduction .....</b>	<b>1</b>
1.1 Magnetocaloric effect.....	2
1.2 Room-temperature magnetocaloric applications .....	3
1.3 Room-temperature magnetocaloric materials .....	3
1.4 $M_5XB_2$ family of compounds .....	4
1.5 Thesis outline .....	5
References .....	6
 <b>Chapter 2 Theoretical aspects .....</b>	 <b>9</b>
2.1 Introduction .....	9
2.2 Thermodynamics .....	9
2.2.1 Gibbs free energy and Maxwell relations for magnetic systems.....	9
2.2.2 Magnetic entropy change and the adiabatic temperature change .....	10
2.3 Order of the magnetic phase transition .....	12
2.3.1 Landau model .....	12
2.3.2 Field exponent for the magnetic entropy change .....	13
2.4 Magnetic neutron diffraction .....	15
References .....	18
 <b>Chapter 3 Experimental techniques.....</b>	 <b>19</b>
3.1 Introduction .....	19
3.2 Sample preparation .....	19
3.2.1 High-energy planetary ball milling .....	19
3.2.2 Annealing .....	20
3.2.3 $^{11}\text{B}$ and field-oriented samples .....	20
3.3 Structure characterization .....	21
3.3.1 X-ray powder diffraction .....	21
3.3.2 Neutron powder diffraction .....	21

3.4 Differential Scanning Calorimetry .....	22
3.5 Magnetization measurements .....	22
3.5.1 SQUID and VSM magnetometers .....	22
3.5.2 Mössbauer spectroscopy .....	23
References.....	24

## **Chapter 4 Magnetocaloric properties of $\text{Mn}_5(\text{Si,P})\text{B}_2$ compounds..... 25**

4.1 Introduction .....	25
4.2 Experimental details .....	26
4.3 Results and discussion .....	28
4.3.1 The crystalline structures .....	28
4.3.2 Magnetocaloric effect .....	31
4.3.3 Magnetic structure .....	37
4.4 Conclusions .....	42
References.....	44

## **Chapter 5 Effect of Cr doping on the Magnetocaloric Properties of $\text{Mn}_5(\text{Si,P})\text{B}_2$**

### **Compounds ..... 49**

5.1 Introduction .....	49
5.2 Experimental methods .....	50
5.3 Results and discussion .....	50
5.3.1 Crystalline structures .....	50
5.3.2 Magnetocaloric effect .....	52
5.3.3 Neutron diffraction study .....	55
5.4 Conclusions .....	58
References.....	59

## **Chapter 6 Effect of V doping on the Magnetocaloric Properties of $\text{Mn}_5(\text{Si,P})\text{B}_2$**

<b>Compounds</b>	<b>61</b>
6.1 Introduction	61
6.2 Experimental methods	62
6.3 Results and discussion	62
6.3.1 Crystalline structures and phase analysis	62
6.3.2 Magnetocaloric effect	65
6.3.3 Neutron diffraction study	69
6.4 Conclusions	72
References	73

## **Chapter 7 Effect of Simultaneous Doping of Fe and Cr on the Magnetocaloric**

<b>Properties of <math>\text{Mn}_5(\text{Si,P})\text{B}_2</math> Compounds</b>	<b>75</b>
7.1 Introduction	75
7.2 Experimental details	76
7.3 Results and discussion	76
7.3.1 Fe doped $\text{Mn}_5(\text{Si,P})\text{B}_2$ compounds	76
7.3.1.1 Structural and magnetic properties	76
7.3.1.2 Mössbauer Spectroscopy and neutron diffraction study	78
7.3.2 (Fe, Cr) doped $\text{Mn}_5(\text{Si,P})\text{B}_2$ compounds	80
7.3.2.1 The crystalline structures and phase analysis	80
7.3.2.2 Magnetocaloric effect	82
7.3.2.3 Neutron diffraction study	84
7.4 Conclusions	86
References	87
<b>Summary</b>	<b>89</b>
<b>Outlook</b>	<b>93</b>

<b>Appendix .....</b>	<b>95</b>
<b>Acknowledgements .....</b>	<b>99</b>
<b>List of publications .....</b>	<b>103</b>
<b>Curriculum Vitae .....</b>	<b>105</b>

# Chapter 1

## **Introduction**

Throughout the history of human development, the discovery and mastery of the efficient use of energy has played a key role. Every time a new energy source is discovered it is skillfully used to bring progress to human society. With the rapid development of science and technology in the past century, the demand for energy has also been rising. For now, fossil fuels are still the most dominant energy source, which includes natural resources such as coal, oil and natural gas. These energy sources not only emit a large amount of greenhouse gases in the energy conversion, the non-renewability of these energy sources and their shortages have made people realize that it's critical to find new energy conversion processes that are more environmentally friendly and more efficient.

Refrigerators, heat pumps and air conditioners, as essential technologies in our lives, consume a considerable amount of energy. The vast majority of these technologies is based on the traditional vapor-compression technique, which still shows significant room for improvement in efficiency, as small instruments achieve only 20% of the efficiency that is achievable in the Carnot cycle [1, 2]. Even more remarkably, the greenhouse gases emitted by vapor-compression contributed to about 8% CO<sub>2</sub> equivalent of the total global emissions [3, 4]. In recent years magnetocaloric cooling and magnetocaloric heat pumps have received widespread attention as a promising alternatives to the traditional cooling and heat pump technologies, due to their environmental friendliness and high efficiency [5-7].

In this chapter, the magnetocaloric effect and its applications, the magnetocaloric materials and the  $M_5XB_2$  material system studied in this thesis, are introduced.

## 1.1 Magnetocaloric effect

The magnetocaloric effect (MCE) is the phenomenon that under adiabatic conditions a temperature change ( $\Delta T_{ad}$ ) is observed when a magnetic field is applied (or removed) [8, 9]. At constant temperature the MCE results in a related isothermal magnetic entropy change ( $\Delta S_M$ ) when a magnetic field is applied (or removed). In 1917, Weiss and Piccard discovered a reversible temperature change (0.7 K) in Ni upon applying and removing an applied magnetic field of 1.5 T near the ferromagnetic Curie temperature ( $T_C$ ) [10]. The MCE is generally most pronounced near a magnetic phase transition. Fig. 1.1 shows the temperature dependent total entropy curve near the  $T_C$  of a magnetocaloric material. Due to the presence of an external field the total entropy curve shift to higher temperatures in a ferromagnetic material. In the illustrated cycle the following steps are distinguished: (1) in the process of adiabatic magnetization, the constant total entropy causes a temperature increase  $\Delta T_{ad}$ . (2) Then the system releases its heat from the temperature increase to the environment. (3) During the adiabatic demagnetization the temperature decreases. (4) The system absorbs heat from the surrounding to achieve the initial temperature. The system undergoes two adiabatic processes (1 and 3) and two isofield processes (2 and 4) to complete the whole cycle. The mentioned  $\Delta S_M$  and  $\Delta T_{ad}$  are important parameters for magnetocaloric materials. In theory, the higher their values, the better their application prospects. However, in addition to these two parameters, there are other important parameters to be considered in practical applications, such as the presence of an adjustable working temperature, the mechanical and chemical stability and the thermal conductivity of the material.

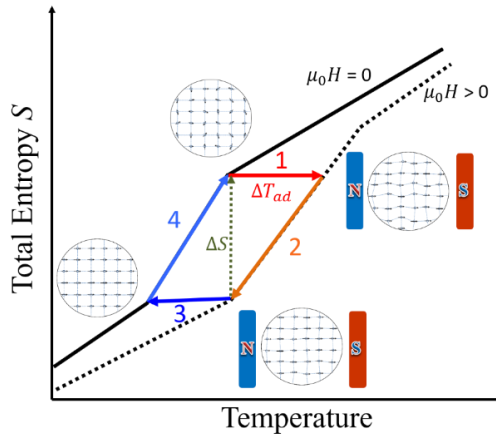


**Fig. 1.1**  $S$ - $T$  diagram in a Brayton cycle for the ferromagnetic-to-paramagnetic transition in magnetic materials.

### 1.2 Room-temperature magnetocaloric applications

This thesis focuses on near room-temperature magnetocaloric applications and materials. The near room-temperature applications of the MCE have received widespread attention in: (i) magnetic cooling, (ii) magnetic heat pumps and (iii) magnetic energy conversion of heat by thermomagnetic generators and thermomagnetic motors [11, 12]. Magnetocaloric materials (MCMs) play a key role in these magnetocaloric devices with different material requirements for different applications. For example, magnetocaloric cooling and heat pumps require MCMs with a high  $\Delta S_M$  and  $\Delta T_{ad}$  (usually a high  $\Delta S_M$  is accompanied by a high  $\Delta T_{ad}$ ), which are the key parameters to characterize the cooling (or heating) ability. Of course, it is not desirable to obtain a larger MCE by increasing the magnetic field. Efficient MCE materials are required to have high  $\Delta S_M$  and  $\Delta T_{ad}$  for a field change in low magnetic fields (usually 1 T). Generally, high  $\Delta S_M$  materials are first-order phase transition (FOPT) materials, where the transition is generally accompanied by thermal hysteresis  $\Delta T_{hys}$ . The presence of thermal hysteresis results in an irreversible process that prevents the cycle from being completed. The  $\Delta S_M$  and  $\Delta T_{ad}$  of second-order phase transition (SOPT) materials are lower than those in FOPT materials, and no thermal hysteresis is observed in SOPT materials. Materials that combine the advantage of both phase transitions, are known as critical point (CP) materials and are positioned at the boundary between FOPT and SOPT materials. Thermomagnetic generators and motors do not suffer from thermal hysteresis, as long as the temperature difference between the hot temperature source and the cold temperature source is greater than the thermal hysteresis.

### 1.3 Room-temperature magnetocaloric materials

In recent years, the research of near room-temperature MCMs has made great achievements, and many material systems have been explored. Due to the large MCE near room temperature, Gd has frequently been used in magnetocaloric refrigeration prototypes and it is regarded as benchmark material for the near room-temperature MCMs [13,14]. The  $\Delta T_{ad}$  value for field changes of 1.0 and 1.5 T are 2.6 and 4.0 K, respectively. In 1997, Pecharsky and Gschneidner [15] discovered the giant magnetocaloric effect (GMCE) of  $\text{Gd}_5\text{Si}_2\text{Ge}_2$  near room temperature with a  $T_C$  of 274 K, and a maximum  $\Delta S_M$  in a field change of 5 T that can reach  $18.5 \text{ J kg}^{-1}\text{K}^{-1}$ . The calculated  $\Delta T_{ad}$  is 30% higher than that of Gd. Subsequent studies found that the  $T_C$  of this compound can be tuned by varying the Si/Ge ratio. In 2002, Tegus and co-workers reported the GMCE in the  $\text{MnFeP}_{0.45}\text{As}_{0.55}$  compound [16]. Not only is the magnetic entropy change greater than that of Gd, but also it has wider working temperature range, as  $T_C$  can be adjusted between 160 and 340 K by chemical substitution [9].

Subsequently, a large amount of research has been done on the Mn-Fe-P-Ge and Mn-Fe-P-Si compounds [16-21]. FeRh alloys [22,23] and Heusler alloys [24-26] are also widely studied as room-temperature MCMs. The research on these material systems is relatively mature, and each material system has its own advantages and disadvantages. Problems related to a poor mechanical stability or expensive raw materials need to be solved. Finding new material systems that potentially meet the application requirements is therefore of interest.

#### 1.4 $M_5XB_2$ family of compounds

The  $M_5XB_2$  ( $M = \text{Fe, Mn, Co, V, Cr}$  and  $X = \text{Si, P, S}$ ) materials system was previously studied for permanent magnet applications. In 1959 and 1960, Aronsson and co-workers [27, 28] reported that  $M\text{-Si-B}$  ( $M = \text{Mn, Fe, Co}$ ) compounds could under appropriate experimental conditions crystallize in the tetragonal  $\text{Cr}_5\text{B}_3$  type crystal-structure with  $I4/mcm$  symmetry (space group 140). Later Rundqvist found that Fe-P-B alloys could also form in this structure [29]. The  $T_C$  of  $\text{Fe}_5\text{SiB}_2$  and  $\text{Fe}_5\text{PB}_2$  were reported to be 784 K [30] and 639 K [31], respectively. The high  $T_C$  values were the reason this system was considered as a potential permanent magnet material. In 2009, Almeida calculated the  $T_C$  of  $\text{Mn}_5\text{SiB}_2$  to be in the range from 469 to 492 K and found a saturation magnetization of  $5.5 \times 10^5 \text{ Am}^{-1}$  [32]. Many studies on doping with  $3d$  elements (Co, Cr, etc.) have been performed for  $(\text{Mn,Fe})_5(\text{Si,P})\text{B}_2$  alloys [33-39]. Interestingly, Ericsson [40] and Cedervall [41] reported a spin reorientation around 170 K in  $\text{Fe}_5\text{SiB}_2$ , where the magnetic moment was oriented along the  $c$  axis at low temperatures and in the  $a$ - $b$  plane after the spin reorientation. In 2010, Xie and coworkers [33] proposed that the  $\text{Mn}_5\text{PB}_2$  compound had the potential to be used as a room-temperature MCM as the  $T_C$  of 311 K is close to room temperature. Co doped  $\text{Fe}_5\text{PB}_2$  compounds are also a good option, as the  $T_C$  of  $\text{Fe}_5\text{PB}_2$  compounds can be adjusted from 662 to 152 K by the introduction of Co [38].

In this study, we systematically investigated the MCE in  $M_5XB_2$  ( $M = \text{Fe, Mn, V, Cr}$  and  $X = \text{Si, P}$ ) materials. The results show that  $T_C$  in these materials can be adjusted continuously in a temperature range around room temperature, which makes them suitable for near room-temperature applications, like magnetocaloric generators that convert low-temperature waste heat into electricity.

### 1.5 Thesis outline

The purpose of work presented in this thesis is to investigate whether  $M_5XB_2$  ( $M = \text{Fe}, \text{Mn}, \text{V}, \text{Cr}$  and  $X = \text{Si}, \text{P}$ ) material system has potential as a room-temperature magnetocaloric application material by studying its crystal and magnetic structure, and magnetocaloric properties.

In *Chapter 2*, we provide some theoretical aspects related to the magnetocaloric effect, crystal and magnetic structure characterization used later in the thesis, as well as the field exponent that is used to distinguish FOPT and SOPT materials based on the Landau theory.

In *Chapter 3*, a brief review is presented on experimental set-ups and techniques for the sample preparation, the crystal and magnetic structural characterization and the determination of the magnetic properties.

In *Chapter 4*, we focused on a systematic study of effect of different Si/P ratio on the crystal and magnetic structure, and magnetocaloric properties of  $\text{Mn}_5(\text{Si},\text{P})\text{B}_2$  compounds. The compounds have ferromagnetic ordering below the transition temperature, magnetic moments along the  $a$ - $b$  plane. Interestingly, we found that the  $T_C$  of the compounds can be continuously adjusted near room temperature, and present a considerable  $\Delta M$  in a temperature change of 30 K. These properties make the  $\text{Mn}_5(\text{Si},\text{P})\text{B}_2$  compounds a good candidate material for room-temperature magnetocaloric energy harvesting applications. And the absence of thermal hysteresis and latent heat is another advantage of the  $\text{Mn}_5(\text{Si},\text{P})\text{B}_2$  compounds.

In *Chapter 5*, the effect of Cr doping on the crystal and magnetic structure, and magnetocaloric properties of  $\text{Mn}_5(\text{Si},\text{P})\text{B}_2$  compounds was studied. The Cr has almost no effect on the order of magnetic transition, and the Cr doped sample still exhibits SOPT characteristics. The Curie temperature, saturation magnetization and isothermal magnetic entropy change of the compounds decrease with the Cr content.

In *Chapter 6*, we explore the effect of V doping on the properties of  $\text{Mn}_5(\text{Si},\text{P})\text{B}_2$  compounds. The V decreases the Curie temperature, saturation magnetization and isothermal magnetic entropy change of the compounds. We also discuss the influence of impurity phases  $\text{Mn}_2\text{B}$  and  $\text{Mn}_2\text{P}$  on the magnetization of samples.

In *Chapter 7*, we present the magnetocaloric properties of  $(\text{Mn},\text{Fe},\text{Cr})_5(\text{Si},\text{P})\text{B}_2$  compounds, and the occupancy preference of Fe and Cr in the unit cell was characterized by neutron diffraction. The magnetocaloric properties of the compound have a strong dependence on the Fe/Cr ratio, Fe and Cr have opposite effects on the magnetocaloric properties.

## References

- [1] C. O. R. Negrão, C. J. L. Hermes, Energy and cost savings in household refrigerating appliances: A simulation-based design approach, *Appl. Energy* 88, (2011) 3051.
- [2] S. Choi, U. Han, H. Cho, H. Lee, Review: Recent advances in household refrigerator cycle technologies, *Appl. Therm. Eng.* 132, (2018) 560.
- [3] D. Coulomb, J. L. Dupont, V. Morlet, The Impact of the Refrigeration Sector on ClimateChange, 35th Informatory Note on Refrigeration Technologies, Technical Report, International Institute of Refrigeration, Paris, France (2017).
- [4] Y. Hwang, Harmonization of the Life Cycle Climate Performance Methodology, 32nd Informatory Note on Refrigeration Technologies, Technical Report, International Institute of Refrigeration, Paris, France (2016).
- [5] A. J. Barclay, W. A. Steyert, Active magnetic regenerator, U.S. Patent 4,332,135, (1982).
- [6] R. E. Rosensweig, *Ferrohydrodynamics*, Dover Publications, Inc., Mineola, NY (1985).
- [7] L. D. Kirol and M. W. Dacus, Rotary Recuperative Magnetic Heat Pump, *Adv. Cryog. Eng.*, (1988) 757.
- [8] E. Brück, O. Tegus, X. W. Li, F. R. de Boer, K. H. J. Buschow, Magnetic refrigeration towards room-temperature applications, *Physica B* 327, (2003) 431.
- [9] O. Tegus, E. Brück, K. H. J. Buschow, F. R. de Boer, Transition-metal-based magnetic refrigerants for room-temperature applications, *Nature* 415, (2002) 150.
- [10] P. Weiss and A. Piccard, Le phénomène magnétocalorique, *J. Phys. Theor. Appl.* 7, (1917) 103.
- [11] A. Kitanovski, Energy Applications of Magnetocaloric Materials, *Adv. Energy Mater.* 10, (2020) 1903741.
- [12] E. Brück, Developments in magnetocaloric refrigeration, *J. Phys. D: Appl. Phys.* 38, (2005) R381.
- [13] S. G. Min, K. S. Kim, S. C. Yu, H. S. Suh and S. W. Leed, Magnetocaloric properties of  $Gd_{1-x}B_x$  ( $x = 0, 0.06, 0.09, 0.12$ ) alloys, *J. Magn. Magn. Mater.* 303, (2006) e440.
- [14] A. M. Tishin, A. V. Derkach, Y. I. Spichkin, M. D. Kuz'min, A. S. Chernyshov, K. A. Gschneidner Jr., V. K. Pecharsky, Magnetocaloric effect near a second-order magnetic phase transition, *J. Magn. Magn. Mater.* 310, (2007) 2800.
- [15] V. K. Pecharsky and K. A. Gschneidner. Some common misconceptions concerning magnetic refrigerant materials. *J. Appl. Phys.* 90, (2001) 4614.
- [16] O. Tegus, B. Fuquan, W. Dagula, L. Zhang, E. Brück, F. R. de Boer, K. H. J. Buschow, Magnetic-entropy change in  $Mn_{1.1}Fe_{0.9}P_{0.7}As_{0.3-x}Ge_x$ , *J. Alloy. Compd.* 396, (2005) 6.

- [17] N.T. Trung, Z.Q. Ou, T.J. Gortenmulder, O. Tegus, K.H.J. Buschow, E. Brück, Tunable thermal hysteresis in MnFe(P,Ge) compounds, *J. Appl. Phys.* 99, (2006) 08Q107.
- [18] H. Yibole, F. Guillou, Y.K. Huang, G.R. Blake, A.J.E. Lefering, N.H. van Dijk, E. Brück, First-order ferromagnetic transition in single-crystalline (Mn,Fe)<sub>2</sub>(P,Si), *Appl. Phys. Lett.* 107, (2015) 162403.
- [19] Z. Q. Ou, L. Zhang, N. H. Dung, L. van Eijck, A. M. Mulders, M. Avdeev, N. H. van Dijk, E. Brück, Neutron diffraction study on the magnetic structure of Fe<sub>2</sub>P-based Mn<sub>0.66</sub>Fe<sub>1.29</sub>P<sub>1-x</sub>Si<sub>x</sub> melt-spun ribbons, *J. Magn. Mater.* 340, (2013) 80.
- [20] X. F. Miao, L. Caron, J. Cedervall, P. C. M. Gubbens, P. Dalmas de Réotier, A. Yaouanc, F. Qian, A. R. Wildes, H. Luetkens, A. Amato, N. H. van Dijk, E. Brück, Short-range magnetic correlations and spin dynamics in the paramagnetic regime of (Mn,Fe)<sub>2</sub>(P,Si), *Phys. Rev. B* 94, (2016) 014426.
- [21] F. Guillou, S. Liting, O. Haschuloo, Z. Q. Ou, E. Brück, O. Tegus, H. Yibole, Room temperature magnetic anisotropy in Fe<sub>2</sub>P-type transition metal based alloys, *J. Alloys Comp.* 800, (2019) 403.
- [22] S. A. Nikitin, G. Myalikgulyev, A. M. Tishin, M. P. Annaorazov, K. A. Asatryan, A. L. Tyurin, The magnetocaloric effect in Fe<sub>49</sub>Rh<sub>51</sub> compound, *Phys. Lett. A* 148, (1990) 363.
- [23] M. P. Annaorazov, K. A. Asatryan, G. Myalikgulyev, S. A. Nikitin, A. M. Tishin, A. L. Tyurin, Alloys of the Fe-Rh system as a new class of working material for magnetic refrigerators, *Cryogenics* 32, (1992) 867.
- [24] F. X. Hu, B. G. Shen, J. R. Sun, Magnetic entropy change in Ni<sub>51.5</sub>Mn<sub>22.7</sub>Ga<sub>25.8</sub> alloy, *Appl. Phys. Lett.* 76, (2000) 3460.
- [25] M. Pasquale, C. P. Sasso, L. H. Lewis, L. Giudici, T. Lograsso, D. Schlagel, Magnetostructural transition and magnetocaloric effect in Ni<sub>55</sub>Mn<sub>20</sub>Ga<sub>25</sub> single crystals, *Phys. Rev. B* 72, (2005) 094435.
- [26] J. Marcos, L. Mañosa, A. Planes, Multiscale origin of the magnetocaloric effect in Ni-Mn-Ga shape-memory alloys, *Phys. Rev. B* 68, (2003) 094401.
- [27] B. Aronsson, G. Lundgren, X-Ray investigations on Me-Si-B System I, *Acta Chemica Scandinavica* 13, (1959) 433.
- [28] B. Aronsson, I. Engström, X-Ray investigations on Me-Si-B System II, *Acta Chemica Scandinavica* 14, (1960) 1403.
- [29] S. Rundqvist, X-Ray investigations of the Ternary System Fe-P-B. Some Feature of the Systems Cr-P-B, Mn-P-B, Co-P-B and Ni-P-B, *Acta Chemica Scandinavica* 16, (1962) 1.
- [30] R. Wäppling, T. Ericsson, L. Häggström, Y. Andersson, Magnetic Properties of Fe<sub>5</sub>SiB<sub>2</sub> and related compounds, *J. Physique Colloques* C6, (1976) 591.

- [31] L. Häggström, R. Wäppling, T. Ericsson, Mössbauer and X-Ray Studies of  $\text{Fe}_5\text{PB}_2$ , *J. Solid State Chem.* 13, (1976) 84.
- [32] D. M. de Almeida, C. Bormio-Nunes, C. A. Nunes, A. A. Coelho, G. C. Coelho, Magnetic characterization of  $\text{Mn}_5\text{SiB}_2$  and  $\text{Mn}_5\text{Si}_3$  phases, *J. Magn. Magn. Mater.* 321, (2009) 2578.
- [33] Z. G. Xie, D. Y. Geng, Z. D. Zhang, Reversible room-temperature magnetocaloric effect in  $\text{Mn}_5\text{PB}_2$ , *Appl. Phys. Lett.* 97, (2010) 202504.
- [34] M. A. McGuire, D. S. Parker, Magnetic and structural properties of ferromagnetic  $\text{Fe}_5\text{PB}_2$  and  $\text{Fe}_5\text{SiB}_2$  and effects of Co and Mn substitutions, *J. Appl. Phys.* 118, (2015) 163903.
- [35] M. Werwiński, Magnetic properties of  $\text{Fe}_5\text{SiB}_2$  and its alloys with P, S, and Co, *Phys. Rev. B* 93, (2016) 174412.
- [36] D. Hedlund, J. Cedervall, A. Edström, M. Werwiński, S. Kontos, O. Eriksson, J. Rusz, P. Svedlindh, M. Sahlberg, K. Gunnarsson, Magnetic properties of the  $\text{Fe}_5\text{SiB}_2$ – $\text{Fe}_5\text{PB}_2$  system, *Phys. Rev. B* 96, (2017) 094433.
- [37] M. Werwiński, Magnetocrystalline anisotropy of  $\text{Fe}_5\text{PB}_2$  and its alloys with Co and 5d elements: A combined first-principles and experimental study, *Phys. Rev. B* 98, (2018) 214431.
- [38] J. Cedervall, E. Nonnet, D. Hedlund, L. Häggström, T. Ericsson, M. Werwiński, A. Edström, J. Rusz, P. Svedlindh, K. Gunnarsson, M. Sahlberg, Influence of Cobalt Substitution on the Magnetic Properties of  $\text{Fe}_5\text{PB}_2$ , *Inorg. Chem.* 57 (2018) 777.
- [39] J. Thakur, P. Rani, M. Tomar, V. Gupta, H. S. Saini, M. K. Kashyap, Tailoring in-plane magnetocrystalline anisotropy of  $\text{Fe}_5\text{SiB}_2$  with Cr-substitution, *AIP Conference Proceedings* 2115, (2019) 030506.
- [40] T. Ericsson, L. Häggström, R. Wäppling, Spin Rotation in  $\text{Fe}_5\text{SiB}_2$ , *Phys. Scr.* 17, (1978) 83.
- [41] J. Cedervall, S. Kontos, T. C. Hansen, O. Balmes, F. J. Martinez-Casado, Z. Matej, P. Beran, P. Svedlindh, K. Gunnarsson, M. Sahlberg, Magnetostructural transition in  $\text{Fe}_5\text{SiB}_2$  observed with neutron diffraction, *J. Solid State Chem.* 235, (2016) 113.

# Chapter 2

## Theoretical aspects

### 2.1 Introduction

To delve further into the research background and the feasibility of the experiments in this work, I will briefly introduce the theoretical foundations involved in this thesis. Thermodynamic theory serves as the basis for the motivation and design of the experiments, while Landau phase transition theory elucidates the definitions and distinctions of first and second-order phase transitions. The Field exponent for the magnetic entropy change further proposes the quantitative analysis of phase transition based on the Landau phase transition theory. Additionally, the section on Neutron Magnetic Diffraction elucidates the rationale behind applying neutron diffraction to magnetic materials.

### 2.2 Thermodynamics

#### 2.2.1 Gibbs free energy and Maxwell relations for magnetic systems

The state of a thermodynamic system can be described by the state function of the system, for a magnetic medium, by the Gibbs free energy of the system. With an external magnetic field  $\mu_0 H$ , pressure  $p$  and temperature  $T$  its Gibbs free energy can be expressed as:

$$G = U - TS + pV - \mu_0 HM \quad (2.1)$$

Where  $U$  is the internal energy,  $S$  the entropy,  $V$  the volume, and  $M$  the magnetization. Thus, the differential form of the Gibbs free energy for a magnetic material is:

$$dG = -SdT + Vdp - \mu_0 MdH \quad (2.2)$$

The total differential of Equation (2.2) is:

$$dG(T, H) = \left(\frac{\partial G}{\partial T}\right)_{p, H} dT + \left(\frac{\partial G}{\partial p}\right)_{T, H} dp + \left(\frac{\partial G}{\partial H}\right)_{p, T} dH \quad (2.3)$$

This leads to:

$$S = -\left(\frac{\partial G}{\partial T}\right)_{p, H} \quad (2.4)$$

$$V = \left(\frac{\partial G}{\partial p}\right)_{T, H} \quad (2.5)$$

$$M = -\frac{1}{\mu_0} \left(\frac{\partial G}{\partial H}\right)_{p, T} \quad (2.6)$$

After taking the partial derivatives of  $p$  and  $T$  for formulas (2.4) and (2.5), we get:

$$\left(\frac{\partial S}{\partial p}\right)_{T, H} = -\left(\frac{\partial^2 G}{\partial T \partial p}\right)_H \quad (2.7)$$

$$\left(\frac{\partial V}{\partial T}\right)_{p, H} = \left(\frac{\partial^2 G}{\partial p \partial T}\right)_H \quad (2.8)$$

Since the result is independent of the order of partial derivatives, we obtain:

$$\left(\frac{\partial S}{\partial p}\right)_{T, H} = -\left(\frac{\partial V}{\partial T}\right)_{p, H} \quad (2.9)$$

Similarly, we can get:

$$\frac{1}{\mu_0} \left(\frac{\partial S}{\partial H}\right)_{T, p} = \left(\frac{\partial M}{\partial T}\right)_{H, p} \quad (2.10)$$

Equation (2.10) is the Maxwell relation for a magnetic medium, very important for magnetic systems.

### 2.2.2 Magnetic entropy change and the adiabatic temperature change

The total differential of the entropy of a magnetic system can be written as:

$$dS(T, H) = \left(\frac{\partial S}{\partial T}\right)_{H, p} dT + \left(\frac{\partial S}{\partial H}\right)_{T, p} dH - \left(\frac{\partial S}{\partial p}\right)_{T, H} dp \quad (2.11)$$

For the isothermal and isobaric process ( $dT = 0, dp=0$ ), it can be simplified as:

$$dS(T, H) = \left(\frac{\partial S}{\partial H}\right)_{T, p} dH \quad (2.12)$$

The entropy of the magnetic medium consists of lattice entropy  $S_l$ , magnetic entropy  $S_m$  and electron entropy  $S_e$ . In magnetocaloric applications, the magnetic entropy  $S_m$  and lattice entropy  $S_l$  are mainly considered, as the contribution of the electron entropy  $S_e$  on the total entropy is generally negligible near room temperature. In an adiabatic magnetization process, the value of  $S_m$  decreases with the degree of ordering. Since the total entropy  $S_{tot}$  is fixed under adiabatic conditions, a decrease in  $S_m$  leads to an increase in  $S_l$  in the form of heat.

Integration of Eq. (2.12) leads to:

$$\Delta S_M(T, \Delta H) = \int_{H_i}^{H_f} \left( \frac{\partial S}{\partial H} \right)_{T,p} dH \quad (2.13)$$

Substitute Eq. (2.10) into Eq. (2.13) yields:

$$\Delta S_M(T, \Delta H) = \int_{H_i}^{H_f} \mu_0 \left( \frac{\partial M}{\partial T} \right)_{H,p} dH \quad (2.14)$$

The magnetic entropy change of the system for a field change of  $\mu_0 \Delta H$  is given by Eq. (2.14).

The heat capacity  $C_p$  is defined in the second law of thermodynamics:

$$C_p(T, H) = T \left( \frac{\partial S}{\partial T} \right)_{H,p} \quad (2.15)$$

Combining Eqs. (2.10), (2.11) and (2.15) yields:

$$dT = - \frac{T}{C_p(T, H)} \left( \frac{\partial M}{\partial T} \right)_{H,p} \mu_0 dH \quad (2.16)$$

by taking the integral for Eq. (2.16), we get:

$$\Delta T_{ad}(T, \Delta H) = - \int_{H_i}^{H_f} \frac{T}{C_p(T, H)} \left( \frac{\partial M}{\partial T} \right)_{H,p} \mu_0 dH \quad (2.17)$$

By measuring  $C_p(T, H)$  and the temperature-dependent  $M$  under different applied fields, we can calculate the adiabatic temperature change  $\Delta T_{ad}$  of the system by Eq. (2.17). If we assume that the magnetic field has little effect on  $C_p$ ,  $T/C_p(T, H) \approx \text{Constant}$ , it can be simplified as:

$$\Delta T_{ad}(T, \Delta H) = - \frac{T}{C_p(T, H)} \Delta S_M(T, \Delta H) \quad (2.18)$$

Although Eq. (2.18) has been simplified compared to Eq. (2.17), it can approximate the  $\Delta T_{ad}$  of the magnetic system under specific experimental conditions.

## 2.3 Order of the magnetic phase transition

### 2.3.1 Landau model

The type of phase transition is an important parameter for magnetocaloric materials. FOPT materials generally have high magnetic entropy changes, but are generally accompanied by thermal hysteresis. Conversely SOPT material do not exhibit thermal hysteresis, but the magnetic entropy change is relatively low. Theoretically, the FOPT material without thermal hysteresis is the ideal magnetocaloric material, but it is usually difficult to achieve. Therefore, materials tuned into a critical region with low hysteresis and yet high entropy change taking advantages of the two types of phase transitions are a good compromise. Thus, it is important to investigate the type of magnetic phase transition for magnetocaloric materials. The type of magnetic phase transition can be classified according to Landau by the discontinuities of derivatives of the Gibbs free energy  $G$  with respect to thermodynamic variables. For example, entropy  $S$  and volume  $V$  can be expressed as  $-\left(\frac{\partial G}{\partial T}\right)_{p,H}$ ,  $\left(\frac{\partial G}{\partial p}\right)_{T,H}$ , and  $-\frac{1}{\mu_0}\left(\frac{\partial G}{\partial H}\right)_{p,T}$  the first-order partial derivatives of the Gibbs free energy  $G$  with respect to  $T$ ,  $p$  or  $H$ , respectively. If the first-order derivatives such as  $S$ ,  $V$  and  $M$ , show discontinuous changes during the phase transition, then the transition corresponds to a first-order phase transition. The heat capacity  $C_p = T\left(\frac{\partial S}{\partial T}\right)_p = -T\frac{\partial^2 G}{\partial T^2}$  is a second-order derivative of  $G$ . If only this second derivative is undergoing a discontinuous change at the phase transition, then the transition corresponds to a second-order phase transition.

For a magnetic system, the Gibbs free energy can be represented by a Taylor expansion of order parameter  $M$  [3]:

$$G = \frac{\alpha}{2}M^2 - \frac{\beta}{4}M^4 + \frac{\gamma}{6}M^6 - \mu_0 HM \quad (2.19)$$

where  $\mu_0 H$  is the external magnetic field. Suppose  $\alpha = \alpha_0(T - T_0)$ , where  $\alpha_0 > 0$ ,  $\beta$  and  $\gamma \geq 0$  are constant, and  $T_0$  is the characteristic temperature, the type of ferromagnetic-paramagnetic (FM-PM) phase transition depends on the value of  $\beta$ : (i)  $\beta < 0$  refers to a FOPT; (ii)  $\beta > 0$  refers to a SOPT, and  $\beta = 0$  is a critical point (CP). For the SOPT, the third term can be neglected,  $\gamma = 0$ . In the absence of an external magnetic field, there is an energy barrier for the FOPT at  $T = T_0$ , and the magnetic order cannot be transformed into a disordered state. A higher temperature is required to cross this energy barrier (as shown in Fig. 2.1), and  $T_c > T_0$ . This is why the FOPT materials are frequently accompanied by thermal hysteresis. However, there is no energy barrier in the SOPT and CP materials, resulting in  $T_c = T_0$ , without thermal hysteresis.

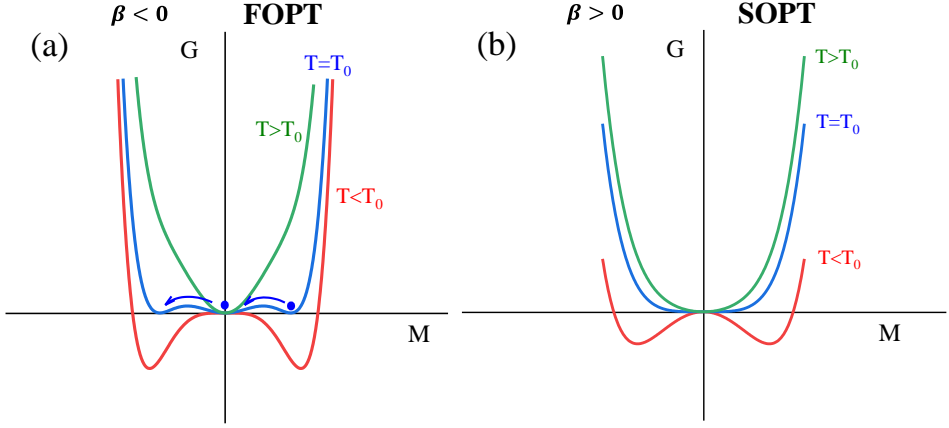


**Fig. 2.1** Schematic diagram of the first-order phase transition (FOPT) and the second-order phase transition (SOPT).  $G$  is the Gibbs free energy and  $M$  is the magnetic order parameter.

### 2.3.2 Field exponent for the magnetic entropy change

The magnetic entropy change  $\Delta S_M$  of the magnetic system at the phase transition can be calculated by Eq. (2.14). The value of  $\Delta S_M$  depends on the external magnetic field  $\mu_0 H$ , and can be expressed as:

$$\Delta S_M \propto H^n \quad (2.20)$$

where the field exponent  $n$  is a function of temperature and magnetic field, in general, and can be expressed as [4]:

$$n(T, H) = \frac{d \ln(|\Delta S_M|)}{d \ln(H)} \quad (2.21)$$

Van Dijk [5] demonstrated that these predictions are also found when the Landau model [6] is applied to describe the phase transition, and calculated the exponent  $n$  in the high-temperature region  $T \gg T_0$ , the low-temperature region  $T \ll T_0$  and at the characteristic temperature  $T = T_0$  for FOPT, SOPT and CP, respectively. It is found that  $n \approx 2$  and  $n \approx 1$  at  $T \gg T_0$  and  $T \ll T_0$ , regardless of the type of the phase transition. As shown in Fig. 2.2, at the characteristic temperature  $T = T_0$ , the field exponent  $n$  for the FOPT, SOPT and CP tends to be 0,  $2/3$  and  $2/5$ , respectively. Although the value of  $n$  tends to 2 at high temperatures (in the PM state), different phase transition types show completely different behaviors near to the transition temperature: SOPT and CP gradually approach

2, while the FOPT undergoes a divergence,  $n \rightarrow \infty$ , and then tends to 2. These results provide a basis for judging the phase transition type in magnetic materials.

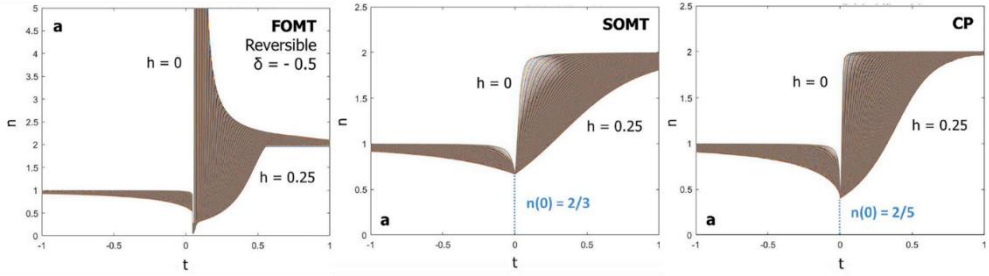


**Fig. 2.2** Field exponent of the entropy change  $n = d \ln(|\Delta s|)/d \ln(h)$  for the reversible FOPT, SOPT and CP as a function of the reduced temperature  $t$  for different reduced magnetic fields  $h = 0$  to  $0.25$ , where  $t = (T - T_0)/T_0$  and  $h = \mu_0 H/\mu_0 H_0$  [4].

**Table 2.1** Definition, characteristics and the field exponent  $n$  value for the FOPT, SOPT and CP.

	FOPT	SOPT	CP
Definition	The first derivatives of Gibbs free energy has a discontinuous change: $S = -\left(\frac{\partial G}{\partial T}\right)$ and $V = \left(\frac{\partial G}{\partial p}\right)$	The second derivatives of the Gibbs free energy have a discontinuous change: $C_p = -T \frac{\partial^2 G}{\partial T^2}$	Landau Gibbs free energy: $G_L = \frac{\alpha}{2} M^2 + \frac{\beta}{4} M^4 + \frac{\gamma}{6} M^6 - \mu_0 H M$ , with $\beta=0$ .
Characteristic	Accompanied by thermal hysteresis and latent heat, lattice distortion, large magnetic entropy	No distortion in the lattice, small magnetic entropy change and the heat capacity has a discontinuous change	with negligible thermal hysteresis and latent heat.
Field exponent for the entropy change $n$	$T \gg T_0$ : $n \approx 2$ $T \ll T_0$ : $n \approx 1$ $T = T_0$ : $n = 0$	$T \gg T_0$ : $n \approx 2$ $T \ll T_0$ : $n \approx 1$ $T = T_0$ : $n = 2/3$	$T \gg T_0$ : $n \approx 2$ $T \ll T_0$ : $n \approx 1$ $T = T_0$ : $n = 2/5$

## 2.4 Magnetic neutron diffraction

The magnetic properties of a magnetic material are directly determined by its magnetic structure and understanding its magnetic structure plays a key role in investigating the material properties. Neutron diffraction is an effective technique to explore magnetic structures. In this thesis, the technique was used to study the magnetic structure and properties of materials. Below the characteristics of magnetic neutron powder diffraction are briefly introduced.

For the study of the crystalline structure of materials, X-ray scattering is often the technique of choice, as X-ray sources are much more abundant. Neutrons interact with the nuclei, in contrast to X-rays that interact with the electrons. Neutrons are most sensitive to specific atoms (or isotopes) while X-rays are most sensitive to the heaviest atoms (that contain a large number of electrons). Furthermore, due to the magnetic dipole moment of the neutron it interacts with the local magnetic field of the atoms. In the diffraction pattern of a magnetically ordered material, additional information about magnetic order and the size of the magnetic moments can be obtained from the magnetic scattering that is found in addition to the nuclear scattering [7]. The intensity of the magnetic diffraction peak  $I$  is proportional to the square of the magnetic scattering length  $b_m$ :

$$I \propto b_m^2. \quad (2.22)$$

The magnetic scattering length  $b_m$  is proportional to the magnetic moment  $\mu$ :

$$b_m \propto p_0 \mu \quad (2.23)$$

where  $p_0 = 2.699 \text{ fm}/\mu_B$ . And the magnetic form factor  $f_m(\mathbf{Q}) = \int s(r) \exp[i \mathbf{Q} \cdot \mathbf{r}] d^3 \mathbf{r} \mu_B$  also plays an important role in the intensity of the magnetic peaks:

$$I \propto b_m^2 = p_0 \mu f_m(\mathbf{Q}) \sin \alpha \quad (2.24)$$

where  $f_m(\mathbf{Q})$  decreases rapidly with the scattering angle. Fig. 2.3 shows an example of  $f_m(\mathbf{Q})$  as a function of the scattering angle for  $\text{Nd}^{3+}$ . Obviously, in magnetic scattering the low-angle diffraction peaks have a stronger intensity, which will provide valuable information for magnetic structure analysis (as it allows for a separation of the nuclear and the magnetic scattering).

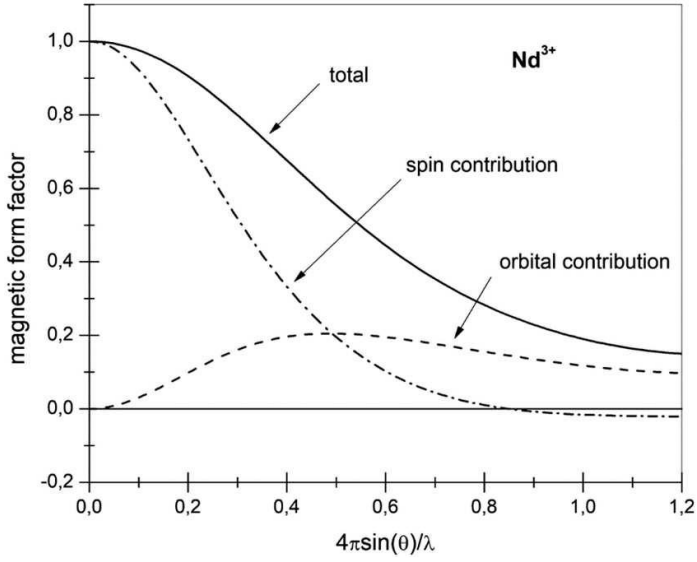


**Fig. 2.3** Magnetic form factor  $f_m(Q)$  as a function of the wave vector transfer  $Q$  for  $\text{Nd}^{3+}$  [8].

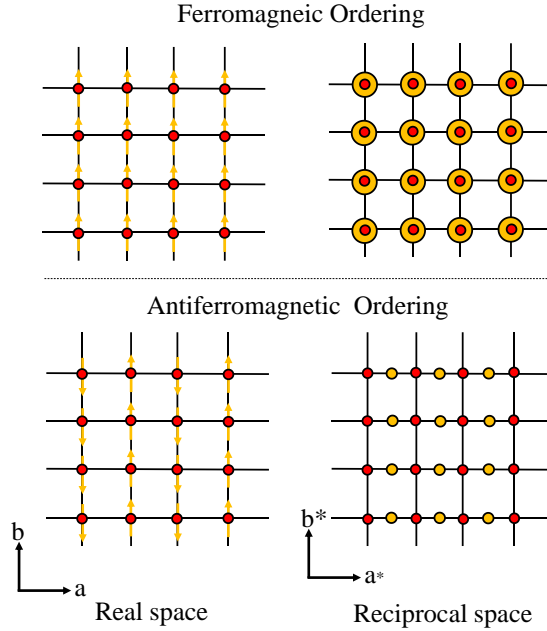


**Fig. 2.4** Schematic diagram of ferromagnetic and antiferromagnetic lattice in two-dimensional both in real-space (with the orientation of the magnetic moments) and in reciprocal space [9].

In formula (2.24),  $\alpha$  is the angle between the scattered neutron and the magnetic moment, thus the  $\sin(\alpha)$  term provides information on the direction of the magnetic moment. In a same lattice structure with a different magnetic structure, the magnetic structures contribute differently to the diffraction pattern. In Fig. 2.4 we take a two-dimensional structure as an example to show the influence of the different magnetic structures both in real space and in reciprocal space. In the case of FM order, the size of the magnetic unit is equal to the lattice unit cell, and the magnetic lattice completely coincides with the nuclear lattice in reciprocal space. For the shown AFM order, the magnetic unit cell is twice as large as the lattice unit cell, and the magnetic unit cell is  $1/2$  of the nuclear unit cell in reciprocal space. Experimentally, we will observe new peaks in the diffraction pattern for such AFM order.

## **References**

- [1] A. M. Tishin and Y. I. Spichkin, The magnetocaloric effect and its Applications (Bristol: Institute of Physics Publishing, 2003).
- [2] M. D. Kuzmin and A. M. Tishin, Magnetocaloric effect. part 1: An introduction to various aspects of theory and practice, *Cryogenics* 32, (1992) 545.
- [3] J. M. D. Coey, Magnetism and Magnetic Materials, Cambridge University Press, New York, (2009).
- [4] J. Y. Law, V. Franco, L. M. Moreno-Ramírez, A. Conde, D. Y. Karpenkov, I. Radulov, K. P. Skokov, O. Gutfleisch, A quantitative criterion for determining the order of magnetic phase transitions using the magnetocaloric effect, *Nature Comm.* 9, (2018) 2680.
- [5] N.H. van Dijk, Landau model evaluation of the magnetic entropy change in magnetocaloric materials, *J. Magn. Mater.* 529, (2021) 167871.
- [6] L. D. Landau, On the theory of phase transitions. I., *Zh. Eksp. Teor. Fiz.* 7, (1937) 19.
- [7] K. Lefmann, Neutron Scattering: Theory, Instrumentation, and Simulation, Niels Bohr Institute, University of Copenhagen, (2007).
- [8] S.K. Sharma, D.S. Verma, L.U. Khan, S. Kumar, S.B. Khan, Handbook of Materials Characterization, Springer Nature Switzerland AG, (2018).
- [9] E. Ressouche. Reminder: Magnetic structures description and determination by neutron diffraction. École thématique de la Société Française de la Neutronique, (2014).

# Chapter 3

## Experimental techniques

### 3.1 Introduction

A novel magnetocaloric materials system  $M_5XB_2$  ( $M = \text{Fe, Mn, V, Cr}$  and  $X = \text{Si, P}$ ) has been investigated to determine its potential as a room temperature magnetocaloric material in this study. To facilitate reproducibility and verification of the results, this chapter provides a detailed account of the experimental methods, equipment used, and data analysis methods. By presenting comprehensive experimental details, this chapter aims to enable fellow researchers to replicate the experiments, validate the findings, and offer insights into the methodology employed in this study. The samples were prepared by high-energy ball milling, melt spinning, and annealing techniques. The crystal structure, magnetic structure and phase analysis were characterized by X-Ray Powder Diffraction (XRD), Neutron Diffraction (ND), Scanning Electron Microscope (SEM) and Energy Dispersive Spectroscopy (EDS). The magnetic properties were measured by superconducting quantum interference device (SQUID), vibrating sample magnetometer (VSM) and Mössbauer Spectroscopy. Differential Scanning Calorimetry (DSC) was used for the heat capacity measurements.

### 3.2 Sample preparation

#### 3.2.1 High-energy planetary ball milling

High-energy ball milling is a widely used technique for grinding and mixing materials. A planetary ball mill (PM100, Retsch) was used to prepare the samples in this thesis. As shown in Fig. 3.1, since the jar and the plate are rotating in opposite directions, the balls in the jar will collide randomly, grinding the sample into smaller particles, and mixing them thoroughly down to atomic scale as particles are being cold welded as soon as they

are below a few micron diameter. The total mass of 10 g of starting materials was ground in a stainless steel jar with a rotation speed of 350 rpm for 10 hours under an argon atmosphere, with a sample-to-balls mass ratio of 1:4.

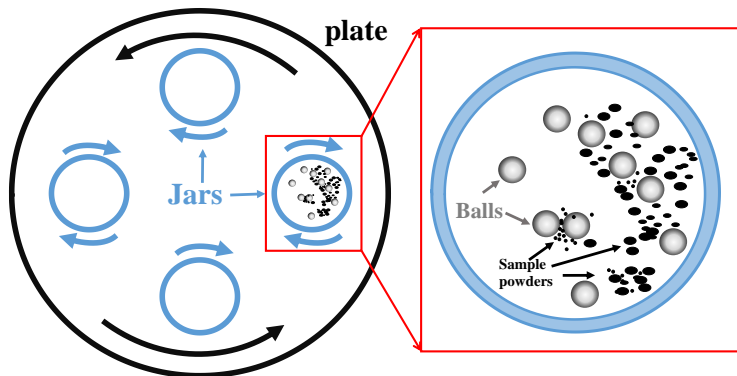


Fig. 3.1 Schematic illustration of a planetary ball mill.

### 3.2.2 Annealing

The ball-milled samples were pressed into tablets with a diameter of 1 cm, and a thickness of about 0.5 cm, then sealed in a quartz tube containing 200 mbar of high-purity argon. The sealed samples were annealed in the furnace at 1150 °C for 24 hours and then quenched into water. The melt-spun ribbons were also sealed in quartz tubes containing high-purity argon, and annealed at 1150 °C for 2 hours before quenching.

### 3.2.3 $^{11}\text{B}$ and field-oriented samples

Natural B is composed of 80%  $^{11}\text{B}$  and 20%  $^{10}\text{B}$  isotopes [1]. The absorption cross-section  $\sigma_{a,th}$  of isotope  $^{10}\text{B}$  for neutrons is as high as  $3838 \times 10^{-28} \text{ m}^2$  ( $\sigma_{a,th} < ^{11}\text{B} > = 0.0055 \times 10^{-28} \text{ m}^2$ ) [2], which seriously affects the detected intensity of the scattered neutrons. To avoid this effect, we used the  $^{11}\text{B}$  isotope to re-prepare some of the samples for ND experiments using the same procedure as the previous parent sample produced with natural B. To achieve a sample with aligned magnetic moments, starting material was ground into small particles and passed through a 30  $\mu\text{m}$  sieve, then mixed

with slow-curing glue and placed into a magnetic field (1 T) for 24 hours at room temperature.

### 3.3 Structure characterization

#### 3.3.1 X-ray powder diffraction

Room-temperature XRD was carried out using an PANalytical X-Pert PRO employing Cu- $K_\alpha$  radiation in a  $2\theta$  range of 10-100°. An Anton Paar TTK450 Low-Temperature Chamber was used for the temperature-dependent XRD measurement in the temperature range from 298 to 450 K (in a  $2\theta$  range of 25-60°). Due to problems with the instrumental temperature calibration, a linear fitting was carried out for 5 points in the negative thermal expansion (NTE) temperature region and 4 points in the high-temperature thermal expansion region, respectively. After setting the crossover point of these two fitting lines as the transition temperature, corrected the transition temperature of the temperature-dependent XRD data based on the transition temperature obtained from magnetic measurement. The lattice structure refinements were carried out using the Rietveld method [3] implemented in the Fullprof software [4].

#### 3.3.2 Neutron powder diffraction

XRD is derived from the interaction between incident X-rays and the electrons around the atoms, which is less sensitive to the lighter elements with a small number of electrons in the atom, such as B and C. Alternatively, neutron diffraction (ND) can distinguish different atoms in the lattice structure due to difference in coherent neutron scattering length  $b_c$  and can relatively accurately detect the lattice-site occupation of the light atoms B and C. The coherent neutron scattering length  $b_c$  of the elements covered in this thesis are shown in Table 3.1. Neutron diffraction can provide accurate and detailed crystal structure information, that is complementary to XRD. Furthermore, due to its magnetic dipole moment the neutron interacts with the local magnetic field of the atoms. As a result, ND can provide information about the magnetic structure of the samples. The ND measurements described in this thesis were performed on the neutron powder diffractometer PEARL at the TU Delft with an incident wavelength of 1.665 Å [5]. The measurements were carried out at temperatures of 80, 298 and 530 K, and the sample powder was contained in a vanadium can. The lattice and magnetic structure refinements were carried out using the Rietveld method [3] and the Fullprof software [4].

## Chapter 3 Experimental techniques

**Table 3.1** Coherent neutron scattering length  $b_c$  for  $^{10}\text{B}$ ,  $^{11}\text{B}$ , Si, P, V, Cr, Mn and Fe.

	$^{10}\text{B}$	$^{11}\text{B}$	Si	P	V	Cr	Mn	Fe
Z	5	5	14	15	23	24	25	26
$b_c$ (fm)	-0.1-1.066i	6.65	4.14	5.13	-0.38	3.63	-3.73	9.45

### 3.4 Differential Scanning Calorimetry

A Differential Scanning Calorimeter (DSC) determines the heat capacity of a material by measuring the heat flow difference between the sample and a reference as a function of the temperature. The heat capacity measurements were carried out on a TA-Q2000 instrument (TA Instrument Company) equipped with a liquid nitrogen cooling system. The sweeping rate selected for the DSC measurements in this study was  $10 \text{ Kmin}^{-1}$ .

### 3.5 Magnetization measurements

#### 3.5.1 SQUID and VSM magnetometers

Temperature-dependent and field-dependent magnetization measurements were performed in a superconducting quantum interference device (SQUID) magnetometer (Quantum Design MPMS) with reciprocating sample option (RSO) in the temperature range from 5 to 370 K. Powder samples with a mass of 1.5 - 3 mg were inserted into a gelatin capsule and mounted in a plastic straw with diamagnetic contribution of the order of  $10^{-8} \text{ Am}^2$  for measurements in the SQUID. Temperature-dependent magnetization measurements were measured in the temperature range from 5 to 370 K for heating and cooling with a speed of 2 K/min in applied magnetic fields of 0.01 and 1 T. In this thesis, the  $dM/dT$  of the temperature-dependent magnetization in a field of 0.01 T was used to determine the ferromagnetic transition temperature  $T_C$ . The temperature-dependent magnetization data under 12 different magnetic fields (0.05, 0.10, 0.20, 0.40, 0.60, 0.80, 1.00, 1.20, 1.40, 1.60, 1.80 and 2.00) were used to calculate the isothermal magnetic entropy change  $\Delta S_m$ . The field-dependent magnetization measurements were performed at 5 and 300 K in magnetic fields from 0 to 5 T. The magnetic measurements at temperatures higher than 370 K were performed in a

VersaLab vibrating sample magnetometer (VSM) with an oven function. For measurements in the VSM, the powder samples were pressed into a small tablet with a mass of 4 - 7 mg and glued to a sample holder with a thermocouple.

### **3.5.2 Mössbauer spectroscopy**

The Mössbauer effect refers to recoilless resonant emission and absorption of gamma-rays by atoms in a crystal [6]. In 1958, Mössbauer discovered the nuclear resonance absorption of  $^{191}\text{Ir}$  solid and explained this unexpected phenomenon [7]. He was awarded the Nobel Prize in Physics in 1961 for this discovery. The energy levels of the atomic nuclei in a solid will be split or shifted to varying degrees due to the influence of the surrounding electric and magnetic fields. The magnetic field at the site of the atomic nucleus and the information of the crystal structure can be analyzed through the spectroscopic energy scans resulting in isomer shift, quadrupole and hyperfine splitting. Transmission  $^{57}\text{Fe}$  Mössbauer spectra for the  $(\text{Mn,Fe})_5(\text{Si,P})\text{B}_2$  compounds in Chapter 7 were collected at 120 K with a sinusoidal velocity spectrometer using a  $^{57}\text{Co}(\text{Rh})$  source. A velocity calibration was carried out using an  $\alpha\text{-Fe}$  foil at room temperature. The source and the absorbing samples were kept at the same temperature during the measurements. The Mössbauer spectra were fitted using the Mosswin 4.0 program [8].

### References

- [1] J. R. de Laeter, J. K. Böhlke, P. de Bièvre, H. Hidaka, H. S. Peiser, K. J. R. Rosman, P. D. P. Tayler, Atomic weights of the elements: Review 2000 (IUPAC Technical Report), *Pure Appl. Chem.* 75, (2003) 683.
- [2] K. Lefmann, *Neutron Scattering: Theory, Instrumentation, and Simulation*, Niels Bohr Institute, University of Copenhagen, (2007).
- [3] H. M. Rietveld, A profile refinement method for nuclear and magnetic structures. *J. Appl. Cryst.* 2, (1969) 65.
- [4] J. Rodriguez-Carvajal, Recent advances in magnetic-structure determination by neutron powder diffraction, *Physica B* 192, (1993) 55.
- [5] L. van Eijck, L. D. Cussen, G. J. Sykora, E. M. Schooneveld, N. J. Rhodes, A. A. van Well, C. Pappas, Design and performance of a novel neutron powder diffractometer: PEARL at TU Delft, *J. Appl. Cryst.* 49, (2016) 1398.
- [6] D. P. E. Dickson and F. J. Berry, *Mössbauer spectroscopy*, Cambridge University Press, New York, (1986).
- [7] R. L. Mössbauer, Kernresonanzabsorption von gammastrahlung in  $\text{Ir}^{191}$ , *Naturwissenschaften* 45, (1958) 538.
- [8] Z. Klencsár, Mössbauer spectrum analysis by evolution algorithm, *Nucl. Instr. Meth. Phys. Res. B* 129, (1997) 527.

# Chapter 4

## **Magnetocaloric properties of $Mn_5(Si,P)B_2$ compounds**

### **4.1 Introduction**

There is a great deal of waste heat generated in modern industrial processes. The waste heat emitted by industrial processes is about 72% of all electrical energy produced worldwide in 2016 [1]. This industrial waste heat can partly be re-used if it is effectively utilized. In most cases the temperature of the produced industrial waste heat is only moderately higher than room temperature (300 - 400 K) [2]. Nevertheless, conventional thermoelectric generators are inefficient in this temperature range and expensive [3, 4]. There have been several attempts to utilize the waste heat for energy harvesting. For example, magnetocaloric generators (or magnetocaloric motors) [5], shape memory alloy-based heat engines [6], as well as thermoacoustic engines [7] have been investigated. Among them, the magnetocaloric generator converts thermal energy into electrical energy by the difference in magnetization of soft magnetic materials at different temperatures. This energy harvesting concept was proposed by Nikola Tesla [8, 9] as far back as the end of the 19<sup>th</sup> century. However, in order to use the concept efficiently it required the development of new magnetocaloric materials. Initially, magnetocaloric materials were studied for magnetic cooling applications, where the magnetic entropy change of the material induced by a change in applied magnetic field is converted into thermal energy [10-12]. It was later found that the inverse process in a power cycle could also be used for energy harvesting [13, 14]. In recent years, the research of near room-temperature magnetocaloric materials (MCMs) has made great achievements, and many material systems have been explored: Gd and Gd alloys [15-19],  $Fe_2P$ -based [11, 20-24],  $La(Fe,Si)_{13}$  based [25, 26], FeRh alloys [27, 28] and Heusler alloys [29-31]. The research on these material systems is relatively mature, and each material system has its own advantages and disadvantages. Problems related to a poor mechanical stability or expensive raw materials often limit the applicability of the

established MCMs. Finding new material systems that potentially meet the application requirements is therefore of interest.

The  $M_5XB_2$  ( $M = Fe, Mn, Co, V, Cr$  and  $X = Si, P, S$ ) materials system was previously studied for permanent magnet applications. In 1959 and 1960, Aronsson and Lundgren [32, 33] reported that  $M-Si-B$  ( $M = Mn, Fe, Co$ ) compounds could, under appropriate experimental conditions, crystallize in the tetragonal  $Cr_5B_3$  crystal structure with  $I4/mcm$  symmetry (space group 140). Later, Rundqvist found that  $Fe-P-B$  alloys could also form in this structure [34]. The Curie temperatures of  $Fe_5SiB_2$  and  $Fe_5PB_2$  were reported to be 784 K [35] and 639 K [36], respectively. The high  $T_C$  values were the reason this system was considered as a potential permanent magnet material. In 2009, Almeida calculated the Curie temperature of  $Mn_5SiB_2$  to be in the range of 469 - 492 K and found a saturation magnetization of  $5.5 \times 10^5 \text{ Am}^{-1}$  [37]. Many studies on doping with  $3d$  elements ( $Co, Cr$ , etc.) have been performed for  $(Mn,Fe)_5(Si,P)B_2$  alloys [38-44]. Interestingly, Ericsson [45] and Cedervall [46] reported a spin reorientation around 170 K in  $Fe_5SiB_2$ , where the magnetic moment was oriented along the  $c$  axis at low temperatures and in the  $a-b$  plane above the spin reorientation temperature of 170 K. In 2010, Xie and coworkers [38] proposed that the  $Mn_5PB_2$  compound had the potential to be used as a room-temperature MCM as the Curie temperature of 311 K is close to room temperature. Co doped  $Fe_5PB_2$  compounds are also a good candidates for room-temperature MCMs, as the Curie temperature of the  $Fe_5PB_2$  compounds can be adjusted from 662 down to 152 K by the introduction of Co [43].

In this study, we investigated whether  $Mn_5(Si,P)B_2$  compounds have the potential to be used as MCMs for energy harvesting applications. The Si/P ratio was adjusted over the full range, and the lattice structure was analyzed by XRD and ND measurements. The magnetocaloric properties and magnetic structure were revealed by magnetic measurements and ND studies at low temperature. The results show that the Curie temperature of the compounds can be adjusted continuously in a wide temperature range above room temperature. A relatively high magnetization difference was found for a fixed temperature span around the magnetic transition. This makes them suitable for magnetocaloric energy harvesting applications that efficiently convert low-temperature waste heat into electricity.

### 4.2 Experimental details

The polycrystalline  $Mn_5SiB_2$  compound was prepared by ball-milling the starting materials Mn (99.6% purity), Si (99+% purity), B (99.4% purity) at a speed of 350 rpm for 10 hours in a stainless steel jar with a sample-to-balls mass ratio of 1:4. The  $Mn_5PB_2$  compound and the other compounds containing P were prepared with starting

materials of MnP (96.08% purity), Mn (99.6% purity) and B (99.4% purity) powder by ball-milling at a speed of 350 rpm. The ball-milled samples were pressed into tablets with a diameter of 1 cm and a thickness of about 0.5 cm, and subsequently sealed in a quartz tube filled with 200 mbar of high-purity argon. The sealed samples were annealed in a furnace at 1150 °C for 24 hours and then quenched in water. Room-temperature XRD was carried out with a PANalytical X-Pert PRO using Cu- $K_\alpha$  radiation. ND measurements were performed on the neutron powder diffractometer PEARL at the research reactor of the TU Delft [47]. Temperature-dependent XRD measurements were performed with an Anton Paar TTK450 temperature chamber. Differences in sample temperature and the control temperature were calibrated by comparing the Curie temperature obtained from XRD and SQUID magnetisation. Powder Neutron Diffraction data were collected at 80, 298 and 520 K using a fixed neutron wave length of  $\lambda = 1.665 \text{ \AA}$ . The samples were placed in a vanadium can with a diameter of 0.7 mm. The lattice structure and magnetic structure refinements were carried out using the Rietveld method [48] and the Fullprof software [49]. For the magnetic structure analysis in the ferromagnetic state we used the occupancies and internal coordinates obtained for the paramagnetic state at high temperatures. Magnetic measurements were carried out in a superconducting quantum interference device (SQUID) magnetometer (Quantum Design MPMS). Temperature-dependent magnetization was measured with a sweep rate of 2 K/min. The magnetic measurements at temperatures above 370 K and the heat capacity in a magnetic field of 1 T were performed in a VersaLab vibrating-sample magnetometer (VSM) with an oven function. The heat capacity measurements were carried out by Differential Scanning Calorimetry (DSC) measurements using a TA-Q2000 instrument (TA Instrument Company), equipped with a liquid nitrogen cooling system. The sweeping rate selected for the DSC measurements in this study was 10 K/min. Natural B is composed of 80%  $^{11}\text{B}$  and 20%  $^{10}\text{B}$  [50]. The absorption cross-section for thermal neutrons  $\sigma_{a,th}$  at a neutron velocity of  $2200 \text{ ms}^{-1}$  for the  $^{10}\text{B}$  isotope is as high as  $3838 \times 10^{-28} \text{ m}^2$ , while for the  $^{11}\text{B}$  isotope it corresponds to only  $0.0055 \times 10^{-28} \text{ m}^2$  [51]. This means that the presence of the  $^{10}\text{B}$  isotope seriously affects the scattered intensity of the neutrons as a result of absorption. To avoid this effect, we used  $^{11}\text{B}$  to re-prepare three samples  $Mn_5Si^{11}B_2$ ,  $Mn_5Si_{0.5}P_{0.5}^{11}B_2$  and  $Mn_5P^{11}B_2$  for ND experiments using the same procedure as the previous parent sample (prepared with natural boron). The effect of crystallite orientation along an applied magnetic field in powder samples was studied by grinding the powder into small particles and then passing it through a  $30 \text{ }\mu\text{m}$  sieve. These powder samples were mixed with glue and placed in a magnetic field (of 1 T) for 24 hours at room temperature.

### 4.3 Results and discussion

#### 4.3.1 The crystalline structures

XRD investigations confirm that the  $Mn_5Si_{1-x}P_xB_2$  ( $0 \leq x \leq 1$ ) compounds all crystallize in the  $Cr_5B_3$ -type tetragonal structure with space group  $I4/mcm$ . Fig. 4.1(a) shows the XRD patterns taken at room temperature for the  $Mn_5Si_{1-x}P_xB_2$  ( $x = 0.0, 0.6, 0.8$  and  $1.0$ ) compounds. For  $0.0 \leq x \leq 0.5$  no additional diffraction peaks were observed besides the ones from the  $Mn_5SiB_2$  main phase. However, a hexagonal  $Mn_2P$  impurity phase emerges for  $x > 0.5$  and increases with the P content, as shown in Fig. 4.1(b). When Si is completely replaced by P ( $x = 1$ ), the  $Mn_2P$  impurity phase reaches a weight fraction of 6.2 wt.%. Fig. 4.1(c) and (d) show the lattice parameters  $a$  and  $c$ , the  $c/a$  ratio and the unit-cell volume  $V$  of the  $Mn_5Si_{1-x}P_xB_2$  ( $0 \leq x \leq 1$ ) main phase as a function of P content. The lattice parameters obtained by XRD were  $a = 5.61032(5) \text{ \AA}$ ,  $c = 10.44349(9) \text{ \AA}$  for  $Mn_5SiB_2$  ( $x = 0$ ) and  $a = 5.53276(6) \text{ \AA}$ ,  $c = 10.47474(12) \text{ \AA}$  for  $Mn_5PB_2$  ( $x = 1$ ), in good agreement with former studies [37, 38]. Table 4.1 lists the lattice parameters and unit cell volume for the whole range of P doping. As expected the introduction of P reduced the unit-cell volume, as the atomic radius of P (0.98  $\text{\AA}$ ) is slightly smaller than Si (1.11  $\text{\AA}$ ). The change in the unit cell with P substitution is found to be anisotropic, as the changes in lattice parameters  $a$  and  $c$  have an opposite sign: the unit cell is stretched along the  $c$  axis, and compressed in the  $a$ - $b$  plane. The effect of the lattice structure is important for the magnetic properties since it causes changes in the relative distances between the magnetic atoms and thus affects the magnetic coupling.

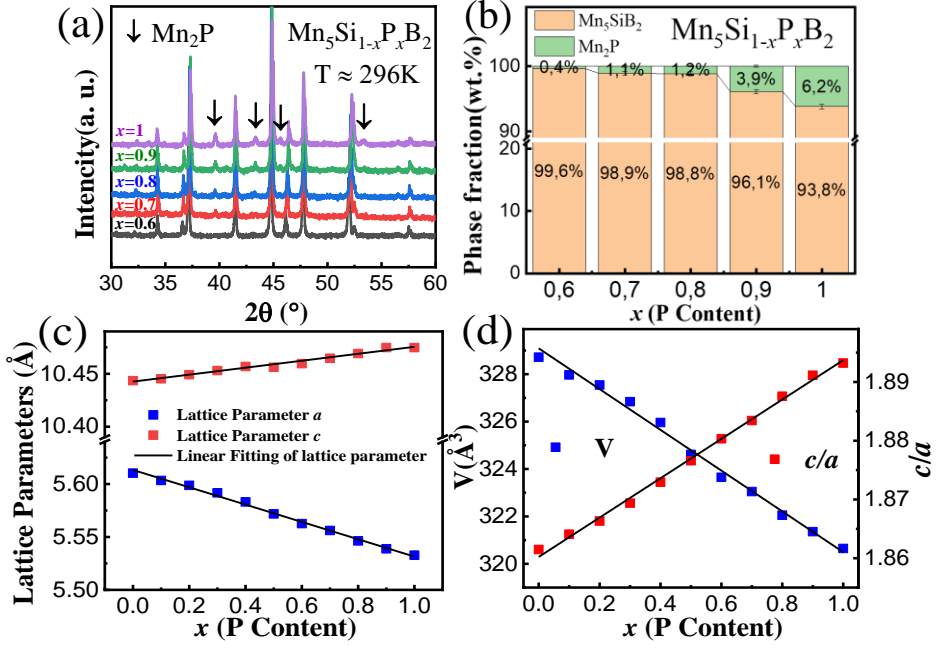


**Fig. 4.1** (a) XRD patterns of  $Mn_5Si_{1-x}P_xB_2$  ( $x = 0.0, 0.6, 0.8$  and  $1.0$ ) compounds. The peaks of the secondary  $Mn_2P$  phase are indicated by black arrows. (b) Weight fractions of the main and secondary phase for the  $Mn_5Si_{1-x}P_xB_2$  ( $0.6 \leq x \leq 1$ ) compounds. (c) Lattice parameters of the main phase in the  $Mn_5Si_{1-x}P_xB_2$  ( $0.6 \leq x \leq 1$ ) compounds as a function of the P content. (d) Unit-cell volume and  $c/a$  ratio of the main phase in the  $Mn_5Si_{1-x}P_xB_2$  ( $0 \leq x \leq 1$ ) compounds as a function of the P content.

**Table 4.1** Lattice parameters  $a$  and  $c$ , unit-cell volume  $V$ , saturation magnetization  $M_S$  and ferromagnetic transition temperature  $T_C$  for the  $Mn_5Si_{1-x}P_xB_2$  ( $0 \leq x \leq 1$ ) compounds. The lattice parameters and unit-cell volume were obtained by room-temperature XRD,  $M_S$  from SQUID magnetometer measurements at 5 K and  $T_C$  from SQUID magnetometer measurements in an applied field of 0.01 T.

$x$	$a$ (Å)	$c$ (Å)	$V$ (Å <sup>3</sup> )	$M_S$ (Am <sup>2</sup> kg <sup>-1</sup> )	$M_S$ (μ <sub>B</sub> /f.u.)	$T_C$ (K)
0.0	5.61032(4)	10.44349(9)	328.716(5)	105.56	6.13	406
0.1	5.60345(5)	10.44529(11)	327.968(5)	101.54	5.90	398
0.2	5.59878(4)	10.44915(9)	327.543(4)	105.16	6.12	386
0.3	5.59174(4)	10.45302(8)	326.840(4)	102.17	5.95	374
0.4	5.58316(4)	10.45688(9)	325.959(4)	101.16	5.90	359
0.5	5.57184(4)	10.45612(11)	324.614(5)	97.33	5.68	346
0.6	5.56262(5)	10.45959(11)	323.648(5)	100.43	5.86	339
0.7	5.55612(4)	10.46460(9)	323.047(4)	97.75	5.71	329
0.8	5.54635(4)	10.46912(8)	322.051(4)	99.25	5.81	318
0.9	5.53888(4)	10.47478(9)	321.358(4)	94.12	5.51	309
1.0	5.53276(6)	10.47474(12)	320.647(6)	91.07	5.34	305

In Fig. 4.2(a) the XRD pattern for the  $^{11}\text{B}$  containing sample  $\text{Mn}_5\text{P}^{11}\text{B}_2$ , which was prepared for the ND measurements, is shown. The  $\text{Mn}_5\text{P}^{11}\text{B}_2$  compound also crystallized in  $\text{Cr}_5\text{B}_3$ -type structure (94.5 wt.%) and is accompanied by a small amount of the  $\text{Mn}_2\text{P}$  impurity phase (5.5 wt.%). Fig. 4.2(b) shows the lattice parameters of the main phase in  $\text{Mn}_5\text{Si}_{1-x}\text{P}_x\text{B}_2$  (natural B) and in  $\text{Mn}_5\text{Si}_{1-x}\text{P}_x^{11}\text{B}_2$  (with  $^{11}\text{B}$ ) for  $x = 0.0, 0.5$  and  $1.0$ . The XRD data at room temperature are almost identical. It can be seen that the introduction of  $^{11}\text{B}$  has no significant effect on the formation of the main phase. The room-temperature (298 K) XRD and the high-temperature (520 K) and low-temperature (80 K) ND data show the same trend. The ND pattern for the  $\text{Mn}_5\text{P}^{11}\text{B}_2$  compound in the paramagnetic state ( $T = 520\text{K}$ ) is shown in Fig. 4.2(c). The ND refinement confirms that this series of compounds crystallizes in the  $\text{Cr}_5\text{B}_3$ -type tetragonal structure, in good agreement with XRD results. We found that Mn occupies the  $16l$  and  $4c$  sites, Si/P the  $4a$  site and B the  $8h$  site (consistent with previous results). Häggström and coworkers [36] reported that part of the B occupies the  $4a$  site in  $\text{Fe}_5\text{PB}_2$ . We did however not observe evidence for this in  $\text{Mn}_5\text{Si}_{1-x}\text{P}_x^{11}\text{B}_2$  ( $0 \leq x \leq 1$ ) compounds. The refined structural parameters from the ND measurements in the paramagnetic state are listed in Table 4.2.

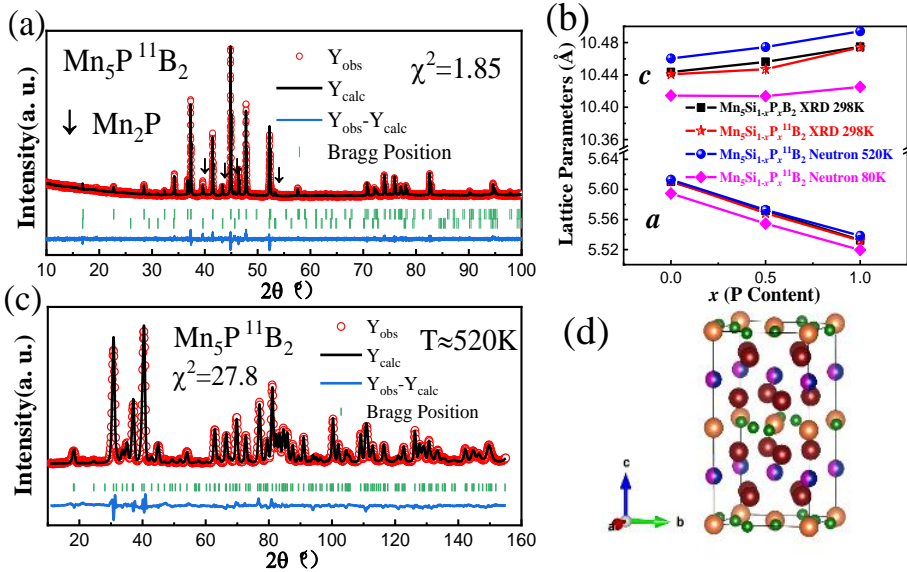


**Fig. 4.2** (a) Room-temperature XRD pattern for the  $\text{Mn}_5\text{P}^{11}\text{B}_2$  compound. The contribution from the  $\text{Mn}_2\text{P}$  phase is indicated by black arrows. (b) Lattice parameters of the main phase for  $\text{Mn}_5\text{Si}_{1-x}\text{P}_x\text{B}_2$  ( $x = 0.0, x = 0.5$  and  $x = 1.0$ ) and  $\text{Mn}_5\text{Si}_{1-x}\text{P}_x^{11}\text{B}_2$  ( $x = 0.0, x = 0.5$  and  $x = 1.0$ ) measured by XRD (at 298 K) and ND (at 80 and 520 K). (c) ND pattern of  $\text{Mn}_5\text{P}^{11}\text{B}_2$  compound in the paramagnetic state ( $T = 520\text{K}$ ). (d) Crystal structure of  $\text{Mn}_5(\text{Si,P})\text{B}_2$ . The different elements at the different sites are represented with dark brown for Mn at the  $16l$  site, light brown for Mn at the  $4c$  site, purple/blue for Si/P at the  $4a$  site and green for B at the  $8h$  site.

## Chapter 4 Magnetocaloric properties of $Mn_5(Si,P)B_2$ compounds

**Table 4.2** Structural parameters of  $Mn_5Si_{1-x}P_xB_2$  ( $x = 0.0$ ,  $x = 0.5$  and  $x = 1.0$ ) in the paramagnetic state by ND. The numbers in parentheses are the refined errors. All the compounds crystallize in the  $Cr_5B_3$ -type structure with space group  $I4/mcm$  with Mn1 at the  $16l$  ( $x_1$ ,  $x_1+1/2$ ,  $z$ ) site, Mn2 at the  $4c$  (0, 0, 0) site, P/Si at the  $4a$  (0, 0,  $1/4$ ) site and B at the  $8h$  ( $x_2$ ,  $x_2+1/2$ , 0) Site.

Parameters	$Mn_5Si^{11}B_2$	$Mn_5Si_{0.5}P_{0.5}^{11}B_2$	$Mn_5P^{11}B_2$
$a(\text{\AA})$	5.61296(8)	5.57277(109)	5.53694(10)
$c(\text{\AA})$	10.46029(9)	10.47449(402)	10.48970(37)
$V(\text{\AA}^3)$	329.555(11)	325.294(154)	321.590(14)
$16l$ $x_1$	0.16719(14)	0.16840( 209)	0.16950(19)
$z$	0.13821(14)	0.13936( 205)	0.14007(19)
$8h$ $x_2$	0.61724(13)	0.61619( 204)	0.61679(17)
$4a$ Occ(Si/P)	-	0.400(52)/0.600(52)	-
$R_p(\%)$	5.76	6.83	6.59
$R_{wp}(\%)$	7.62	10.4	9.19

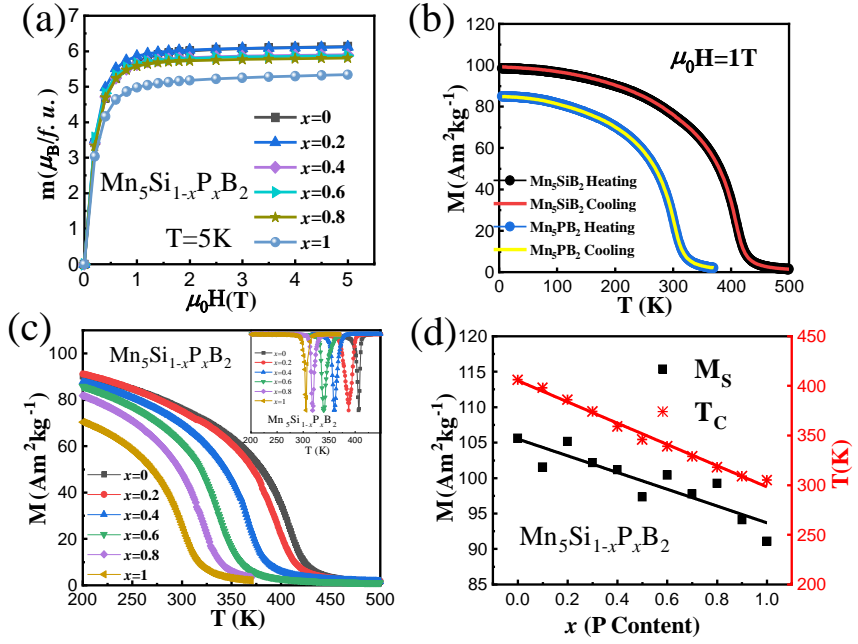
### 4.3.2 Magnetocaloric effect

Fig. 4.3(a) shows the  $M$ - $\mu_0 H$  curves measured at a temperature of 5 K. All magnetization curves show a typical soft ferromagnetic behavior without any magnetic hysteresis, where magnetic saturation is effectively reached at 1 T. The saturation magnetization ( $M_s$ ) of  $Mn_5SiB_2$  and  $Mn_5PB_2$  corresponds to 6.13 and 5.34  $\mu_B/\text{f.u.}$ , respectively. The  $M_s$  value for all the  $Mn_5Si_{1-x}P_xB_2$  ( $0 \leq x \leq 1$ ) compounds is listed in Table 4.1. The average magnetic moment per manganese atom in  $Mn_5SiB_2$  and  $Mn_5PB_2$  is 1.37 and 1.12  $\mu_B/\text{atom}$ , respectively. Wappling and coworkers [35] reported an average magnetic moment in  $Mn_5SiB_2$  and  $Mn_5PB_2$  of 1.6 and 1.1  $\mu_B/\text{atom}$ , respectively. The results for the  $Mn_5PB_2$  compound are consistent, but  $Mn_5SiB_2$  has a higher value in his report, which may be an overestimation since their calculation is based on NMR data. De Almeida and coworkers reported a magnetization for  $Mn_5SiB_2$  that corresponds to 0.946  $\mu_B/\text{atom}$  at 300 K [37], which is slightly higher than our result of 0.882  $\mu_B/\text{atom}$ . The saturation magnetization of the  $Mn_5Si_{1-x}P_xB_2$  compounds was found to depend on the Si/P ratio, as shown in Fig. 4.3(d). The introduction of P reduces the saturation magnetization.

Fig. 4.3(b) shows the temperature dependent magnetization ( $M$ - $T$ ) curves of  $Mn_5SiB_2$  and  $Mn_5PB_2$  for heating and cooling in an applied field of 1 T. The compounds show a ferromagnetic-to-paramagnetic phase transition near room temperature with a transition temperature  $T_C$  of 406 and 305 K, respectively. The transition temperature was obtained

from the extreme value in the first derivative of the corresponding  $M$ - $T$  curves in low magnetic field (0.01 T). These results are in good agreement with the values of 411 and 312 K previously reported by Wäppling and coworkers [35]. Xie and coworkers [38] reported a slightly lower value of 302 K for  $Mn_5PB_2$ . Heating and cooling  $M$ - $T$  curves coincide without thermal hysteresis, suggesting that these compounds show a second-order phase transition (SOPT) at  $T_C$ . The  $M$ - $T$  curves in a field of 1 T and the first derivatives of the  $M$ - $T$  curves in a field of 0.01 T are shown in Fig. 4.3(c). The value of  $T_C$  shows a strong dependence on the Si/P ratio and decreased with P content. An increase in P content of 10 at.% causes a decrease in  $T_C$  of about 10 K, resulting in  $dT_C/dx \approx 1$  K/at.%. The  $T_C$  values of the  $Mn_5Si_{1-x}P_xB_2$  ( $0 \leq x \leq 1$ ) compounds are listed in Table 4.1. The results are similar to those observed by Wäppling *et al.* [35] and Häggström *et al.* [36] for  $Fe_5SiB_2$  -  $Fe_5PB_2$  compounds. Fig. 4.3(d) shows  $T_C$  as a function of the P content, indicating that  $T_C$  in the  $Mn_5Si_{1-x}P_xB_2$  ( $0 \leq x \leq 1$ ) compounds can be varied continuously in the temperature range from 305 to 406 K by adjusted the Si/P ratio. This fulfills one important application requirements of MCMs that the transition temperature can be adjusted continuously over the temperature range of interest for the application.

For the magnetocaloric energy harvesting cycle low-grade waste heat  $Q_{in}$  is used as an energy source, and the magnetization difference caused by the material after being heated will cause the change of Gibbs free energy:  $E_M = -\mu_0 \Delta M H$ , and this can be convert into kinetic or electrical energy, where the  $\Delta M = M_{cold} - M_{hot}$  is the magnetization difference between the two reference temperatures above ( $T_{hot}$ ) and below ( $T_{cold}$ ) the phase transition temperature ( $T_C$ ). A key property for magnetic energy harvesting materials is the thermodynamic efficiency  $\eta = -\mu_0 \Delta M H / Q_{in}$ , defined by the ratio of the upper-limit magnetic energy  $E_M$  and the required heat  $Q_{in}$  [13]. In Fig. 4.4, we show the  $M$ - $T$  and  $C_p$ - $T$  curves in the vicinity of the transition temperature for the  $Mn_5Si_{0.5}P_{0.5}B_2$  compounds and the  $\Delta M$  and  $Q_{in}$  values for a temperature span  $\Delta T$  of 30 K symmetrically placed around  $T_C$ . According to a study by Dzekan and coworkers [52], FOPT materials generally have a relatively high  $\Delta M$ , but due to the presence of latent heat, the required input heat energy  $Q_{in}$  is also significant, which in turn reduces its efficiency. Although the  $\Delta M$  of the SOPT materials are generally smaller than the  $\Delta M$  of FOPT materials, the absence of thermal hysteresis and the smaller  $Q_{in}$  make them competitive. In our study,  $\Delta M$  for  $Mn_5PB_2$  and  $Mn_5Si_{0.5}P_{0.5}B_2$  compounds are 28.1 and 31.1  $Am^2kg^{-1}$ , respectively. The  $\Delta M$  of these two compounds is comparable to those for Heusler alloys, as reported by Dzekan and coworkers [52]. The  $\Delta M$  values for  $Mn_5PB_2$  and  $Mn_5Si_{0.5}P_{0.5}B_2$  compounds are higher than the majority of the reported Heusler alloys. The  $Q_{in}$  values for the  $Mn_5PB_2$  and  $Mn_5Si_{0.5}P_{0.5}B_2$  compounds correspond to 18.8 and 20.9  $kJkg^{-1}$ , respectively. The value of  $\Delta M$  and  $Q_{in}$  for the  $Mn_5Si_{1-x}P_xB_2$  ( $x = 0.0, 0.5$  and  $1.0$ ) compounds are shown in Table 4.3.



**Fig. 4.3** (a) Field-dependent magnetization of the  $Mn_5Si_{1-x}P_xB_2$  ( $x = 0.0, 0.2, 0.4, 0.6, 0.8$  and  $1.0$ ) compounds measured at  $5 K$ . (b) Temperature-dependent magnetization of the  $Mn_5SiB_2$  and  $Mn_5PB_2$  compounds in a field of  $1 T$  for heating and cooling. (c) Temperature-dependent magnetization of the  $Mn_5Si_{1-x}P_xB_2$  ( $x = 0.0, 0.2, 0.4, 0.6, 0.8$  and  $1.0$ ) compounds. The inset shows the reduced first derivative of the low-field  $M-T$  curve in a field of  $0.01 T$ . (d) Values of  $T_C$  (red) and  $M_S$  (black) for  $Mn_5Si_{1-x}P_xB_2$  ( $0 \leq x \leq 1$ ) as a function of the P content  $x$ .

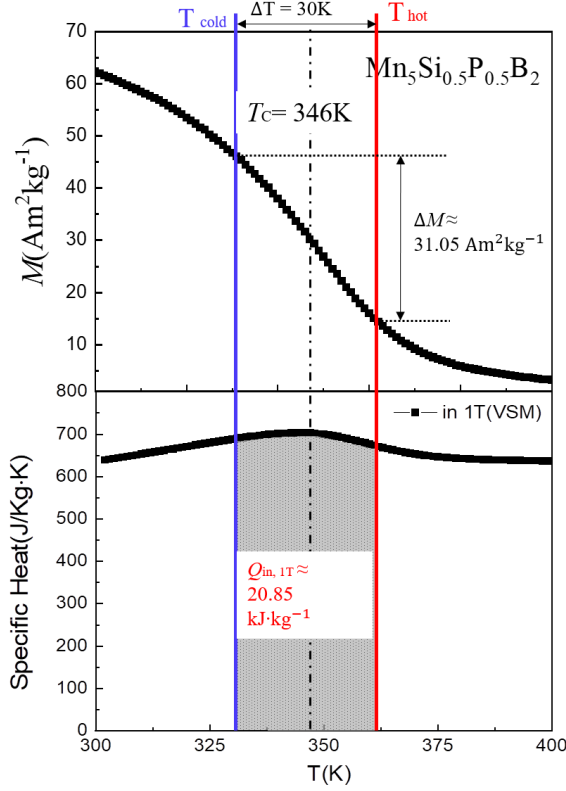


**Fig. 4.4** (a)  $M$ - $T$  curve of  $\text{Mn}_5\text{Si}_{0.5}\text{P}_{0.5}\text{B}_2$  compound near the Curie temperature in a magnetic field of 1 T, where  $\Delta M$  is the difference in magnetization for a temperature span of  $\Delta T = T_{\text{hot}} - T_{\text{cold}} = 30\text{ K}$ . (b) Temperature dependence of the heat capacity. The input heat  $Q_{\text{in}}$  is defined by the integral of the heat capacity over the temperature span of  $\Delta T = 30\text{ K}$ .

The specific heat capacity as a function of temperature for the  $\text{Mn}_5\text{Si}_{1-x}\text{P}_x\text{B}_2$  ( $x = 0.0, 0.2, 0.4, 0.6, 0.8$  and  $1.0$ ) compounds is shown in Fig. 4.5(a). A discontinuous step in the specific heat capacity is observed at the transition temperature, which is characteristic for a SOPT. We calculated the isothermal magnetic entropy change of the compounds from the  $M$ - $T$  data at different magnetic field changes ( $0.05 - 2\text{ T}$ ) using equation  $\Delta S_M(T)_{\Delta H} = \int_{H_i}^{H_f} \mu_0 \left( \frac{\partial M(T, H)}{\partial T} \right)_H dH$  [15]. The estimated isothermal magnetic entropy change is shown in Fig. 4.5(b) for a field change of  $\Delta \mu_0 H = 1\text{ T}$  (for a field between 0 and 1 T). The transition temperature moves to lower temperatures for an increase in P content. The corresponding maximum  $|\Delta S_M|$  for  $\text{Mn}_5\text{SiB}_2$ ,  $\text{Mn}_5\text{Si}_{0.5}\text{P}_{0.5}\text{B}_2$  and  $\text{Mn}_5\text{PB}_2$  in a field change of 1 T is 1.90, 1.33 and 1.35  $\text{Jkg}^{-1}\text{K}^{-1}$ , respectively. For comparison, the

isothermal magnetic entropy curve of Gd is also shown in Fig. 4.5(b). The maximum value of  $|\Delta S_M|$  for our sample is slightly lower than the value of  $2.46 \text{ Jkg}^{-1}\text{K}^{-1}$  of Gd. The maximum magnetic entropy change  $|\Delta S_{M, \max}|$  for  $Mn_5Si_{1-x}P_xB_2$  ( $x = 0.0, 0.5$  and  $1.0$ ) compounds are listed in Table 4.3.

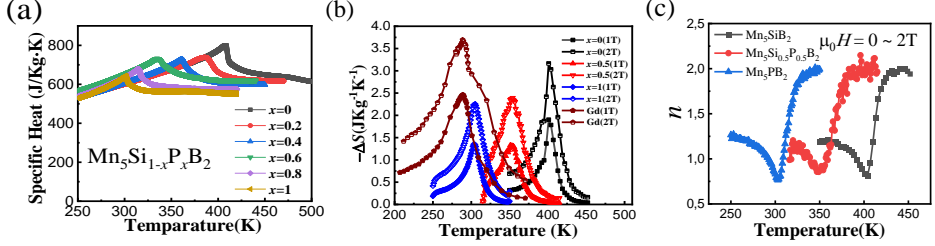


**Fig. 4.5** (a) Temperature dependence of the specific heat capacity of the  $Mn_5Si_{1-x}P_xB_2$  ( $x = 0.0, 0.2, 0.4, 0.6, 0.8$  and  $1.0$ ) compounds. (b) Magnetic entropy change  $-\Delta S_M$  as a function of temperature for a field change of 1 and 2T. The data for Gd have been added as reference. (c) Field exponent of the magnetic entropy change  $n = \frac{d \ln(|\Delta S_M|)}{d \ln(H)}$  for the  $Mn_5Si_{1-x}P_xB_2$  ( $x = 0.0, 0.5$  and  $1.0$ ) compounds.

**Table 4.3** Calculated  $|\Delta S_{M, \max}|$  and  $\Delta M$  and  $Q_{in}$  ( $\Delta T = 30\text{K}$ ) for  $Mn_5Si_{1-x}P_xB_2$  ( $x = 0.0, 0.5$  and  $1.0$ ) in 1 and 2 T, data for Gd from literatures [52, 53] and Gd in this work are shown as a comparison.

	Applied field	Gd (in this work)	Gd	$Mn_5SiB_2$	$Mn_5Si_{0.5}P_{0.5}B_2$	$Mn_5PB_2$
$\Delta S_{M, \max}$ ( $\text{Jkg}^{-1}\text{K}^{-1}$ )	0-1 T	2.46	2.8 [53]	1.90	1.33	1.35
	0-2 T	3.69	---	3.16	2.36	2.26
$\Delta M$ ( $\text{Am}^2\text{kg}^{-1}$ )	1 T	63.4	77 [52]	---	31.05	28.12
$Q_{in}$ ( $\text{kJkg}^{-1}$ )	1 T	---	19.2 [52]	---	20.85	18.88

The  $M$ - $T$  and DSC curves of these compounds show typical SOPT characteristics. Law and coworkers [54] proposed a quantitative analysis to evaluate the nature of the phase transition. The magnetic entropy change is proposed to scale as a power law with the magnetic field  $|\Delta S_M| \propto H^n$ , where the exponential  $n = \frac{d \ln(|\Delta S_M|)}{d \ln(H)}$  will demonstrate a

sharp change near the transition temperature. Using the Bean and Rodbell model [55] it was demonstrated that it can distinguish whether a material shows a FOPT or a SOPT by evaluating the field exponent  $n$  across the phase transition. For materials with a FOPT, the maximum value of the field exponent  $n_{max}$  is greater than 2, while it remains equal or less than 2 for a SOPT (this is also the case for the critical point between the FOPT and the SOPT). Moreover, the minimum value for the field exponent  $n_{min}$  is also characteristic for the transition where  $n_{min} = 2/3$  for the SOPT,  $n_{min} = 2/5$  for the critical point between the FOPT and the SOPT and  $n_{min} < 2/5$  for the FOPT. Van Dijk [56] later demonstrated that these predictions are also found when the Landau model [57] is applied to describe the phase transition. Fig. 4.5(c) shows the temperature dependence of the field exponent  $n$  for the  $Mn_5Si_{1-x}P_xB_2$  ( $x = 0.0, 0.5$  and  $1.0$ ) compounds. The maximum value for the field exponent does not exceed the value of 2 in the vicinity of the phase transition. The minimum value for the field exponent  $n_{min}$  is very similar for all three compounds and reaches a value slightly above  $2/3$ . All these observations confirm that these three materials show a SOPT.

Temperature-dependent XRD was used to characterize the magneto-elastic coupling in the  $Mn_5SiB_2$  compound. Fig. 4.6(a) shows the unit-cell volume as a function of temperature for  $Mn_5SiB_2$  in the temperature range from 298 to 429 K. Interestingly, the volume of the unit cell reduces with temperature in a narrow temperature range (360 - 400 K) below  $T_C$ . In this temperature range a weak negative thermal expansion (NTE) is observed, which originates from the temperature-dependent magneto-elastic coupling. In the low-temperature range (well below  $T_C$ ), all the magnetic moments are well aligned along the easy direction, and the magnetic moments deviate from the easy direction, while with the increase in temperature the magnetic order gradually collapses when the temperature approaches  $T_C$ . As the magneto-elastic coupling scales with the magnetic order, the lattice may experience a negative thermal expansion in case the magnetic order weakens when  $T_C$  is approached. Above the ferromagnetic transition temperature, the magnetic order vanishes, and thereby also the magneto-elastic coupling, resulting in the conventional thermal expansion of the paramagnetic state  $V_{PM}$  [58, 59]. In Fig. 4.6(a) the magneto-elastic contribution in the magnetically ordered state is estimated from the extrapolated temperature dependence of the unit-cell volume of the paramagnetic state. The difference  $\Delta V$  between the experimental data  $V_{exp}$  of the ferromagnetic state and the extrapolated paramagnetic state  $V_{PM}$  can be regarded as the contribution from the magneto-elastic coupling. The gradual variation in the unit-cell volume as a function of the temperature near  $T_C$  between 400 and 410 K, is expected to reflect the short-range order in the paramagnetic state (just above  $T_C$ ). It is interesting to note that the NTE is strongly anisotropic. As shown in Fig. 4.6(b) the negative thermal expansion is only observed within the  $a$ - $b$  plane ( $a$  axis) and not along the  $c$  axis. This is related to the magnetic structure of the compound, which we will discuss in the next section.

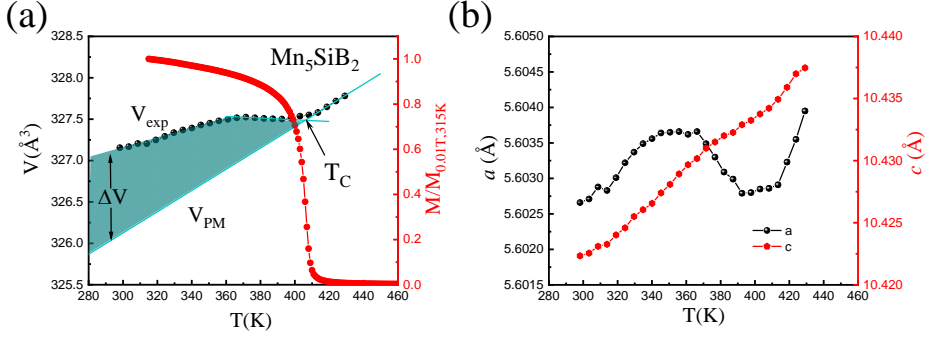


**Fig. 4.6** (a) Temperature dependence of the unit-cell volume  $V$  and the normalized  $M-T$  curve in a magnetic field of 0.01T for the  $Mn_5SiB_2$  compound. The ferromagnetic transition temperature  $T_C$  is indicated by the arrow. (b) Temperature dependence of the lattice parameters  $a$  and  $c$  for the tetragonal  $Mn_5SiB_2$  compound.

### 4.3.3 Magnetic structure

Magnetic anisotropy of the materials is also an important factor for magnetocaloric applications, especially for the magnetocaloric generators. As polycrystalline soft magnetic materials are used in generators, a low magnetic anisotropy means the materials can be magnetized more easily in relatively low magnetic fields, resulting in a larger magnetization difference for a given temperature span. To determine the magnetic structure of the  $Mn_5Si_{1-x}P_xB_2$  ( $0 \leq x \leq 1$ ) compounds, ND was carried out in both the ferromagnetic and the paramagnetic state. For the neutron powder diffraction samples containing the  $^{11}B$  isotope (instead of natural B) were prepared with composition  $Mn_5Si_{1-x}P_x^{11}B_2$  ( $x = 0.0, 0.5$  and  $1.0$ ). It is necessary to ensure that the  $Mn_5Si_{1-x}P_x^{11}B_2$  compounds have the same lattice structure and magnetic properties as the corresponding mother compounds prepared with natural boron. In the phase analysis section we have discussed that the  $^{11}B$  samples have the same lattice structure as the mother compounds. For the  $M-\mu_0H$  curves in Fig. 4.7(a) and the  $M-T$  curves in Fig. 4.7(b), the  $^{11}B$  compounds shows almost the same characteristics as the natural B containing mother compounds. This means we can confidently use  $^{11}B$  compounds as representative for the magnetic structure in the mother compounds. Fig. 4.8 shows the ND pattern of the  $Mn_5Si^{11}B_2$  compound in both the FM state (80 K) and the PM state (520 K). Due to the magnetic form factor  $f(Q)$  the magnetic scattering (proportional to  $|f(Q)|^2$ ) rapidly attenuates for increasing scattering angles. This means that the peaks in the low-angle scattering range provide most reliable information regarding the magnetic structure in the FM state. We didn't observe any new peaks in the FM state compared to the PM state, indicating that the size of the magnetic unit cell is the same as the nuclear unit cell. This means that the propagation vector for the magnetic structure corresponds

to  $\mathbf{k} = (0,0,0)$ . The most obvious difference between the neutron diffraction patterns of the FM and PM state is the increase in intensity for the (213) and (204) peaks in the FM state, reflecting a relatively strong magnetic contribution.

A representational analysis of space group 140 (tetragonal  $I4/mcm$  symmetry) has been performed with the SARA software package [60]. Table 4.4 shows the possible irreducible representations and the corresponding basis vectors for the magnetic structure in space group 140. According to a previous report [35, 46], this system has two magnetic sites for the Mn atoms: Mn1 at the  $16l$  site and Mn2 at the  $4c$  site. As we observe a single magnetic transition in the DSC and SQUID magnetization measurements, the two magnetic sites are strongly coupled and must be represented by the same irreducible representations, namely  $\Gamma_1$ ,  $\Gamma_3$  and  $\Gamma_9$ . The  $\Gamma_1$  representation is an antiferromagnetic ordering, while our samples show typical ferromagnetic order characteristics in magnetic measurements, so it can be excluded. The  $\Gamma_3$  representation has its basis vector along the  $c$  axis for the two magnetic sites, and the  $\Gamma_9$  representation has its basis vector aligned within the  $a$ - $b$  plane. We used the  $\Gamma_3$  and  $\Gamma_9$  representations to refine the ND data and found that the quality of fit in the refinement was relatively close for these two models, as shown in Fig. 4.9. This makes it difficult to conclude what orientation the magnetic moments have.

In order to determine the direction of its magnetic moment, the  $Mn_5SiB_2$  powder was oriented in a magnetic field at room temperature. Fig. 4.10(a) shows a comparison between the XRD pattern of the field-oriented powder and the free powder sample. The (004) and (006) peaks, which have a plane normal along the  $c$  axis in the oriented sample, all disappear. On the other hand, the (110), (200) and (220) peaks, which have a plane normal in the  $a$ - $b$  plane, are all significantly enhanced. Therefore, we can conclude that in the FM state at room temperature the magnetic moments are oriented within the  $a$ - $b$  plane. Based on the tetragonal  $I4/mcm$  symmetry of space group 140, there are two possible orientations within the  $a$ - $b$  plane, namely: (100) or (110).

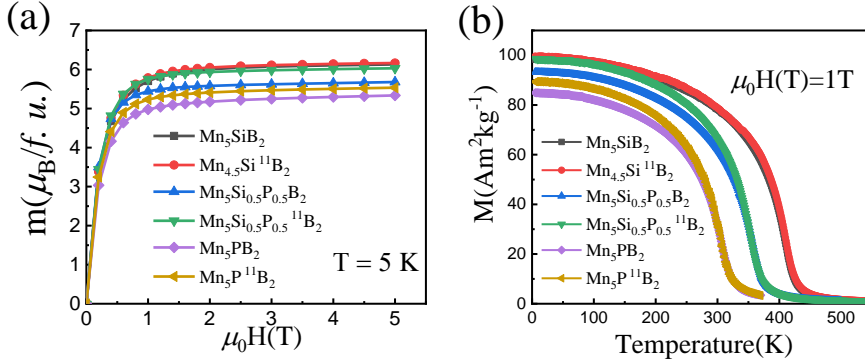


**Fig. 4.7** (a) Field-dependent magnetization of the  $Mn_5Si_{1-x}P_xB_2$  and  $Mn_5Si_{1-x}P_x^{11}B_2$  ( $x = 0.0, 0.5$  and  $1.0$ ) compounds at a temperature of 5 K. (b) Temperature-dependent magnetization of the  $Mn_5Si_{1-x}P_xB_2$  and  $Mn_5Si_{1-x}P_x^{11}B_2$  ( $x = 0.0, 0.5$  and  $1.0$ ) compounds in an applied field of 1 T.

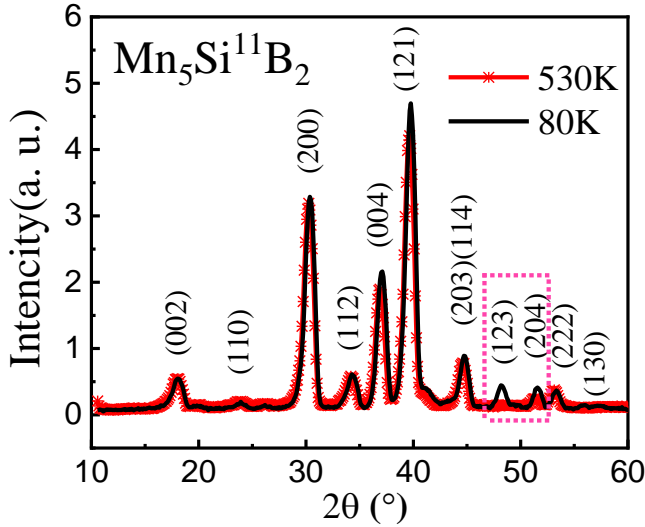


**Fig. 4.8** Neutron diffraction patterns for the  $Mn_5Si^{11}B_2$  compound in the ferromagnetic state (80 K) and in the paramagnetic state (520 K).

According to the calculated contribution of the magnetic scattering to the ND pattern in Fig. 4.10(b), it is concluded that low-angle diffraction peaks of the (002) and (101) crystal planes will be observed if the magnetic moments are aligned along the (110) direction, this is not the case in our result, no magnetic contribution is observed on

## Chapter 4 Magnetocaloric properties of $Mn_5(Si,P)B_2$ compounds

these two peaks (see Fig. 4.8). We therefore conclude that the magnetic moments are oriented along the (100) direction.

This result also explains the observed anisotropy in the negative thermal expansion. As the magnetic moments are arranged in the  $a$ - $b$  plane, the effect of the magnetic moment on the thermal expansion is much larger in this direction than along the  $c$  axis. Fig. 4.10(c) shows the obtained magnetic structure of  $Mn_5SiB_2$ .

**Table 4.4** Representational analysis results for space group 140 (tetragonal  $I4/mcm$  symmetry) with propagation vector  $\mathbf{k} = (0,0,0)$  and two magnetic sites at  $16l$  and  $4c$  given by SARAh. For each magnetic site, the possible magnetic ordering was given: antiferromagnetic (AFM) or ferromagnetic (FM), and the number of basis vectors  $\Phi_i$ .

Irreducible Representation	Magnetic $16l$ site		Magnetic $4c$ site	
	$\Phi$ in $a$ - $b$ plane	$\Phi$ in $c$ axis	$\Phi$ in $a$ - $b$ plane	$\Phi$ in $c$ axis
$\Gamma_1$	1 (AFM)	0	0	1 (AFM)
$\Gamma_2$	1 (AFM)	1 (AFM)	0	0
$\Gamma_3$	1 (AFM)	1 (FM)	0	1 (FM)
$\Gamma_4$	1 (AFM)	0	0	0
$\Gamma_5$	1 (AFM)	1 (AFM)	0	0
$\Gamma_6$	1 (AFM)	0	0	0
$\Gamma_7$	1 (AFM)	0	0	0
$\Gamma_8$	1 (AFM)	1 (AFM)	0	0
$\Gamma_9$	2 (FM) 4 (AFM)	0	2 (FM) 4 (AFM)	0
$\Gamma_{10}$	4 (AFM)	2 (FM)	0	0

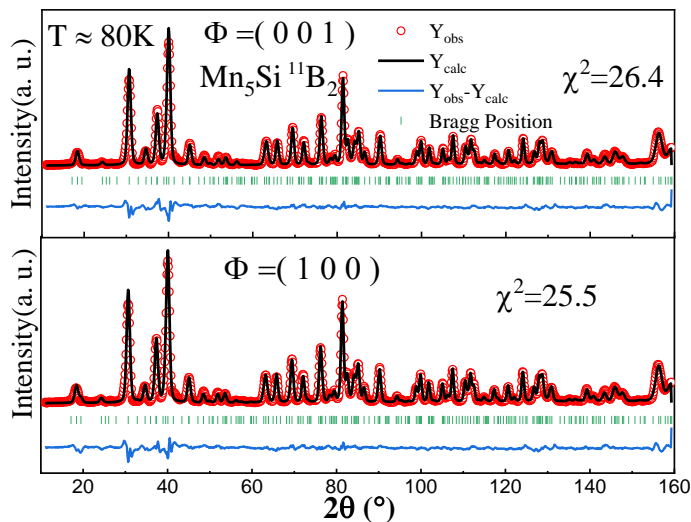


**Fig. 4.9** Comparison of the neutron powder diffraction refinements for the  $Mn_5Si^{11}B_2$  compound in the ferromagnetic state using different basis functions, with  $\Phi = (001)$  at the top and  $\Phi = (100)$  at the bottom.

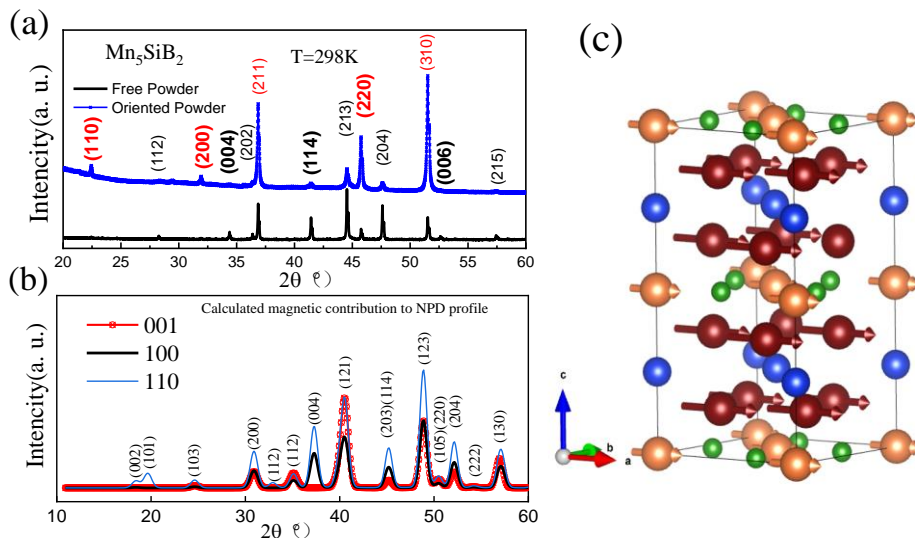


**Fig. 4.10** (a) Field-oriented powder and free powder XRD patterns of the  $Mn_5SiB_2$  compound in the ferromagnetic state at room temperature (298 K). (b) The comparison of the calculated magnetic contributions for three different magnetic moment directions in free powder ND:  $\Phi = (001)$ ,  $(100)$  and  $(110)$ . (c) Magnetic structure of the  $Mn_5Si^{11}B_2$  compound in the ferromagnetic state. The length of arrow corresponds to the size of the magnetic moment.

Fig. 4.11(a) shows the total magnetic moment per formula unit obtained by ND refinement and SQUID magnetization for the  $\text{Mn}_5\text{Si}_{1-x}\text{P}_x\text{B}_2$  ( $x = 0.0, 0.5$  and  $1.0$ ) compounds. The total magnetic moment decreases with increasing P content. It is worth noting that the values from the ND data are higher than those from the SQUID data. This may be because the magnetization is not fully saturated yet in an applied field of 5 T. To check this Fig. 4.11(b) shows a plot of  $M$  as a function of  $1/\mu_0 H$ . From this plot the saturation magnetization can be estimated by a linear fit of the curve. In order to avoid the effect of demagnetizing fields, only the data above 1 T were used. The saturation magnetization obtained by fitting in Fig. 4.11(a) is slightly higher than those of the SQUID magnetization data in 5 T, but still slightly lower than the magnetization obtained by ND. Fig. 4.11(c) shows the individual magnetic Mn moments for the two inequivalent positions (Mn1 at the  $16l$  site and Mn2 at the  $4c$  site) obtained by ND. The magnetic moment of Mn is larger at the  $16l$  site than at the  $4c$  site, consistent with the reported result for  $\text{Mn}_5\text{SiB}_2$  by Wäppling and coworkers [35]. The introduction of P has a different effect on the two magnetic moments: the moment on the  $16l$  site decreases with P content, while the moment on the  $4c$  site remains more or less constant with increasing P content.

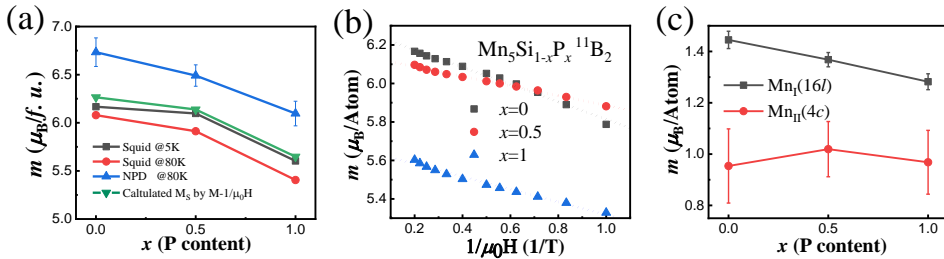


**Fig. 4.11** (a) Saturation magnetization of the  $\text{Mn}_5\text{Si}_{1-x}\text{P}_x\text{B}_2$  compounds ( $x=0.0, 0.5$  and  $1.0$ ) obtained by neutron diffraction and SQUID magnetization at different temperatures. (b) Magnetization versus  $1/\mu_0 H$  curve for the  $\text{Mn}_5\text{Si}_{1-x}\text{P}_x\text{B}_2$  compounds ( $x = 0.0, 0.5$  and  $1.0$ ). (c) Magnetic moments for Mn1 at the  $16l$  site and Mn2 at the  $4c$  site in the tetragonal lattice of the  $\text{Mn}_5\text{Si}_{1-x}\text{P}_x\text{B}_2$  compounds ( $x = 0.0, 0.5$  and  $1.0$ ).

#### 4.4 Conclusions

The magnetocaloric properties, lattice and magnetic structure of the  $\text{Mn}_5\text{Si}_{1-x}\text{P}_x\text{B}_2$  compounds have been studied in the whole range of P substitution ( $0 \leq x \leq 1$ ). All compounds crystallize in the tetragonal  $\text{Cr}_5\text{B}_3$ -type structure ( $I4/mcm$  symmetry), where the P atom replaces the Si at the  $4c$  site in the unit cell, which leads to a decrease in the

## Chapter 4 Magnetocaloric properties of $Mn_5(Si,P)B_2$ compounds

unit-cell volume. The  $Mn_5Si_{1-x}P_xB_2$  ( $0.6 \leq x \leq 1.0$ ) compounds are accompanied by a small amount of  $Mn_2P$  impurity phase, 6.2 wt.% for  $x = 1.0$ . As a result of a significant magneto-elastic coupling in the ferromagnetic state,  $Mn_5SiB_2$  exhibits a negative thermal expansion between 360 and 400 K. The neutron diffraction results reveal that the compounds show FM ordering with moments on the Mn atoms oriented within the  $a$ - $b$  plane below the ferromagnetic transition temperature. Although the P doping reduces  $M_S$ , the compounds still exhibit a considerable  $\Delta M$  up to  $31.25 \text{ Am}^2\text{kg}^{-1}$  for  $\Delta T = 30 \text{ K}$  in a applied magnetic field of 1 T. The value of  $T_C$  can continuously be adjusted in the near room temperature range between 305 and 406 K by the Si/P ratio. Although the compounds are not competitive for magnetic cooling due to their lower value of  $|\Delta S_M|$  (1.35 to  $1.90 \text{ Jkg}^{-1}\text{K}^{-1}$  in a field change of 1 T), the considerable  $\Delta M$  and the continuously adjustable  $T_C$  in the temperature range above room temperature makes them promising candidate materials for magnetocaloric energy harvesting applications.

## References

- [1] C. Forman, I. K. Muritala, R. Pardemann, and B. Meyer, Estimating the global waste heat potential, *Renew. Sust. Energ. Rev.* 57 (2016) 1568.
- [2] G. Schierning, Bring on the heat, *Nat. Energy* 3 (2018) 92.
- [3] M. Araiz, Á. Casi, L. Catalán, Á. Martínez, and D. Astrain, Prospects of wasteheat recovery from a real industry using thermoelectric generators: Economic and power output analysis, *Energy Convers. Manage.* 205 (2020) 112376.
- [4] O.P. Dimitriev, Thermomechanical Energy Converters for Harvesting Thermal Energy: A Review, *J. Renew. Mater.* 11 (2023) 4.
- [5] V. Srivastava, Y. Song, K. Bhatti, and R. D. James, The direct conversion of heat to electricity using multiferroic alloys, *Adv. Energy Mater.* 1 (2011) 97.
- [6] Y. Gao, W. Liu, S. Zhu, Thermoplastic polyolefin elastomer blends for multiple and reversible shape memory polymers, *Ind. Eng. Chem. Res.* 58(42) (2019) 19495.
- [7] G.W. Swift, Thermoacoustic engines, *J. Acoust. Soc. Am.* 84(4) (1988) 1145.
- [8] N. Tesla, Thermo-magnetic motor, U.S. patent 396121A (Jan. 15 1889).
- [9] N. Tesla, Pyromagneto-electric generator, U.S. patent 428057A (May 13 1890).
- [10] E. Brück, O. Tegus, X.W. Li, F.R. de Boer, K.H.J. Buschow, Magnetic refrigeration towards room-temperature applications, *Physica B* 327 (2003) 431.
- [11] O. Tegus, E. Brück, K. H. J. Buschow, F. R. de Boer, Transition-metal-based magnetic refrigerants for room-temperature applications, *Nature* 415 (2002) 150.
- [12] A. Kitanovski, Energy Applications of Magnetocaloric Materials, *Adv. Energy Mater.* 10 (2020) 1903741.
- [13] T. Christiaanse and E. Brück, Proof-of-concept static thermomagnetic generator experimental device, *Metall. Mater. Trans. E* 1 (2013) 36.
- [14] A. Waske, D. Dzekan, K. Sellschopp, D. Berger, A. Stork, K. Nielsch and S. Fähler, Energy harvesting near room temperature using a thermomagnetic generator with a pretzel-like magnetic flux topology, *Nat. Energy* 4 (2019) 68.
- [15] V.K. Pecharsky and K.A. Gschneidner, Jr., Giant Magnetocaloric Effect in  $Gd_5(Si_2Ge_2)$ , *Phys. Rev. Lett.* 78 (1997) 4494.
- [16] L. Morellon, J. Blasco, P.A. Algarabel, M.R. Ibarra, Nature of the first-order antiferromagnetic-ferromagnetic transition in the Ge-rich magnetocaloric compounds  $Gd_5(Si_xGe_{1-x})_4$ , *Phys. Rev. B* 62 (2000) 1022.
- [17] A.O. Pecharsky, K.A. Gschneidner Jr., V.K. Pecharsky, C.E. Schindler, The room temperature metastable/stable phase relationships in the pseudo-binary  $Gd_5Si_4$ - $Gd_5Ge_4$  system, *J. Alloys Comp.* 338 (2002) 126.
- [18] Y. Mozharivskyj, A.O. Pecharsky, V.K. Pecharsky, G.J. Miller, On the High-Temperature Phase Transition of  $Gd_5Si_2Ge_2$ , *J. Am. Chem. Soc.* 127 (2005) 317.
- [19] L. Morellon, P.A. Algarabel, M.R. Ibarra, J. Blasco, and B. Garcia-Landa, Magnetic-field-induced structural phase transition in  $Gd_5(Si_{1.8}Ge_{2.2})$ , *Phys. Rev. B* 58 (1998) R14721.

- [20] N.T. Trung, Z.Q. Ou, T.J. Gortenmulder, O. Tegus, K.H.J. Buschow, E. Brück, Tunable thermal hysteresis in  $MnFe(P,Ge)$  compounds, *J. Appl. Phys.* 99 (2006) 08Q107.
- [21] H. Yibole, F. Guillou, Y.K. Huang, G.R. Blake, A.J.E. Lefering, N.H. van Dijk, E. Brück, First-order ferromagnetic transition in single-crystalline  $(Mn,Fe)_2(P,Si)$ , *Appl. Phys. Lett.* 107 (2015) 162403.
- [22] Z.Q. Ou, L. Zhang, N.H. Dung, L. van Eijck, A.M. Mulders, M. Avdeev, N.H. van Dijk, E. Brück, Neutron diffraction study on the magnetic structure of  $Fe_2P$ -based  $Mn_{0.66}Fe_{1.29}P_{1-x}Si_x$  melt-spun ribbons, *J. Magn. Magn. Mater.* 340 (2013) 80.
- [23] X.F. Miao, L. Caron, J. Cedervall, P.C.M. Gubbens, P. Dalmas de Réotier, A. Yaouanc, F. Qian, A.R. Wildes, H. Luetkens, A. Amato, N.H. van Dijk, E. Brück, Short-range magnetic correlations and spin dynamics in the paramagnetic regime of  $(Mn,Fe)_2(P,Si)$ , *Phys. Rev. B* 94 (2016) 014426.
- [24] F. Guillou, S. Liting, O. Haschuloo, Z.Q. Ou, E. Brück, O. Tegus, H. Yibole, Room temperature magnetic anisotropy in  $Fe_2P$ -type transition metal based alloys, *J. Alloys Comp.* 800 (2019) 403.
- [25] F.X. Hu, X.L. Qian, J.R. Sun, G.J. Wang, X.X. Zhang, Z.H. Cheng and B.G. Shen, Magnetic entropy change and its temperature variation in compounds  $La(Fe_{1-x}Co_x)_{11.2}Si_{1.8}$ , *J. Appl. Phys.* 92 (2002) 3620.
- [26] Y.F. Chen, F. Wang, B.G. Shen, F.X. Hu, J.R. Sun, G.J. Wang, Z.H. Cheng, Magnetic properties and magnetic entropy change of  $LaFe_{11.5}Si_{1.5}H_y$  interstitial compounds, *J. Phys.: Condens. Matter* 15 (2003) L161.
- [27] S.A. Nikitin, G. Myalikgulyev, A.M. Tishin, M.P. Annaorazov, K.A. Asatryan, A.L. Tyurin, The magnetocaloric effect in  $Fe_{49}Rh_{51}$  compound, *Phys. Lett. A* 148(6-7) (1990) 363.
- [28] M.P. Annaorazov, K.A. Asatryan, G. Myalikgulyev, S.A. Nikitin, A.M. Tishin, A.L. Tyurin, Alloys of the Fe-Rh system as a new class of working material for magnetic refrigerators, *Cryogenics* 32 (1992) 867.
- [29] F.X. Hu, B.G. Shen, J.R. Sun, Magnetic entropy change in  $Ni_{51.5}Mn_{22.7}Ga_{25.8}$  alloy, *Appl. Phys. Lett.* 76 (2000) 3460.
- [30] M. Pasquale, C.P. Sasso, L.H. Lewis, L. Giudici, T. Lograsso, D. Schlagel, Magnetostructural transition and magnetocaloric effect in  $Ni_{55}Mn_{20}Ga_{25}$  single crystals, *Phys. Rev. B* 72 (2005) 094435.
- [31] J. Marcos, L. Mañosa, A. Planes, Multiscale origin of the magnetocaloric effect in Ni-Mn-Ga shape-memory alloys, *Phys. Rev. B* 68 (2003) 094401.
- [32] B. Aronsson, G. Lundgren, X-Ray investigations on Me-Si-B System I, *Acta Chemica Scandinavica* 13 (1959) 433.
- [33] B. Aronsson, I. Engström, X-Ray investigations on Me-Si-B System II, *Acta Chemica Scandinavica* 14 (1960) 1403.

- [34] S. Rundqvist, X-Ray investigations of the Ternary System Fe-P-B. Some Feature of the Systems Cr-P-B, Mn-P-B, Co-P-B and Ni-P-B, *Acta Chemica Scandinavica* 16 (1962) 1.
- [35] R. Wäppling, T. Ericsson, L. Häggström, Y. Andersson, Magnetic Properties of  $Fe_5SiB_2$  and related compounds, *J. Physique Colloques* C6 (1976) 591.
- [36] L. Häggström, R. Wäppling, T. Ericsson, Mössbauer and X-Ray Studies of  $Fe_5PB_2$ , *J. Solid State Chem.* 13 (1976) 84.
- [37] D.M. de Almeida, C. Bormio-Nunes, C.A. Nunes, A.A. Coelho, G.C. Coelho, Magnetic characterization of  $Mn_5SiB_2$  and  $Mn_5Si_3$  phases, *J. Magn. Magn. Mater.* 321 (2009) 2578.
- [38] Z.G. Xie, D.Y. Geng, Z.D. Zhang, Reversible room-temperature magnetocaloric effect in  $Mn_5PB_2$ , *Appl. Phys. Lett.* 97 (2010) 202504.
- [39] M.A. McGuire, D.S. Parker, Magnetic and structural properties of ferromagnetic  $Fe_5PB_2$  and  $Fe_5SiB_2$  and effects of Co and Mn substitutions, *J. Appl. Phys.* 118 (2015) 163903.
- [40] M. Werwiński, Magnetic properties of  $Fe_5SiB_2$  and its alloys with P, S, and Co, *Phys. Rev. B* 93 (2016) 174412.
- [41] D. Hedlund, J. Cedervall, A. Edström, M. Werwiński, S. Kontos, O. Eriksson, J. Ruzs, P. Svedlindh, M. Sahlberg, K. Gunnarsson, Magnetic properties of the  $Fe_5SiB_2$ – $Fe_5PB_2$  system, *Phys. Rev. B* 96 (2017) 094433.
- [42] M. Werwiński, Magnetocrystalline anisotropy of  $Fe_5PB_2$  and its alloys with Co and 5d elements: A combined first-principles and experimental study, *Phys. Rev. B* 98 (2018) 214431.
- [43] J. Cedervall, E. Nonnet, D. Hedlund, L. Häggström, T. Ericsson, M. Werwiński, A. Edström, J. Ruzs, P. Svedlindh, K. Gunnarsson, M. Sahlberg, Influence of Cobalt Substitution on the Magnetic Properties of  $Fe_5PB_2$ , *Inorg. Chem.* 57 (2018) 777.
- [44] J. Thakur, P. Rani, M. Tomar, V. Gupta, H.S. Saini, M.K. Kashyap, Tailoring in-plane magnetocrystalline anisotropy of  $Fe_5SiB_2$  with Cr-substitution, *AIP Conf. Proc.* 2115 (2019) 030506.
- [45] T. Ericsson, L. Häggström, R. Wäppling, Spin Rotation in  $Fe_5SiB_2$ , *Phys. Scr.* 17 (1978) 83.
- [46] J. Cedervall, S. Kontos, T.C.Hansen, O. Balmes, F.J. Martinez-Casado, Z. Matej, P. Beran, P. Svedlindh, K. Gunnarsson, M. Sahlberg, Magnetostructural transition in  $Fe_5SiB_2$  observed with neutron diffraction, *J. Solid State Chem.* 235 (2016) 113.
- [47] L. van Eijck, L.D. Cussen, G.J. Sykora, E.M. Schooneveld, N.J. Rhodes, A.A. van Well, C. Pappas, Design and performance of a novel neutron powder diffractometer: PEARL at TU Delft, *J. Appl. Cryst.* 49 (2016) 1398.
- [48] H.M. Rietveld, A profile refinement method for nuclear and magnetic structures. *J. Appl. Cryst.* 2 (1969) 65.

- [49] J. Rodriguez-Carvajal, Recent advances in magnetic-structure determination by neutron powder diffraction, *Physica B* 192 (1993) 55.
- [50] J.R. de Laeter, J.K. Böhlke, P. de Bièvre, H. Hidaka, H.S. Peiser, K.J.R. Rosman, P.D.P. Tayler, Atomic weights of the elements: Review 2000 (IUPAC Technical Report), *Pure Appl. Chem.* 75 (2003) 683.
- [51] K. Lefmann, Neutron Scattering: Theory, Instrumentation, and Simulation, Niels Bohr Institute, University of Copenhagen. (2007).
- [52] D. Dzekan, A. Waske, K. Nielsch and S. Fähler, Efficient and affordable thermomagnetic materials for harvesting low grade waste heat, *APL Mater.* 9 (2021) 011105.
- [53] V.K. Pecharsky and K.A. Gschneidner. Some common misconceptions concerning magnetic refrigerant materials. *J. Appl. Phys.* 90 (2001) 4614.
- [54] J.Y. Law, V. Franco, L.M. Moreno-Ramírez, A. Conde, D.Y. Karpenkov, I. Radulov, K.P. Skokov, O. Gutfleisch, A quantitative criterion for determining the order of magnetic phase transitions using the magnetocaloric effect, *Nature Comm.* 9 (2018) 2680.
- [55] C.P. Bean and D.S. Rodbell, Magnetic disorder as a first-order phase transformation, *Phys. Rev.* 126 (1962) 104.
- [56] N.H. van Dijk, Landau model evaluation of the magnetic entropy change in magnetocaloric materials, *J. Magn. Magn. Mater.* 529 (2021) 167871.
- [57] L.D. Landau, On the theory of phase transitions. I., *Zh. Eksp. Teor. Fiz.* 7 (1937) 19.
- [58] Y.Z. Song, N. Shi, S.Q. Deng, X.R. Xing, J. Chen, Negative thermal expansion in magnetic materials, *Prog. Mater. Sci.* 121 (2021) 100835.
- [59] Y. Song, Q. Sun, M. Xu, J. Zhang, Y. Hao, Y. Qiao, S. Zhang, Q. Huang, X. Xing, J. Chen, Negative thermal expansion in (Sc,Ti)Fe<sub>2</sub> induced by an unconventional magnetovolume effect, *Mater. Horiz.* 7 (2020) 275.
- [60] A.S. Wills, A new protocol for the determination of magnetic structures using simulated annealing and representational analysis (SARAh), *Physica B* 276-278 (2000) 680.



# Chapter 5

## Effect of Cr doping on the Magnetocaloric Properties of $Mn_5(Si,P)B_2$ Compounds

### 5.1 Introduction

In many material systems, the introduction of new elements plays a key role in the control over the structure and physical properties of the materials. For example, Trung *et al.* used Cr to substitute Mn in the MnCoGe compound and obtained a large magnetic entropy change [1]. In the  $(Mn,Fe)_2(P,Si)$  material system Mn-rich and Fe-rich compounds with different Mn/Fe ratios exhibited completely different magnetocaloric properties [2-5]. In Chapter 4, the effect of changes in the Si/P ratio in  $Mn_5(Si,P)B_2$  compounds on the lattice structure, phase composition, and magnetocaloric properties was discussed. It was shown that the Curie temperature  $T_C$  of  $Mn_5(Si,P)B_2$  compounds can continuously be adjusted from 305 to 406 K, where for all compositions a considerable magnetocaloric effect was observed. In the  $M_5XB_2$  ( $M = Fe, Mn, Co, V, Cr$  and  $X = Si, P, S$ ) materials system, the Fe and Mn compounds have been studied intensively. It was found that the Curie temperature and saturation magnetization of the  $Fe_5(Si,P)B_2$  compounds are higher than that of the  $Mn_5(Si,P)B_2$  compounds. Wäppling and colleagues reported that the Curie temperature of  $Fe_5SiB_2$  and  $Fe_5PB_2$  were 784 and 628 K, respectively [6]. For  $Mn_5SiB_2$  and  $Mn_5PB_2$  the reported Curie temperatures were 411 and 312 K, respectively [7-9]. For other 3d metals, McGuire and Parker reported that Co doping reduced the Curie temperature and saturation magnetization of  $Fe_5SiB_2$  and  $Fe_5PB_2$  compounds [10]. It can be seen that different 3d elements greatly influence the magnetic properties of the  $M_5XB_2$  compounds. Earlier studies on the influence of Cr and Co doping on the  $M_5XB_2$  materials system by DFT calculations focused on the  $Fe_5(Si,P)B_2$  compounds, as these may lead to permanent magnet materials [11-13]. However, no studies have been done on doping of 3d elements in the  $Mn_5(Si,P)B_2$  compounds. With near room-temperature applications in mind, in this chapter the effect

of Cr doping on the structure and the magnetic properties of Mn<sub>5</sub>(Si,P)B<sub>2</sub> compounds has been studied.

## **5.2 Experimental methods**

The Mn<sub>5-x</sub>Cr<sub>x</sub>PB<sub>2</sub> and Mn<sub>5-x</sub>Cr<sub>x</sub>SiB<sub>2</sub> ( $0 \leq x \leq 1$ ) alloys were prepared by high-energy ball milling of the starting materials Mn (99.6% purity), Cr(99.4% purity), MnP (96.08% purity), Si (99+% purity) and B (99.4% purity) in a stainless steel jar rotating at a speed of 350 rpm for 10 hours. For the Mn<sub>5-x</sub>Cr<sub>x</sub>P<sup>11</sup>B<sub>2</sub> ( $x = 0.0, 0.1, 0.3$  and  $0.5$ ) and Mn<sub>4.5</sub>Cr<sub>0.5</sub>Si<sup>11</sup>B<sub>2</sub> compounds studied in the neutron diffraction (ND) experiments, <sup>11</sup>B was used as a starting material instead of natural B. A SQUID magnetometer (Quantum Design MPMS) was employed for magnetic measurements in the temperature range of 5 to 370 K. The magnetic measurements in the temperature range of 315 to 650 K were performed in a VersaLab vibrating-sample magnetometer (VSM) with an oven function. The XRD patterns were collected at room temperature with a PANalytical X-Pert PRO using Cu-K<sub>α</sub> radiation. ND measurements were carried out on the neutron powder diffractometer PEARL at the research reactor of the TU Delft [14] at temperatures of 80 and 530 K. The lattice and magnetic structure refinements were carried out using the Rietveld method [15] and the Fullprof software [16].

## **5.3. Results and discussion**

### **5.3.1 Crystalline structure**

The room-temperature XRD diffraction patterns of the Mn<sub>5-x</sub>Cr<sub>x</sub>PB<sub>2</sub> and Mn<sub>5-x</sub>Cr<sub>x</sub>SiB<sub>2</sub> ( $0 \leq x \leq 1$ ) compounds are shown in Fig. 5.1(a) and (b). Cr doping does not significantly affect the phase composition of the compound. The main phase of all Cr doped samples still crystallizes in the Cr<sub>5</sub>B<sub>3</sub>-type tetragonal structure (as shown in Fig.4.2(d) in Chapter 4), no new impurity was found in the XRD patterns of the Mn<sub>5-x</sub>Cr<sub>x</sub>PB<sub>2</sub> and Mn<sub>5-x</sub>Cr<sub>x</sub>SiB<sub>2</sub> ( $0 \leq x \leq 1$ ) compounds and the content of the Mn<sub>2</sub>P impurity phase shows no obvious dependence on the Cr content in the Mn<sub>5-x</sub>Cr<sub>x</sub>PB<sub>2</sub> compounds, as shown in Fig. 5.1(c). The lattice parameters  $a$  and  $c$ ,  $c/a$  ratio and unit-cell volume  $V$  obtained from room-temperature XRD refinements of Mn<sub>5-x</sub>Cr<sub>x</sub>PB<sub>2</sub> and Mn<sub>5-x</sub>Cr<sub>x</sub>SiB<sub>2</sub> ( $0 \leq x \leq 1$ ) compounds are shown in Fig. 5.2. Compared with the Mn<sub>5-x</sub>Cr<sub>x</sub>SiB<sub>2</sub>, the Mn<sub>5-x</sub>Cr<sub>x</sub>PB<sub>2</sub> compounds show a different dependence on the Cr content. As shown in Fig. 5.2 (a) and (b) the lattice parameter  $a$  gradually increases with Cr content, while there is no significant change in  $c$ , leading to a decrease in the  $c/a$  ratio. Although Cr in the metallic state is generally considered to be smaller than Mn, the dependence of lattice parameters  $a$  and  $c$  on the Cr content leads to an increase in unit-

## Chapter 5 Effect of Cr doping on the Magnetocaloric Properties of $\text{Mn}_5(\text{Si,P})\text{B}_2$ Compound

cell volume  $V$  with Cr content. For the  $\text{Mn}_{5-x}\text{Cr}_x\text{SiB}_2$  compounds, the unit-cell volume  $V$  from a room-temperature XRD refinement shows no monotonous dependence on the Cr content: it decreases in the range of  $0.0 \leq x \leq 0.5$  and increases for  $x = 1$ . This phenomenon will be discussed in the next section on magnetic properties. The  $c/a$  ratio of the  $\text{Mn}_{5-x}\text{Cr}_x\text{SiB}_2$  and  $\text{Mn}_{5-x}\text{Cr}_x\text{PB}_2$  compounds show a similar gradual reduction with the Cr content.

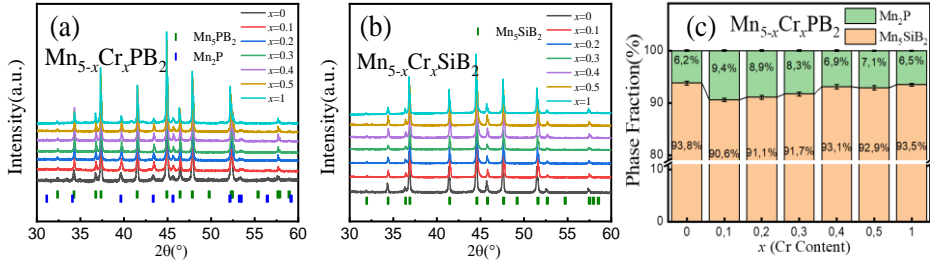


**Fig. 5.1** Room-temperature XRD patterns of (a)  $\text{Mn}_{5-x}\text{Cr}_x\text{PB}_2$  and (b)  $\text{Mn}_{5-x}\text{Cr}_x\text{SiB}_2$  ( $0 \leq x \leq 1$ ) compounds. (c) Phase concentration of the  $\text{Mn}_{5-x}\text{Cr}_x\text{PB}_2$  ( $0 \leq x \leq 1$ ) compounds.

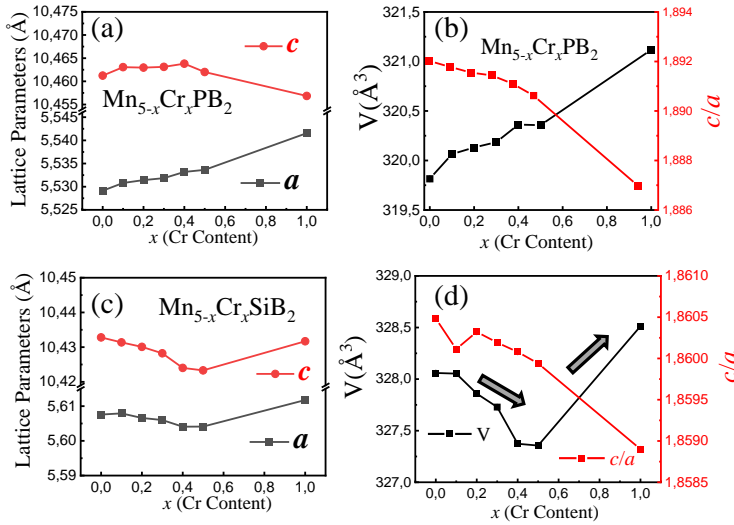


**Fig. 5.2** (a) Lattice parameters  $a$  and  $c$  of the  $\text{Mn}_{5-x}\text{Cr}_x\text{PB}_2$  ( $0 \leq x \leq 1$ ) compounds. (b) Unit-cell volume  $V$  and the  $c/a$  ratio of the  $\text{Mn}_{5-x}\text{Cr}_x\text{PB}_2$  ( $0 \leq x \leq 1$ ) compounds. (c) Lattice parameters  $a$  and  $c$  of the  $\text{Mn}_{5-x}\text{Cr}_x\text{SiB}_2$  ( $0 \leq x \leq 1$ ). (d) Unit-cell volume  $V$  and  $c/a$  ratio of the  $\text{Mn}_{5-x}\text{Cr}_x\text{SiB}_2$  ( $0 \leq x \leq 1$ ) compounds.

### 5.3.2 Magnetocaloric effect

The field-dependent magnetization for the Mn<sub>5-x</sub>Cr<sub>x</sub>PB<sub>2</sub> and Mn<sub>5-x</sub>Cr<sub>x</sub>SiB<sub>2</sub> ( $0 \leq x \leq 1$ ) compounds at a temperature of 5 K is shown in Fig. 5.3(a) and (b) for magnetic fields up to 5 T. The magnetization curves of all Cr doped compounds show ferromagnetic characteristics. As shown in Fig. 5.3 (c) the saturation magnetisation  $M_S$  of the compounds gradually decreases with the introduction of Cr. The decrease in  $M_S$  caused by the introduction of each 10 at.% Cr was 11.6 and 11.3 Am<sup>2</sup>kg<sup>-1</sup>, for the Si- and P compounds, respectively. Fig. 5.3(d) and (e) show the temperature-dependent magnetization curve of the Mn<sub>5-x</sub>Cr<sub>x</sub>PB<sub>2</sub> and Mn<sub>5-x</sub>Cr<sub>x</sub>SiB<sub>2</sub> ( $0 \leq x \leq 1$ ) compounds in a magnetic field of 1 T. The compounds undergo a FM-PM transition upon heating. The transition temperature  $T_C$  gradually shifts to lower temperatures with increasing Cr content. The effect of Cr doping on the Curie temperature of the two groups of compounds is almost the same:  $dT_C/dx \approx 5.4\text{-}5.7$  K/at.% Cr. The decrease of  $M_S$  and  $T_C$  indicates that the magnetic coupling and total magnetic moment of the compounds decreases with Cr doping. In the structural analysis of the previous section, we found that the introduction of Cr leads to the expansion of the lattice, which directly affects the distance between the magnetic ions. Moreover, because Cr has different electronic properties than Mn, it affects the density of electron states near the Fermi level, leading to a decrease in the magnetic moments, resulting in a reduction in  $M_S$  and  $T_C$ . The unit-cell volume  $V$  of the Mn<sub>5-x</sub>Cr<sub>x</sub>SiB<sub>2</sub> compounds shows a completely different trend in comparison with the Mn<sub>5-x</sub>Cr<sub>x</sub>PB<sub>2</sub> compounds in the compositional range of  $x = 0.1 - 0.5$ . The unit-cell volume of the Mn<sub>5-x</sub>Cr<sub>x</sub>PB<sub>2</sub> compounds increases with the Cr content, while for Mn<sub>5-x</sub>Cr<sub>x</sub>SiB<sub>2</sub> it decreases. The negative thermal expansion effect of the Mn<sub>5</sub>SiB<sub>2</sub> compound near  $T_C$  (mentioned in Chapter 4) plays an important role here. The  $T_C$  of the Mn<sub>5-x</sub>Cr<sub>x</sub>PB<sub>2</sub> compounds are around and below room temperature (194 - 305 K). The XRD measurements were carried out in the paramagnetic state of these compounds, and the negative thermal expansion of the compounds did therefore have almost no influence. For the Mn<sub>5-x</sub>Cr<sub>x</sub>SiB<sub>2</sub> compounds, all the  $T_C$  values are above room temperature. The negative thermal expansion effect may in this case be larger than the effect of Cr doping. These conjectures can also explain why the unit-cell volume of the Mn<sub>4</sub>CrSiB<sub>2</sub> compound with a  $T_C$  of 291 K is larger than that of the mother compound.

The calculated isothermal magnetic entropy change in a magnetic field change of 1 T is shown in Fig. 5.4(a) and (b). Introducing Cr reduces the maximum isothermal magnetic entropy changes  $|\Delta S_{M, \max}|$ . As shown in Fig. 5.4(c), for Si-based and P-based compounds  $|\Delta S_{M, \max}|$  decreased from 1.90 ( $x = 0$ ) and 1.35 ( $x = 0$ ) to 0.88 ( $x = 1$ ) and 0.89 ( $x = 1$ ) Jkg<sup>-1</sup>K<sup>-1</sup>, respectively. The Cr doping has a larger effect on the  $|\Delta S_{M, \max}|$  of the Si-based compounds than on the P-based compounds. The change caused by 10 at.%

of Cr on the Si and P based compounds is 0.51 and 0.24 Jkg<sup>-1</sup>K<sup>-1</sup>, respectively. It is worth to note that the Full Width at Half Maximum (FWHM) of the isothermal magnetic entropy change curve  $|\Delta S_M|$ - $T$  of the compounds (obtained by Gaussian fitting) tends to be widened by Cr doping, as shown in Fig. 5.4(d). Compared with the FOMT materials, the  $|\Delta S_M|$ - $T$  curves of the SOMT materials have in most cases a larger FWHM. Therefore, it can be inferred that the SOMT characteristics of the compounds seem to be enhanced with the Cr content.

In order to further analyse the effect of Cr doping on the phase transition in these compounds, the field exponent for the magnetic entropy change  $n = \frac{d \ln(|\Delta S_M|)}{d \ln(H)}$  [17, 18] is analysed. The results are shown in Fig. 5.5(a) and (b). As described in Section 2.2.2, the field exponent  $n$  of a SOMT material gradually approaches without divergence a value of 2 above the transition temperature. As observed in Fig. 5.5(a) and (b), the temperature evolution of  $n$  shows typical SOMT characteristics for these compounds. In addition, we can analyse the phase transition characteristics by the minimum value of  $n$ . Fig. 5.5(c) and (d) show the minimum value of the field exponent  $n_{\min}$  as a function of Cr content. Theoretically, the minimum value of the field exponent  $n_{\min}$  for the FOPT, SOPT, and CP tends to be 0, 2/3, and 2/5, respectively. The  $n_{\min}$  values of the mother compounds without Cr doping are 0.69 and 0.68, which are close to 2/3, conforming that the mother compounds are SOMT materials. In the Cr doped Mn<sub>5-x</sub>Cr<sub>x</sub>PB<sub>2</sub> and Mn<sub>5-x</sub>Cr<sub>x</sub>SiB<sub>2</sub> ( $0 \leq x \leq 1$ ) compounds, the value of  $n_{\min}$  slightly increased with the Cr content, indicating that the compounds remained to have SOPT characteristics with Cr doping.

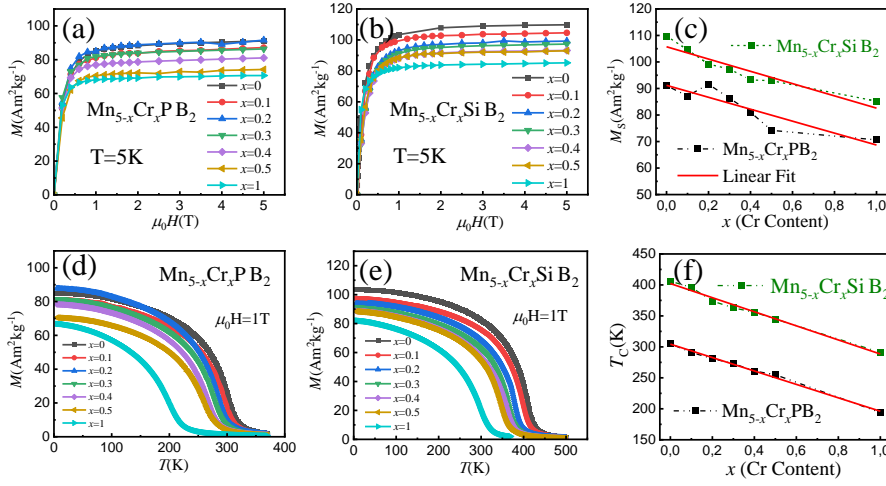


**Fig. 5.3** Field-dependent magnetization of the (a)  $Mn_{5-x}Cr_xPB_2$  and (b)  $Mn_{5-x}Cr_xSiB_2$  ( $0 \leq x \leq 1$ ) compounds at a temperature of 5 K. (c) Saturation magnetization as a function of the Cr content for the  $Mn_{5-x}Cr_xPB_2$  and  $Mn_{5-x}Cr_xSiB_2$  ( $0 \leq x \leq 1$ ) compounds. Temperature-dependent magnetization of the (d)  $Mn_{5-x}Cr_xPB_2$  and (e)  $Mn_{5-x}Cr_xSiB_2$  ( $0 \leq x \leq 1$ ) compounds in a field of 1 T. (f)  $T_C$  as a function of the Cr content for the  $Mn_{5-x}Cr_xPB_2$  and  $Mn_{5-x}Cr_xSiB_2$  ( $0 \leq x \leq 1$ ) compounds.

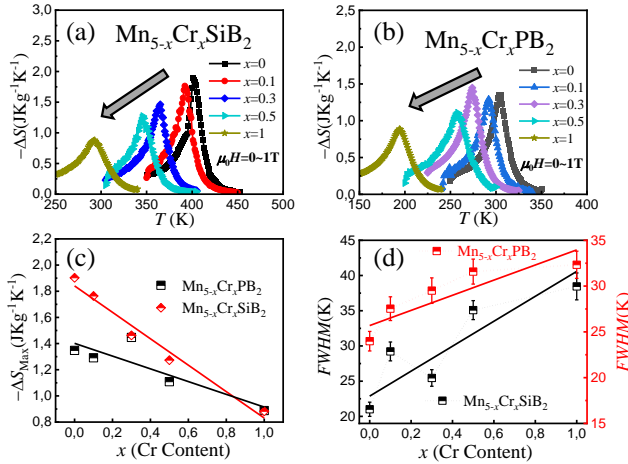


**Fig. 5.4** Isothermal magnetic entropy change  $-\Delta S_M$  as a function of temperature for a field change of 1 T for (a)  $Mn_{5-x}Cr_xPB_2$  and (b)  $Mn_{5-x}Cr_xSiB_2$  ( $x = 0.0, 0.1, 0.3, 0.5$  and  $1.0$ ). (c) Maximum isothermal magnetic entropy change  $-\Delta S_{M,max}$  as a function of the Cr content for the  $Mn_{5-x}Cr_xPB_2$  and  $Mn_{5-x}Cr_xSiB_2$  ( $x = 0.0, 0.1, 0.3, 0.5$  and  $1.0$ ) compounds for a field change of 1 T. (d) Full Width at Half Maximum (FWHM) of the  $|\Delta S_M|$ - $T$  curves in a field change of 1 T for the  $Mn_{5-x}Cr_xPB_2$  and  $Mn_{5-x}Cr_xSiB_2$  ( $x = 0.0, 0.1, 0.3, 0.5$  and  $1.0$ ) compounds.

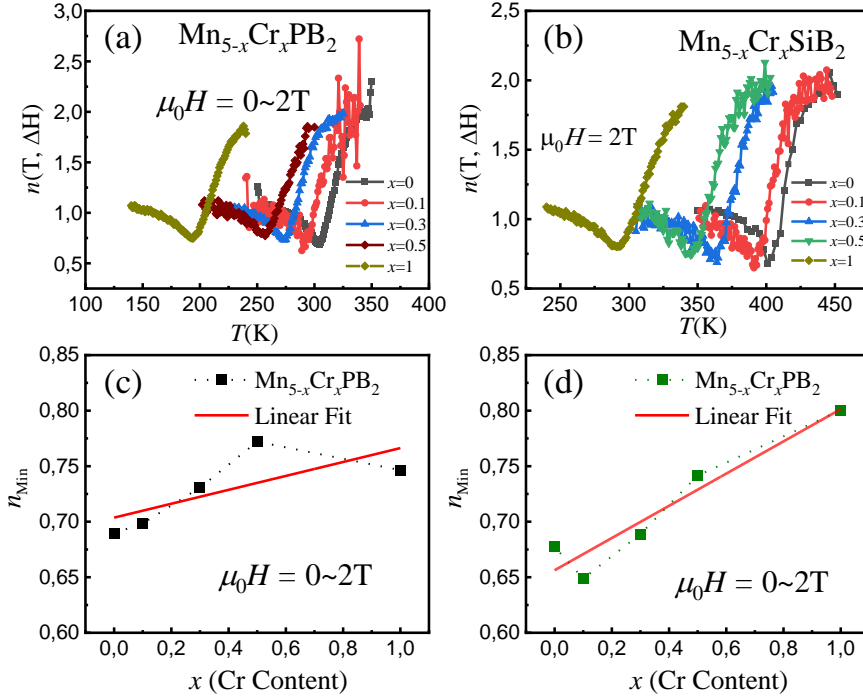


**Fig. 5.5** Field exponent of the magnetic entropy change  $n = \frac{d \ln(\Delta S_m)}{d \ln(H)}$  for the (a)  $Mn_{5-x}Cr_xPB_2$  and (b)  $Mn_{5-x}Cr_xSiB_2$  ( $x = 0.0, 0.1, 0.3, 0.5$  and  $1.0$ ) compounds. Minimum value of the field exponent of the magnetic entropy change  $n$  for the (c)  $Mn_{5-x}Cr_xPB_2$  and (d)  $Mn_{5-x}Cr_xSiB_2$  ( $x = 0.0, 0.1, 0.3, 0.5$  and  $1.0$ ) compounds.

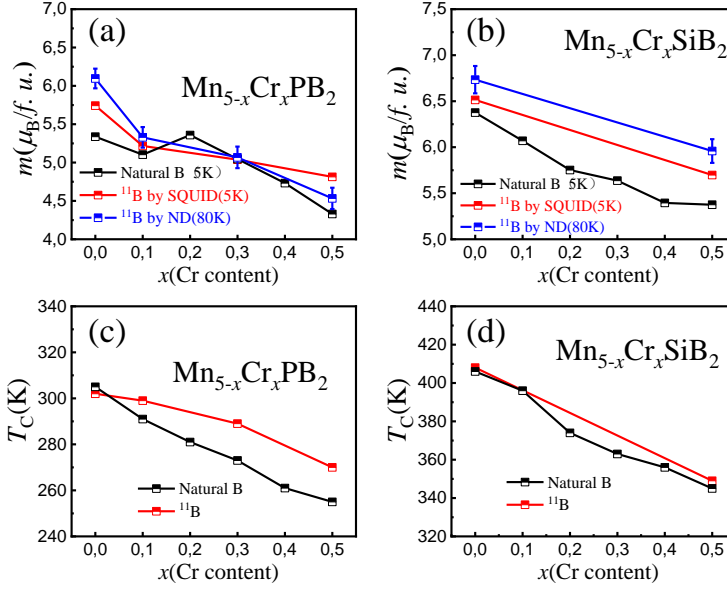
### 5.3.3 Neutron diffraction study

Fig. 5.6 shows the saturation magnetization  $M_s$  and the Curie temperature  $T_C$  of the  $^{11}B$  isotope substituted compounds produced for the neutron diffraction experiments. The  $^{11}B$  containing samples exhibit very similar magnetic properties as the mother compounds: both  $M_s$  and  $T_C$  of the  $Mn_{5-x}Cr_xP^{11}B_2$  ( $x = 0.0, 0.1, 0.3$  and  $0.5$ ) and the  $Mn_{5-x}Cr_xSi^{11}B_2$  ( $x = 0.0$  and  $0.5$ ) compounds decrease with Cr content. The crystal structure refinement of neutron diffraction patterns is in good agreement with the XRD results. The  $^{11}B$  containing compounds crystallize in the  $Cr_5B_3$  structure. In Fig. 5.7 (a) and (b), the  $Mn_{4.5}Cr_{0.5}Si^{11}B_2$  compound was taken as an example to show the neutron diffraction refinements in the paramagnetic state (530 K) and the ferromagnetic state (80 K). Because neutrons are interacting with nuclei of atoms and with the uncompensated magnetic moments of the electrons, neutron diffraction can provide element-specific information about the occupancy and orientation of magnetic moments at specific

crystallographic sites in a crystal. The coherent neutron scattering length  $b_c$  of Mn and Cr is -3.73 and 3.63 fm, respectively. Due to the sign difference neutron diffraction is very sensitive to the Mn/Cr site occupancy.

In our refinements, Cr was assumed to replace Mn at two different magnetic sites, 16l and 4c. The results of the refinement are shown in Fig.5.7 (c), which show that Cr did not randomly replace Mn at the two sites, but prefers to occupy the 16l site. This preferred occupancy was more obvious in the Mn<sub>5-x</sub>Cr<sub>x</sub>P<sup>11</sup>B<sub>2</sub> ( $x = 0.0, 0.1, 0.3$  and  $0.5$ ) compounds. The difference in occupancy in the Mn<sub>4.5</sub>Cr<sub>0.5</sub>Si<sup>11</sup>B<sub>2</sub> compound is not as large as that in the Mn<sub>5-x</sub>Cr<sub>x</sub>P<sup>11</sup>B<sub>2</sub> compounds. In Fig. 5.7 (d) the neutron diffraction patterns of the Mn<sub>4.5</sub>Cr<sub>0.5</sub>Si<sup>11</sup>B<sub>2</sub> compound in the paramagnetic and ferromagnetic states are compared. In the ferromagnetic state, the (123) and (204) diffraction peaks have the most obvious magnetic contribution, which is consistent with the results of the Mn<sub>5</sub>SiB<sub>2</sub> compound in Chapter 4. It can be concluded that Cr has no effect on the magnetic moment orientation in these compounds. The Cr doped compounds were refined with the same magnetic structure as the mother compounds, i.e. the magnetic moments of the two magnetic sites were aligned along the  $a$  axis. The refinement is shown in Fig. 5.7(b). In Fig. 5.6(a) and (b), it can be seen that the total magnetic moment (per formula unit) obtained by neutron diffraction is in good agreement with the SQUID data. The magnetic moments at two magnetic sites 16l and 4c obtained by neutron diffraction of the compounds are shown in Fig. 5.8. For the Mn<sub>5-x</sub>Cr<sub>x</sub>P<sup>11</sup>B<sub>2</sub> compounds the magnetic moment at the 16l site compounds decreased with increasing Cr content, while it has little effect on the moment size at the 4c site (an increase was found however for  $x = 0.5$ ). As mentioned above, as Cr tends to occupy the 16l site, it has a larger effect on the magnetic moment at the 16l site. Since the preference in occupancy in the Mn<sub>4.5</sub>Cr<sub>0.5</sub>Si<sup>11</sup>B<sub>2</sub> compound was lower than in the Mn<sub>5-x</sub>Cr<sub>x</sub>P<sup>11</sup>B<sub>2</sub> compound, this behaviour is not obvious in the Mn<sub>4.5</sub>Cr<sub>0.5</sub>Si<sup>11</sup>B<sub>2</sub> compound. There the magnetic moments at both magnetic sites decreased with Cr.

*Chapter 5 Effect of Cr doping on the Magnetocaloric Properties of  
Mn<sub>5</sub>(Si,P)B<sub>2</sub> Compound*



**Fig. 5.6** Saturation magnetization obtained by neutron diffraction and SQUID magnetization for natural B and  $^{11}\text{B}$  of (a)  $\text{Mn}_{5-x}\text{Cr}_x\text{PB}_2$  and (b)  $\text{Mn}_{5-x}\text{Cr}_x\text{SiB}_2$  compounds.  $T_C$  as a function of Cr content for (c) natural B and (d)  $^{11}\text{B}$  of  $\text{Mn}_{5-x}\text{Cr}_x\text{PB}_2$  and  $\text{Mn}_{5-x}\text{Cr}_x\text{SiB}_2$  compounds.

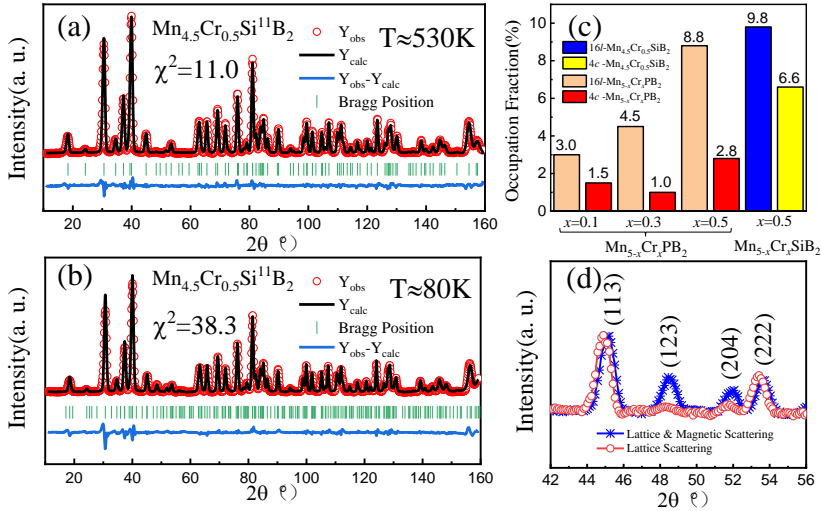


**Fig. 5.7** Neutron diffraction refinements for the  $\text{Mn}_{4.5}\text{Cr}_{0.5}\text{Si}^{11}\text{B}_2$  compound (a) in the paramagnetic state (530 K) and (b) in the ferromagnetic state (80 K). (c) Occupation fraction of Cr on two magnetic sites (16l and 4c) for the  $\text{Mn}_{5-x}\text{Cr}_x\text{P}^{11}\text{B}_2$  ( $x = 0.1, 0.3$  and  $0.5$ ) and  $\text{Mn}_{4.5}\text{Cr}_{0.5}\text{Si}^{11}\text{B}_2$  compounds. (d) Neutron diffraction patterns for the  $\text{Mn}_{4.5}\text{Cr}_{0.5}\text{Si}^{11}\text{B}_2$  compound in the ferromagnetic state (80 K) and in the paramagnetic state (530 K).

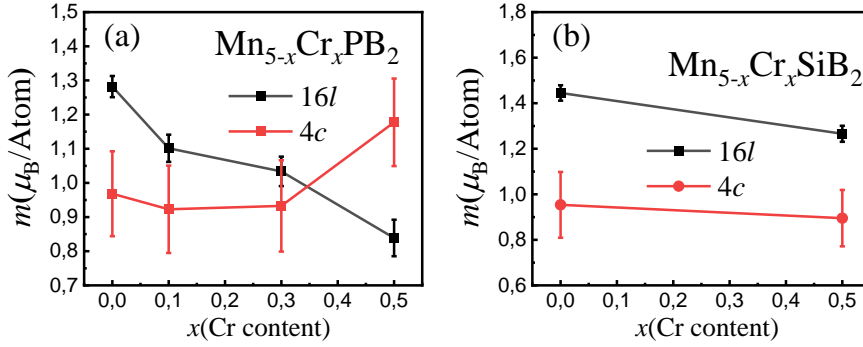


**Fig. 5.8** Magnetic moments at the 16l and 4c sites of (a)  $Mn_{5-x}Cr_xP^{II}B_2$  ( $x = 0.1, 0.3$  and  $0.5$ ) and (b)  $Mn_{5-x}Cr_xSi^{II}B_2$  ( $x = 0.1$  and  $0.5$ ) compounds.

## 5.4 Conclusions

In summary, Cr doping does not affect the phase composition of the compounds. All the Cr doped compounds crystallized in the  $Cr_5B_3$  structure, no new impurity phases were observed in the  $Mn_{5-x}Cr_x(Si,P)B_2$  compounds and the  $Mn_2P$  impurity phase fraction in the  $Mn_{5-x}Cr_xPB_2$  compounds did not show a dependence on the Cr content. The introduction of Cr leads to an unexpected expansion in the lattice of the main phase. This may be due to the more covalent character of the Cr-P bonds compared to the equivalent Cr-Si bonds. The value of  $T_C$  and  $M_S$  decreases with the Cr content. The  $T_C$  of the  $Mn_{5-x}Cr_x(Si, P)B_2$  compounds can continuously be adjusted between 198 and 404 K by Cr doping. Since the lowest Curie temperature of the compounds ( $T_C = 194$  K for  $Mn_4CrPB_2$ ) is far below room temperature, the Cr content was not increased further. All compounds were found to show a SOMT. For  $Mn_{5-x}Cr_xSiB_2$  and  $Mn_{5-x}Cr_xPB_2$  with  $x = 1$  the maximum isothermal magnetic entropy change in a field change of 1 T decreased from 1.90 and 1.35  $Jkg^{-1}K^{-1}$  to 0.88 and 0.89  $Jkg^{-1}K^{-1}$ , respectively. Neutron diffraction results showed that Cr preferentially occupies the 16l site in the crystal lattice. As a consequence, the effect of Cr substitution on the magnetic moment of the 16l site is greater than that of the 4c site. Cr doping has no obvious effect on the magnetic ordering of the compounds. The Cr doped compounds still show ferromagnetic order with the magnetic moments in the  $a$ - $b$  plane.

*Chapter 5 Effect of Cr doping on the Magnetocaloric Properties of  
Mn<sub>5</sub>(Si,P)B<sub>2</sub> Compound*

**References**

- [1] N.T. Trung N, V. Biharie, L. Zhang, L. Caron, K.H.J. Buschow, E. Brück, From single- to double-first-order magnetic phase transition in magnetocaloric Mn<sub>1-x</sub>Ce<sub>x</sub>CoGe compounds, *Appl. Phys. Lett.* 96 (2010) 162507.
- [2] A. Kiecana, C. Kwakernaak, N.H. van Dijk, E. Brück, Effect of the heat treatment on the microstructure, magnetism and magnetocaloric effect in Fe-rich (Mn,Fe)<sub>y</sub>(P,Si) melt-spun ribbons, *J. Alloys Compd.* 932 (2023) 167635.
- [3] X.M. You , M. Maschek, N.H. van Dijk and E. Brück, Magnetic Phase Diagram of the Mn<sub>x</sub>Fe<sub>2-x</sub>P<sub>1-y</sub>Si<sub>y</sub> System, *Entropy MDPI* 2 (2022), 24.
- [4] Z.Q. Ou, L. Zhang, N.H. Dung, L. Caron, E. Brück, Structure, magnetism and magnetocalorics of Fe-rich (Mn,Fe)<sub>1.95</sub>P<sub>1-x</sub>Si<sub>x</sub> melt-spun ribbons, *J. Alloys Compd.* 710 (2017) 446e451.
- [5] Jiawei Lai, Xin Tang, H. Sepehri-Amin, K. Hono, Tuning transition temperature of magnetocaloric Mn<sub>1.8</sub>Fe<sub>0.2</sub>(P<sub>0.59</sub>Si<sub>0.41</sub>)<sub>x</sub> alloys for cryogenic magnetic refrigeration, *Scr. Mater.* 183 (2020) 127.
- [6] R. Wäppling, T. Ericsson, L. Häggström, Y. Andersson, Magnetic Properties of Fe<sub>5</sub>SiB<sub>2</sub> and related compounds, *J. Physique Colloques C6* (1976) 591.
- [7] D.M. de Almeida, C. Bormio-Nunes, C.A. Nunes, A.A. Coelho, G.C. Coelho, Magnetic characterization of Mn<sub>5</sub>SiB<sub>2</sub> and Mn<sub>5</sub>Si<sub>3</sub> phases, *J. Magn. Mater.* 321 (2009) 2578.
- [8] L. Häggström, R. Wäppling, T. Ericsson, Mössbauer and X-Ray Studies of Fe<sub>5</sub>PB<sub>2</sub>, *J. Solid State Chem.* 13 (1976) 84.
- [9] Z.G. Xie, D.Y. Geng, Z.D. Zhang, Reversible room-temperature magnetocaloric effect in Mn<sub>5</sub>PB<sub>2</sub>, *Appl. Phys. Lett.* 97 (2010) 202504.
- [10] M.A. McGuire, D.S. Parker, Magnetic and structural properties of ferromagnetic Fe<sub>5</sub>PB<sub>2</sub> and Fe<sub>5</sub>SiB<sub>2</sub> and effects of Co and Mn substitutions, *J. Appl. Phys.* 118 (2015) 163903.
- [11] M. Werwiński, Magnetic properties of Fe<sub>5</sub>SiB<sub>2</sub> and its alloys with P, S, and Co, *Phys. Rev. B* 93 (2016) 174412.
- [12] M. Werwiński, Magnetocrystalline anisotropy of Fe<sub>5</sub>PB<sub>2</sub> and its alloys with Co and 5d elements: A combined first-principles and experimental study, *Phys. Rev. B* 98 (2018) 214431.
- [13] J. Thakur, P. Rani, M. Tomar, V. Gupta, H.S. Saini, M.K. Kashyap, Tailoring in-plane magnetocrystalline anisotropy of Fe<sub>5</sub>SiB<sub>2</sub> with Cr-substitution, *AIP Conference Proceedings* 2115 (2019) 030506.
- [14] L. van Eijck, L.D. Cussen, G.J. Sykora, E.M. Schooneveld, N.J. Rhodes, A.A. van Well, C. Pappas, Design and performance of a novel neutron powder diffractometer: PEARL at TU Delft, *J. Appl. Cryst.* 49 (2016) 1398.

- [15] H.M. Rietveld, A profile refinement method for nuclear and magnetic structures. J. Appl. Cryst. 2 (1969) 65.
- [16] J. Rodriguez-Carvajal, Recent advances in magnetic-structure determination by neutron powder diffraction, Physica B 192 (1993) 55.
- [17] J.Y. Law, V. Franco, L.M. Moreno-Ramírez, A. Conde, D.Y. Karpenkov, I. Radulov, K.P. Skokov, O.Gutfleisch, A quantitative criterion for determining the order of magnetic phase transitions using the magnetocaloric effect, Nature Comm. 9 (2018) 2680.
- [18] N.H. van Dijk, Landau model evaluation of the magnetic entropy change in magnetocaloric materials, J. Magn. Magn. Mater. 529 (2021) 167871.

# Chapter 6

## Effect of V doping on the Magnetocaloric Properties of

## $Mn_5(Si,P)B_2$ Compounds

### 6.1 Introduction

The  $M_5XB_2$  ( $M = Fe, Mn, Co, V, Cr$  and  $X = Si, P, S$ ) materials system has been studied as a candidate material for permanent magnets, in which the  $Fe_5SiB_2$  and  $Fe_5PB_2$  compounds have received widespread attention due to their high magnetization and high Curie temperature [1-5]. However, the magneto-crystalline anisotropy energy of these compounds is not very strong, resulting in soft-magnetic characteristics, and it is difficult to achieve the magnetic energy product required for use as a permanent magnetic material [6]. Subsequently, people studied the effect of doping different 3d elements on the magnetic properties of  $Fe_5(Si,P)B_2$  compounds [6-9]. It is found that Cr, Mn and Co all reduce the magnetization, and Mn and Co also decrease  $T_C$ , but there is no literature on the effect of Cr on the  $T_C$  of the  $Fe_5(Si,P)B_2$  compounds. In the previous chapter, we discussed the effect of Cr doping on the magnetocaloric properties and structure of  $Mn_5(Si,P)B_2$  compounds. The introduction of Cr not only reduced the magnetization, but also reduced the  $T_C$  of these compounds. Studies on V doping in this system have not yet been published. The only literature that can be found is the analysis of the phase composition of V-Si-B alloys synthesized by arc melting by Reis *et al.* in 2007 [10]. The results showed that it is difficult to form single phase  $V_5SiB_2$  under these experimental conditions for V-Si-B alloys.

In this chapter, we prepared V doped  $Mn_5(Si,P)B_2$  compounds using the same preparation process as the previous two chapters and studied the effect of V doping on the lattice structure, the phase composition and the magnetocaloric properties of the  $Mn_5(Si,P)B_2$  compounds.

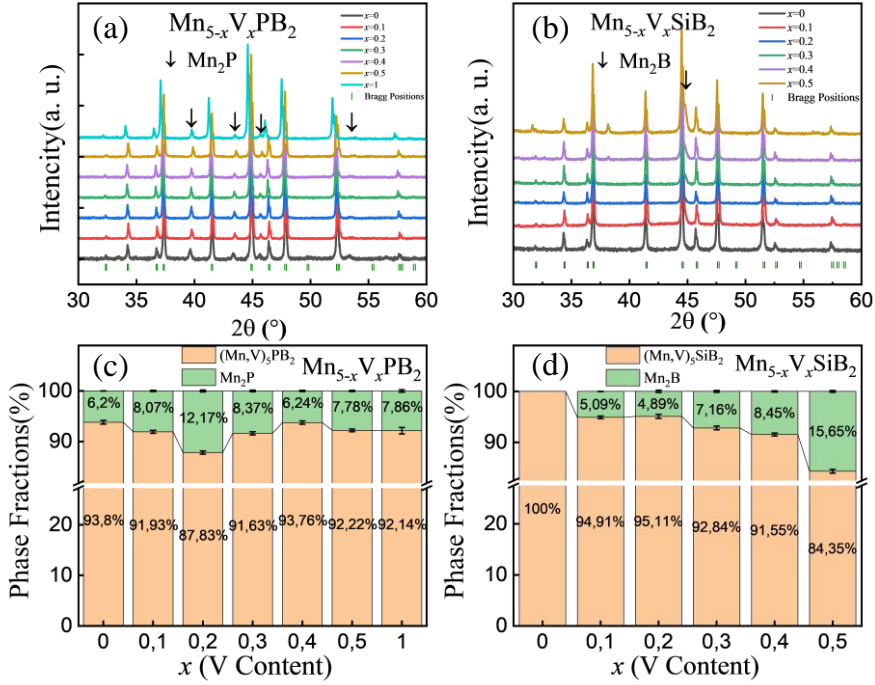
## **6.2 Experimental methods**

Polycrystalline Mn<sub>5-x</sub>V<sub>x</sub>PB<sub>2</sub> ( $0 \leq x \leq 1$ ) and Mn<sub>5-x</sub>V<sub>x</sub>SiB<sub>2</sub> ( $0.0 \leq x \leq 0.5$ ) samples were prepared by ball-milling the starting materials Mn (99.6% purity), V (99.4% purity), MnP (96.08% purity), Si (99+% purity) and B (99.4% purity), as described in Chapter 3. Room-temperature XRD was carried out with a PANalytical X-Pert PRO using Cu-K $\alpha$  radiation. ND measurements were performed on the neutron powder diffractometer PEARL at the research reactor of the TU Delft [11]. The lattice structure and magnetic structure refinements were carried out using the Rietveld method [12] and the Fullprof software [13]. Magnetic measurements were carried out in a superconducting quantum interference device (SQUID) magnetometer (Quantum Design MPMS). The magnetic measurements at a temperature higher than 370 K were performed in a VersaLab vibrating-sample magnetometer (VSM) with an oven function.

## **6.3. Results and discussion**

### **6.3.1 Crystalline structures and phase analysis**

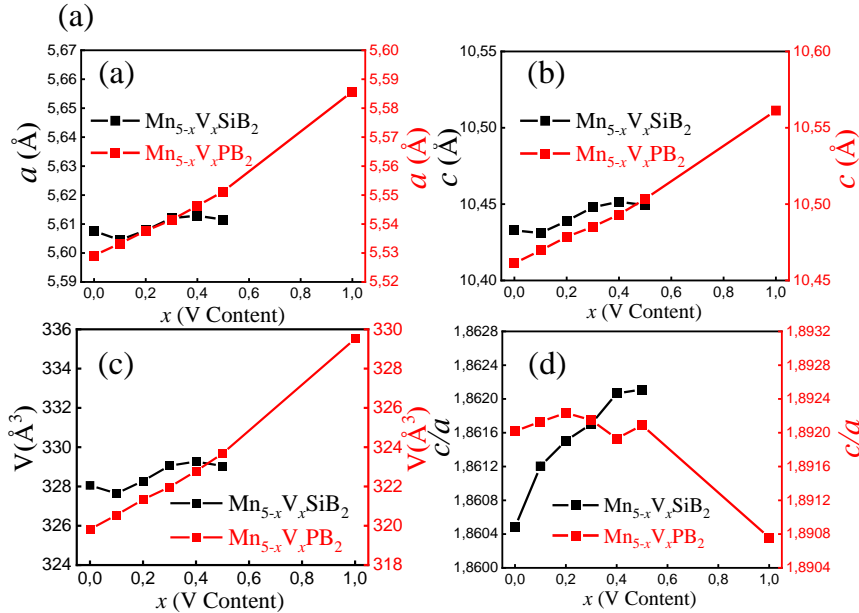
Fig. 6.1(a) and (b) show the room-temperature XRD patterns of Mn<sub>5-x</sub>V<sub>x</sub>PB<sub>2</sub> ( $0 \leq x \leq 1$ ) and Mn<sub>5-x</sub>V<sub>x</sub>SiB<sub>2</sub> ( $0.0 \leq x \leq 0.5$ ) compounds. All the (Mn,V)<sub>5</sub>(SiP)B<sub>2</sub> compounds crystallize into the Cr<sub>5</sub>B<sub>3</sub>-type structure with different contents of Mn<sub>2</sub>P and Mn<sub>2</sub>B as impurity phases. The mother compound Mn<sub>5</sub>PB<sub>2</sub> has been found to contain a small amount of Mn<sub>2</sub>P impurity phase before V doping. The content of the Mn<sub>2</sub>P impurity does not show a significant dependence on the V concentration and remains in the range of 6-12 % for all samples. As shown in Fig. 6.1(c), a stable main phase was formed for the whole range ( $0 \leq x \leq 1$ ) for the Mn<sub>5-x</sub>V<sub>x</sub>PB<sub>2</sub> compounds. For V doping in the Mn<sub>5</sub>SiB<sub>2</sub> compound a new Mn<sub>2</sub>B-type impurity phase is introduced. As can be seen in Fig. 6.1(d) this impurity is quite sensitive to the V content and shows a monotonous increase with the V content, reaching about 16% for  $x = 0.5$ . When 20% of the Mn is replaced by V ( $x = 1$ ), the Mn<sub>4</sub>VSiB<sub>2</sub> compound no longer crystallizes in the Cr<sub>5</sub>B<sub>3</sub> structure.



**Fig. 6.1** XRD patterns of (a)  $Mn_{5-x}V_xPB_2$  ( $0 \leq x \leq 1$ ) and (b)  $Mn_{5-x}V_xSiB_2$  ( $0.0 \leq x \leq 0.5$ ) compounds. The peaks of the  $Mn_2P$  and  $Mn_2B$  impurity phases are indicated by black arrows. Phase fractions of (c)  $Mn_{5-x}V_xPB_2$  ( $0 \leq x \leq 1$ ) and (d)  $Mn_{5-x}V_xSiB_2$  ( $0.0 \leq x \leq 0.5$ ) compounds.

The refined lattice parameters and unit-cell volume of  $Mn_{5-x}V_xPB_2$  ( $0 \leq x \leq 1$ ) and  $Mn_{5-x}V_xSiB_2$  ( $0.0 \leq x \leq 0.5$ ) compounds are shown in Fig. 6.2. The lattice parameters and unit-cell volume  $V$  of the  $Mn_{5-x}V_xPB_2$  compounds increase monotonously with the V content, as the atomic radius of V is larger than Mn [14]. It is worth to note that the  $c/a$  ratio of the  $Mn_{5-x}V_xPB_2$  compounds seems to dependent strongly on the concentration of the  $Mn_2P$  impurity phase. The amount of  $Mn_2P$  phase gradually increases for  $x = 0.0$  to  $0.2$ , leading to an increase of the corresponding  $c/a$  ratio. The  $c/a$  ratio subsequently decreases with decreasing  $Mn_2P$  phase fraction for  $x = 0.3$  to  $0.4$ . The lattice structure of the  $Mn_2P$  type impurity phase has been confirmed, but it is difficult to accurate determine its composition. Assuming that the impurity phase contains only Mn and P, the actual stoichiometric ratio of the mother compound is  $Mn_5P_{0.9}B_{2.1}$ , while the stoichiometric ratio of the V doped sample with  $x = 0.2$  is  $Mn_{4.8}V_{0.22}P_{0.81}B_{2.27}$ . The change in composition of the main phase may lead to a partial replacement of the P at the 4a site by extra B, which may in turn affect the  $c/a$ . Häggström observed a similar

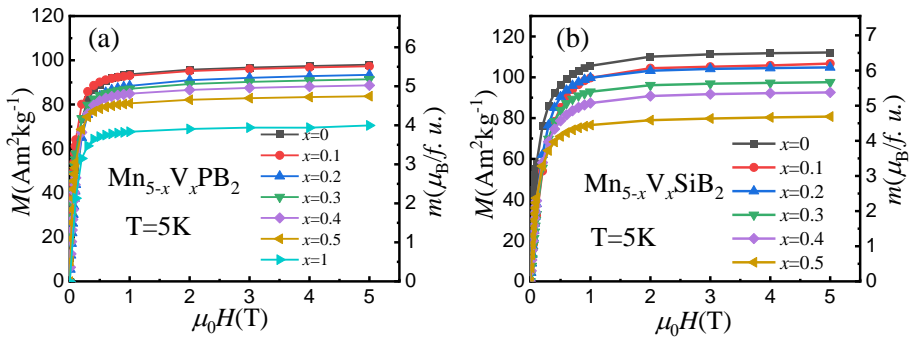
phenomenon in the  $Fe_5PB_2$  compounds, where part of B occupied the 4a site [3]. Since the coherent neutron scattering length  $b_c$  of  $^{11}B$  and P are quite similar, it is difficult to investigate the actual occupation of these two elements within the unit cell by neutron diffraction. The lattice parameters and unit-cell volume of the  $Mn_{5-x}V_xSiB_2$  compounds did not show a monotonously increasing trend. The unit-cell volume of the  $Mn_{4.9}V_{0.1}SiB_2$  compound was slightly smaller than the mother compound, while the unit-cell volume for the  $x = 0.1 - 0.3$  compounds monotonously increased. For  $x = 0.4$  and 0.5 the increase slowed down and even decreased. The unit-cell volume  $V$  strongly depends on the amount of  $Mn_2B$  phase in the  $Mn_{5-x}V_xSiB_2$  compounds. An increase in the  $Mn_2B$  phase fraction leads to a decrease in the unit-cell volume of the main phase. As an example, assuming that the  $Mn_2B$  phase contains only Mn and B, then the main phase composition for the  $x = 0.1$  compound is  $(MnV)_5Si_{1.06}B_{1.97}$ . As the atomic radius of Si is much larger than B, it is difficult to replace B at the 8h site, and the extra Si has a high probability to replace Mn, which leads to a decrease in the unit-cell volume of the main phase.



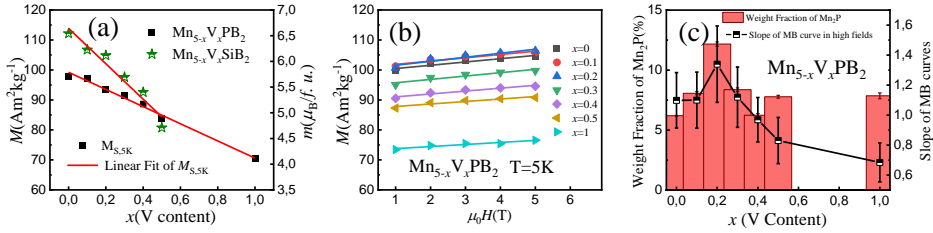
**Fig. 6.2** (a) Lattice parameter  $a$  of  $Mn_{5-x}V_xPB_2$  ( $0 \leq x \leq 1$ ) and  $Mn_{5-x}V_xSiB_2$  ( $0.0 \leq x \leq 0.5$ ) compounds. (b) Lattice parameter  $c$  of  $Mn_{5-x}V_xPB_2$  ( $0 \leq x \leq 1$ ) and  $Mn_{5-x}V_xSiB_2$  ( $0.0 \leq x \leq 0.5$ ) compounds. (c) Unit-cell volume  $V$  of  $Mn_{5-x}V_xPB_2$  ( $0 \leq x \leq 1$ ) and  $Mn_{5-x}V_xSiB_2$  ( $0.0 \leq x \leq 0.5$ ). (d)  $c/a$  ratio of  $Mn_{5-x}V_xPB_2$  ( $0 \leq x \leq 1$ ) and  $Mn_{5-x}V_xSiB_2$  ( $0.0 \leq x \leq 0.5$ ) compounds.

### 6.3.2 Magnetocaloric effect

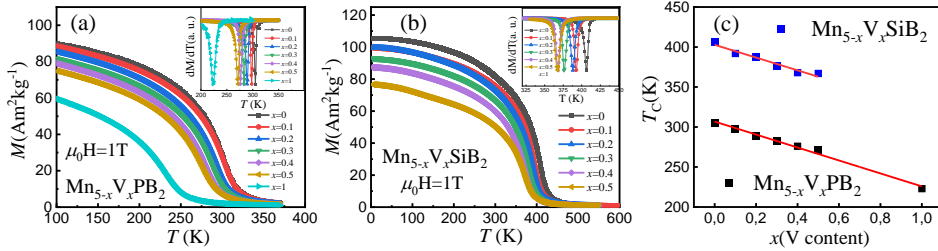
Fig. 6.3 shows the field-dependent magnetization of both series of compounds at 5 K. All samples show typical ferromagnetic characteristics and the magnetization saturates near 1 T. The saturation magnetization  $M_S$  of the compounds decreases with V content, as shown in Fig. 6.4(a). The  $M_S$  of the  $Mn_{5-x}V_xSiB_2$  compounds has a strong dependence on V, and the slope of the linear fit is much larger than for the  $Mn_{5-x}V_xPB_2$  compounds. This is closely related to the  $Mn_2B$  impurity phase in the  $Mn_{5-x}V_xSiB_2$  compounds. As mentioned above, the impurity phase  $Mn_2B$  of the  $Mn_{5-x}V_xSiB_2$  compounds increases with the V content, while V doping has almost no effect on the impurity content of the P compounds. According to the report by Zhou *et al.*,  $Mn_2B$  orders antiferromagnetically [15]. Therefore, an increase in the  $Mn_2B$  phase content must lead to a decrease in the  $M_S$  of the sample. Since the main phase is close to saturation in a field of 1 T, the increase in magnetization at higher fields is attributed to the  $Mn_2B$  phase content. Thus relating the rapid decrease of  $M_S$  for the  $Mn_{5-x}V_xSiB_2$  compounds to the amount of the  $Mn_2B$  phase. Moreover, P samples accompanied by different amount of  $Mn_2P$  impurity phase, and the  $Mn_2P$  phase has a significant impact on the magnetization curve of the sample in the high field (1 to 5 T). Fig. 6.4(b) shows the magnetization curves of the P samples from 1 to 5 T and Fig. 6.4(c) the slope of the high-field magnetization curve together with the  $Mn_2P$  phase fraction as a function of V doping. In Fig. 6.4(c), it can be seen that the slope of the  $M-\mu_0H$  curves at high fields (1 to 5 T) correlates well with the amount of the  $Mn_2P$  phase. According to previous studies on  $Mn_2P$  [16, 17], it has antiferromagnetic ordering, with a Neel temperature of 103 K. The increase in the magnetization of P samples in high field is attributed to antiferromagnetic  $Mn_2P$  impurity.



**Fig. 6.3** Field-dependent magnetization of (a)  $Mn_{5-x}V_xPB_2$  ( $0 \leq x \leq 1$ ) and (b)  $Mn_{5-x}V_xSiB_2$  ( $0.0 \leq x \leq 0.5$ ) compounds at a temperature of 5 K.



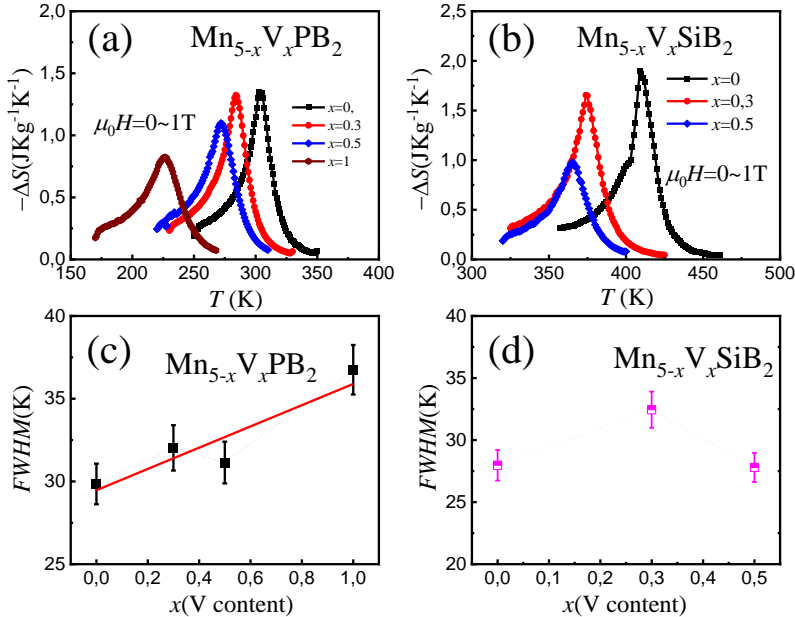
**Fig. 6.4** (a) Saturation magnetization as a function of the V content for the  $Mn_{5-x}V_xPB_2$  ( $0 \leq x \leq 1$ ) and  $Mn_{5-x}V_xSiB_2$  ( $0.0 \leq x \leq 0.5$ ) compounds at a temperature of 5 K. (b) Field-dependent magnetization in applied fields of 1 to 5 T at 5 K. (c) Weight fraction of  $Mn_2P$  in  $Mn_{5-x}V_xPB_2$  ( $x = 0 - 1$ ) and the slope of the  $M$ - $\mu_0 H$  curve in high fields (1 - 5 T).



**Fig. 6.5** Temperature-dependent magnetization of the (a)  $Mn_{5-x}V_xPB_2$  ( $0 \leq x \leq 1$ ) and (b)  $Mn_{5-x}V_xSiB_2$  ( $0.0 \leq x \leq 0.5$ ) compounds in a field of 1 T. The inset shows the normalised first derivative of the low-field  $M$ - $T$  curves in a field of 0.01 T. (c)  $T_C$  as a function of V content  $x$  for the  $Mn_{5-x}V_xPB_2$  ( $0 \leq x \leq 1$ ) and  $Mn_{5-x}V_xSiB_2$  ( $0.0 \leq x \leq 0.5$ ) compounds.

The temperature dependence of the magnetization ( $M$ - $T$ ),  $dM/dT$  and  $T_C$  of the  $Mn_{5-x}V_xPB_2$  ( $0 \leq x \leq 1$ ) and  $Mn_{5-x}V_xSiB_2$  ( $0.0 \leq x \leq 0.5$ ) compounds are shown in Fig. 6.5. The  $T_C$  of both compounds decreases with increasing V content. This dependence of  $T_C$  on V substitution is very similar for both systems. As shown in Fig. 6.5(c), it is found that for each 10 at.% V that is added we find a reduction in  $T_C$  of 40 and 43 K ( $dT_C/dx = -4.0K/at.\%$  and  $-4.3K/at.\%$ ) for the  $Mn_{5-x}V_xPB_2$  and  $Mn_{5-x}V_xSiB_2$  compounds, respectively. The  $T_C$  of the  $Mn_{5-x}V_xPB_2$  compounds decreases to 225 K for  $x = 1$ . Considering that V had almost no effect on the impurity content of the  $Mn_{5-x}V_xPB_2$  compounds, it is expected that compounds with a lower  $T_C$  can be obtained by further increasing the V content.

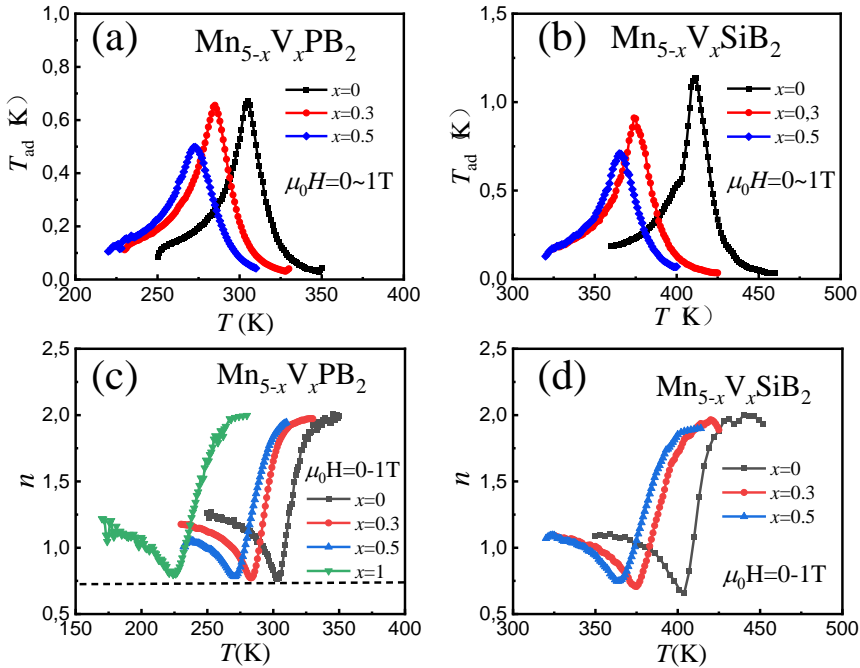
Fig. 6.6(a) and (b) show the calculated isothermal magnetic entropy change  $|\Delta S_M|$  of the Mn<sub>5-x</sub>V<sub>x</sub>PB<sub>2</sub> ( $0 \leq x \leq 1$ ) and Mn<sub>5-x</sub>V<sub>x</sub>SiB<sub>2</sub> ( $0.0 \leq x \leq 0.5$ ) compounds for a magnetic field change of 1 T. The temperature corresponding to the maximum isothermal magnetic entropy change and the maximum isothermal magnetic entropy change  $|\Delta S_{M, \max}|$  decreases with V content. The  $|\Delta S_{M, \max}|$  of the Mn<sub>5-x</sub>V<sub>x</sub>SiB<sub>2</sub> and Mn<sub>5-x</sub>V<sub>x</sub>PB<sub>2</sub> compounds decreases from 1.90 ( $x = 0$ ) and 1.35 ( $x = 0$ ) Jkg<sup>-1</sup>K<sup>-1</sup> to 0.97 ( $x = 0.5$ ) and 0.82 ( $x = 1$ ) Jkg<sup>-1</sup>K<sup>-1</sup>, respectively. The decrease in  $|\Delta S_{M, \max}|$  is expected to be related to an enhancement of the SOPT characteristics induced by V doping. The temperature-dependent magnetic entropy change of a SOPT material generally has a broad peak. We performed a Gaussian fitting on the entropy change curves for a field change of 1 T and analysed the change in the Full Width at Half Maximum (FWHM) as a function of the V content  $x$ . The results are shown in Fig. 6.6(c) and (d). The FWHM of the Mn<sub>5-x</sub>V<sub>x</sub>PB<sub>2</sub> compounds gradually increases with V content, indicating that the introduction of V enhances the SOPT characteristics of the compounds. However, no obvious change was observed in the FWHM data of the Mn<sub>5-x</sub>V<sub>x</sub>SiB<sub>2</sub> compounds.



**Fig. 6.6** Magnetic entropy change  $|\Delta S_M|$  as a function of temperature in a field change of 1 T for (a) Mn<sub>5-x</sub>V<sub>x</sub>PB<sub>2</sub> ( $x = 0.0, 0.3, 0.5$  and  $1.0$ ) and (b) Mn<sub>5-x</sub>V<sub>x</sub>SiB<sub>2</sub> ( $x = 0.0, 0.3$  and  $0.5$ ). Full Width at Half Maximum (FWHM) of the  $|\Delta S_M|$ - $T$  curves in a field change of 1 T for (c) Mn<sub>5-x</sub>V<sub>x</sub>PB<sub>2</sub> ( $x = 0.0, 0.3, 0.5$  and  $1.0$ ) and (d) Mn<sub>5-x</sub>V<sub>x</sub>SiB<sub>2</sub> ( $x = 0.0, 0.3$  and  $0.5$ ).

The adiabatic temperature change  $T_{ad}$  calculated by  $\Delta T_{ad}(T_i, H_f, H_i) \approx -\frac{T_i}{c_H(T_i)} \Delta S(T, H_f, H_i)$  [18] of the  $Mn_{5-x}V_xPB_2$  ( $0 \leq x \leq 1$ ) and  $Mn_{5-x}V_xSiB_2$  ( $0.0 \leq x \leq 0.5$ ) compounds for a change in applied field of 1 T are shown in Fig. 6.7(a) and (b). The  $T_{ad}$  of both the  $Mn_{5-x}V_xPB_2$  and  $Mn_{5-x}V_xSiB_2$  compounds decreased with V content. The  $T_{ad}$  of the  $Mn_{5-x}V_xPB_2$  and  $Mn_{5-x}V_xSiB_2$  compounds decreased from 0.67 and 1.14 K to 0.50 and 0.71 K, respectively.

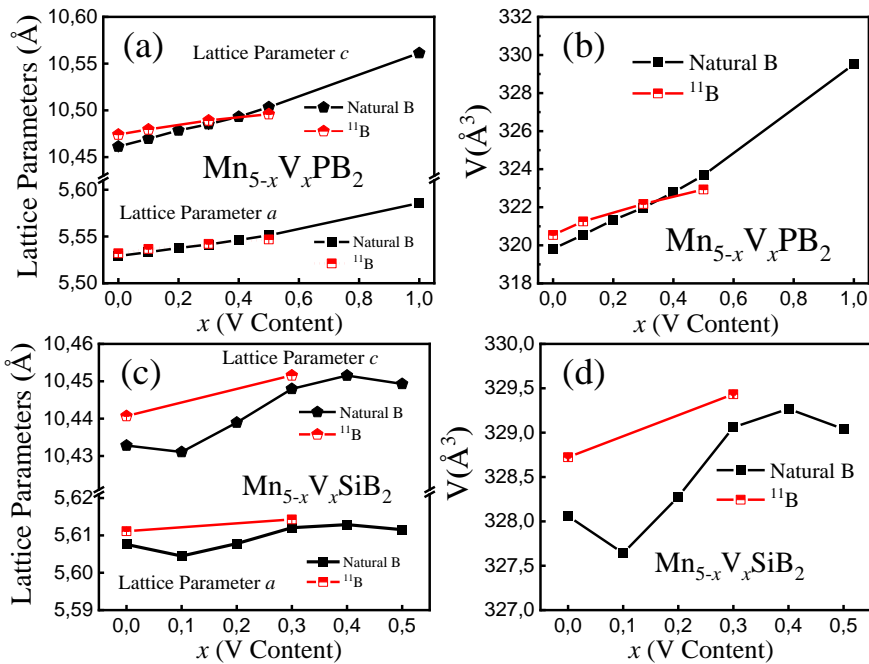
In order to do a quantitative analysis of the effect of V doping on the type of phase transition, we calculated the field exponent for the magnetic entropy change  $n = \frac{d \ln(|\Delta S_m|)}{d \ln(H)}$ . The results are shown in Fig. 6.7 (c) and (d). The field exponent  $n$  of all compounds gradually tends to 2 above the transition temperature. No abrupt change greater than 2 was observed near the phase transition, indicating that all compounds show a SOPT.



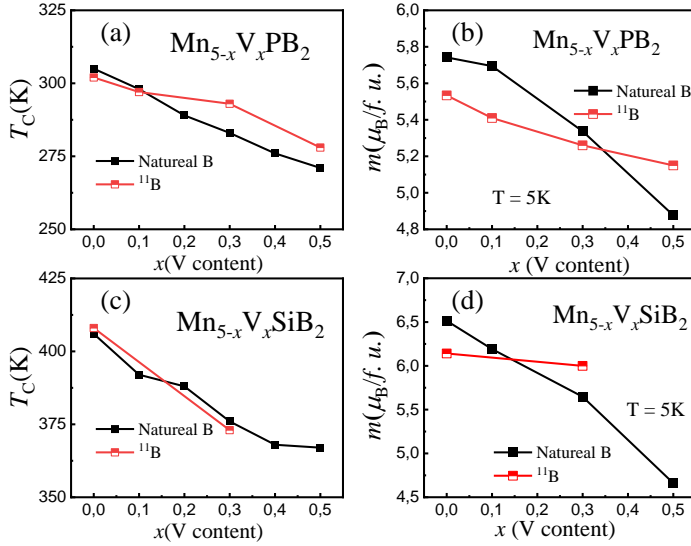
**Fig. 6.7** Adiabatic temperature change  $\Delta T_{ad}$  of for (a)  $Mn_{5-x}V_xPB_2$  ( $x = 0.0, 0.3, 0.5$  and  $1.0$ ) and (b)  $Mn_{5-x}V_xSiB_2$  ( $x = 0.0, 0.3$  and  $0.5$ ) for a field change of 1 T. Field exponent of the magnetic entropy change  $n = \frac{d \ln(|\Delta S_m|)}{d \ln(H)}$  for (c)  $Mn_{5-x}V_xPB_2$  ( $x = 0.0, 0.3, 0.5$  and  $1.0$ ) and (d)  $Mn_{5-x}V_xSiB_2$  ( $x = 0.0, 0.3$  and  $0.5$ ).

### 6.3.3 Neutron diffraction study

<sup>11</sup>B isotope-substituted Mn<sub>5-x</sub>V<sub>x</sub>P<sup>11</sup>B<sub>2</sub> ( $x = 0.0, 0.1, 0.3$  and  $0.5$ ) and Mn<sub>5-x</sub>V<sub>x</sub>Si<sup>11</sup>B<sub>2</sub> ( $x = 0.0$  and  $0.3$ ) compounds were prepared for neutron diffraction to avoid the influence of neutron absorption by natural B. Before discussing the neutron diffraction it must be ensured that the <sup>11</sup>B samples have the same lattice structure and magnetic properties as the natural B samples. The room-temperature XRD analysis results show that Mn<sub>5-x</sub>V<sub>x</sub>P<sup>11</sup>B<sub>2</sub> ( $x = 0.0, 0.1, 0.3$ , and  $0.5$ ) and Mn<sub>5-x</sub>V<sub>x</sub>Si<sup>11</sup>B<sub>2</sub> ( $x = 0.0$  and  $0.3$ ) compounds have the same crystal structure as the natural B samples. The lattice parameters  $a$ ,  $c$  and the unit-cell volume  $V$  of the <sup>11</sup>B and the natural B samples are shown in Fig. 6.8. The lattice parameters and unit-cell volume of the <sup>11</sup>B samples are consistent with those from the natural B compounds. A comparison of  $T_C$  and  $M_S$  of the <sup>11</sup>B compounds with the natural B compounds is given in Fig. 6.9. Although the  $T_C$  and  $M_S$  of the <sup>11</sup>B sample were not exactly the same as the natural B compounds, they show the same V dependence as the natural B compounds: both  $T_C$  and  $M_S$  decrease with increasing V content.



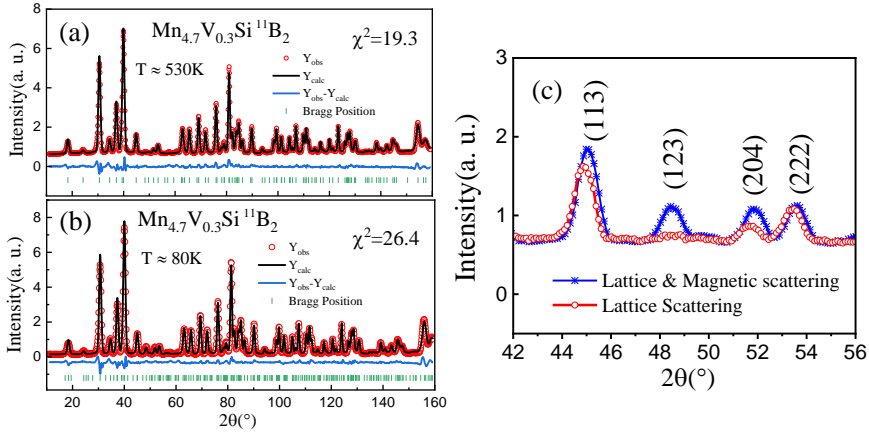
**Fig. 6.8** (a) Lattice parameters  $a$  and  $c$  of the Mn<sub>5-x</sub>V<sub>x</sub>PB<sub>2</sub> and Mn<sub>5-x</sub>V<sub>x</sub>P<sup>11</sup>B<sub>2</sub> compounds. (b) Unit-cell volume  $V$  of the Mn<sub>5-x</sub>V<sub>x</sub>PB<sub>2</sub> and Mn<sub>5-x</sub>V<sub>x</sub>P<sup>11</sup>B<sub>2</sub> compounds. (c) Lattice parameters  $a$  and  $c$  of the Mn<sub>5-x</sub>V<sub>x</sub>SiB<sub>2</sub> and Mn<sub>5-x</sub>V<sub>x</sub>Si<sup>11</sup>B<sub>2</sub> compounds. (d) Unit-cell volume  $V$  of the Mn<sub>5-x</sub>V<sub>x</sub>SiB<sub>2</sub> and Mn<sub>5-x</sub>V<sub>x</sub>Si<sup>11</sup>B<sub>2</sub> compounds.



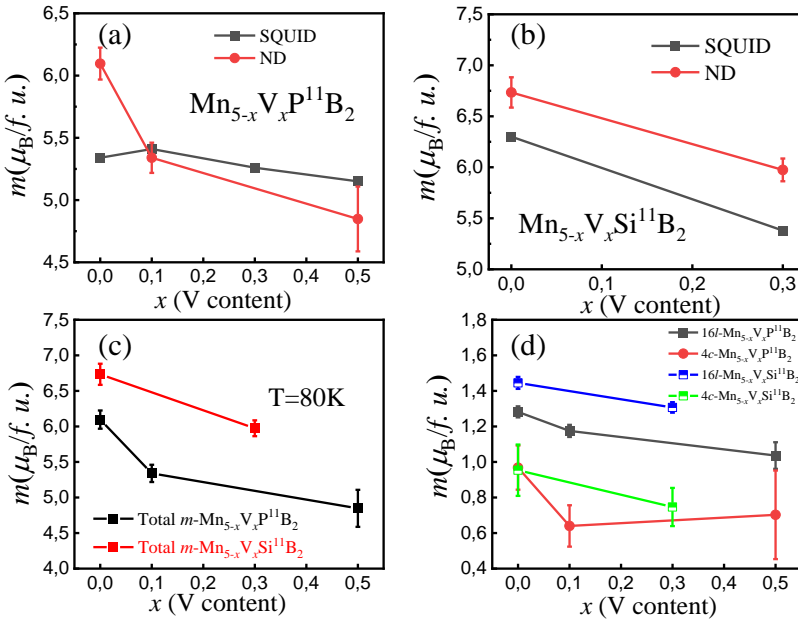
**Fig. 6.9** (a)  $T_C$  and (b) total magnetic moment as a function of V content for the  $Mn_{5-x}V_xPB_2$  and  $Mn_{5-x}V_xP^{11}B_2$  compounds. (c)  $T_C$  and (d) total magnetic moment as a function of the V content for the  $Mn_{5-x}V_xSiB_2$  and  $Mn_{5-x}V_xSi^{11}B_2$  compounds.

Fig. 6.10 shows the neutron diffraction patterns and refinements of the  $Mn_{4.7}V_{0.3}Si^{11}B_2$  compound in the FM and PM states. The neutron diffraction pattern of the  $Mn_{4.7}V_{0.3}Si^{11}B_2$  compound in the FM state has the same magnetic contribution as the mother compound  $Mn_5Si^{11}B_2$ , with significant contributions to the (123) and (204) peaks. We used the same Irreducible Representation ( $\Gamma_9$ ) as the  $Mn_5Si^{11}B_2$  compound for the V doped compounds' magnetic structure refinements [19]. The magnetic moments on the 16l and 4c sites are aligned in the  $a$ - $b$  plane, which indicates that V doping has no effect on the preferred moment alignment in these compounds. The V doped compound has the same magnetic structure as the mother compound. The refinement for the  $Mn_{4.7}V_{0.3}Si^{11}B_2$  compound in FM state is shown in Fig. 6.10(b). The total magnetic moment (per formula unit) obtained by neutron diffraction refinements of the  $Mn_{5-x}V_xP^{11}B_2$  ( $x = 0.0, 0.1, 0.3$  and  $0.5$ ) and  $Mn_{5-x}V_xSi^{11}B_2$  ( $x = 0.0$  and  $0.3$ ) compounds were consistent with the results of SQUID measurements. The magnetic moment of the  $Mn_{4.7}V_{0.3}P^{11}B_2$  and  $Mn_{5-x}V_xSi^{11}B_2$  compounds decreases with the V content, as shown in Fig. 6.11 (a), (b) and (c). Fig. 6.11(d) shows the dependence of the magnetic moments at the different magnetic sites on the V content. The magnetic moments at the two different magnetic sites both decrease with the introduction of V.

*Chapter 6 Effect of V doping on the Magnetocaloric Properties of  
Mn<sub>5</sub>(Si,P)B<sub>2</sub> Compound*



**Fig. 6.10** Neutron powder diffraction refinements for the Mn<sub>4.7</sub>V<sub>0.3</sub>Si<sup>11</sup>B<sub>2</sub> compound (a) in the paramagnetic state (530 K) and (b) in the ferromagnetic (80 K) state. (c) Neutron diffraction patterns for the Mn<sub>4.7</sub>V<sub>0.3</sub>Si<sup>11</sup>B<sub>2</sub> compound in the ferromagnetic state (80 K) and in the paramagnetic state (530 K).



**Fig. 6.11** Total magnetic moment of the (a) Mn<sub>5-x</sub>V<sub>x</sub>P<sup>11</sup>B<sub>2</sub> and (b) Mn<sub>5-x</sub>V<sub>x</sub>Si<sup>11</sup>B<sub>2</sub> compounds obtained by neutron diffraction and SQUID. (c) Total magnetic moment by neutron diffraction refinements of the Mn<sub>5-x</sub>V<sub>x</sub>P<sup>11</sup>B<sub>2</sub> and Mn<sub>5-x</sub>V<sub>x</sub>Si<sup>11</sup>B<sub>2</sub> compounds. (d) Magnetic moments at the 16l and 4c sites in the tetragonal lattice of the Mn<sub>5-x</sub>V<sub>x</sub>P<sup>11</sup>B<sub>2</sub> and Mn<sub>5-x</sub>V<sub>x</sub>Si<sup>11</sup>B<sub>2</sub> compounds.

#### **6.4. Conclusions**

In summary, V doping has a different effect on the phase formation in the  $Mn_{5-x}V_xPB_2$  ( $0 \leq x \leq 1$ ) and  $Mn_{5-x}V_xSiB_2$  ( $0.0 \leq x \leq 0.5$ ) compounds. It has almost no effect on the impurity content of  $Mn_{5-x}V_xPB_2$ , while the fraction of  $Mn_2B$  impurity phase in  $Mn_{5-x}V_xSiB_2$  compounds is quite sensitive to an increase in V content. We were unable to form the  $Cr_5B_3$  phase for V concentrations of  $x \geq 1$  in the  $Mn_{5-x}V_xSiB_2$  system. Since the atomic size of V is larger than Mn, the unit-cell volume expands with increasing V content for all V doped compounds. The value of  $T_C$  can be adjusted by V doping and can cover a temperature range of 225 - 406 K. V doping enhances the SOPT characteristics of the compounds, resulting in a decrease in  $|\Delta S_{M, \max}|$  and  $\Delta T_{ad}$ . V doping has no significant effect on the magnetic structure of the compounds, but it reduced the magnetic moments at the magnetic  $16l$  and  $4c$  sites, resulting in a decrease in the total magnetic moment per formula unit.

*Chapter 6 Effect of V doping on the Magnetocaloric Properties of  
Mn<sub>5</sub>(Si,P)B<sub>2</sub> Compound*

**References**

- [1] B. Aronsson, G. Lundgren, X-Ray investigations on Me-Si-B System I, *Acta Chemica Scandinavica* 13 (1959) 433.
- [2] B. Aronsson, I. Engström, X-Ray investigations on Me-Si-B System II, *Acta Chemica Scandinavica* 14 (1960) 1403.
- [3] L. Häggström, R. Wäppling, T. Ericsson, Mössbauer and X-Ray Studies of Fe<sub>5</sub>PB<sub>2</sub>, *J. Solid State Chem.* 13 (1976) 84.
- [4] R. Wäppling, T. Ericsson, L. Häggström, Y. Andersson, Magnetic Properties of Fe<sub>5</sub>SiB<sub>2</sub> and related compounds, *J. Physique Colloques* C6 (1976) 591.
- [5] D.M. de Almeida, C. Bormio-Nunes, C.A. Nunes, A.A. Coelho, G.C. Coelho, Magnetic characterization of Mn<sub>5</sub>SiB<sub>2</sub> and Mn<sub>5</sub>Si<sub>3</sub> phases, *J. Magn. Magn. Mater.* 321 (2009) 2578.
- [6] M.A. McGuire, D.S. Parker, Magnetic and structural properties of ferromagnetic Fe<sub>5</sub>PB<sub>2</sub> and Fe<sub>5</sub>SiB<sub>2</sub> and effects of Co and Mn substitutions, *J. Appl. Phys.* 118 (2015) 163903.
- [7] M. Werwiński, Magnetic properties of Fe<sub>5</sub>SiB<sub>2</sub> and its alloys with P, S, and Co, *Phys. Rev. B* 93 (2016) 174412.
- [8] M. Werwiński, Magnetocrystalline anisotropy of Fe<sub>5</sub>PB<sub>2</sub> and its alloys with Co and 5d elements: A combined first-principles and experimental study, *Phys. Rev. B* 98 (2018) 214431.
- [9] J. Thakur, P. Rani, M. Tomar, V. Gupta, H.S. Saini, M.K. Kashyap, Tailoring in-plane magnetocrystalline anisotropy of Fe<sub>5</sub>SiB<sub>2</sub> with Cr-substitution, *AIP Conference Proceedings* 2115 (2019) 030506.
- [10] D.A.P. Reis, C.A. Nunes, A. Capri Neto, Caracterização microestrutural e química de ligas V-Si-B, *Revista Brasileira de Aplicações de Vácuo*, 26 (2007) 79.
- [11] L. van Eijck, L.D. Cussen, G.J. Sykora, E.M. Schooneveld, N.J. Rhodes, A.A. van Well, C. Pappas, Design and performance of a novel neutron powder diffractometer: PEARL at TU Delft, *J. Appl. Cryst.* 49 (2016) 1398.
- [12] H.M. Rietveld, A profile refinement method for nuclear and magnetic structures, *J. Appl. Cryst.* 2 (1969) 65.
- [13] J. Rodriguez-Carvajal, Recent advances in magnetic-structure determination by neutron powder diffraction, *Physica B* 192 (1993) 55.
- [14] F.R. de Boer, W.C.M. Mattens, R. Boom, A.R. Miedema, A.K. Niessen, *Cohesion in metals: Transition metal alloys*, North-Holland, (1988).
- [15] C.T. Zhou, J.D. Xing, B. Xiao, J. Feng, X.J. Xie, Y.H. Chen, First principles study on the structural properties and electronic structure of X<sub>2</sub>B (X = Cr, Mn, Fe, Co, Ni, Mo and W) compounds, *Comput. Mater. Sci.* 44 (2009) 1056.

- [16] L. Häggström J. Sjöström and T. Ericsson, A  $^{57}\text{Fe}$  Mössbauer Study of  $\text{Mn}_2\text{P}$ , J. Magn. Magn. Mater. 60 (1986) 171.
- [17] S.H. Na, W. Wu, and J.L. Luo, Anisotropy Properties of  $\text{Mn}_2\text{P}$  Single Crystals with Antiferromagnetic Transition, Chinese Phys. Lett. 37 (2020) 087301.
- [18] M. Foldeaki, R. Chahine, B.R. Gopal, T.K. Bose, X.Y. Liu, J.A. Barclay, Effect of sample preparation on the magnetic and magnetocaloric properties of amorphous  $\text{Gd}_{70}\text{Ni}_{30}$ , J. Appl. Phys. 83 (1998) 2727.
- [19] A.S. Wills, A new protocol for the determination of magnetic structures using simulated annealing and representational analysis (SARAh), Physica B 276-278 (2000) 680.

# Chapter 7

## **Effect of Simultaneous Doping of Fe and Cr on the Magnetocaloric Properties of $Mn_5(Si,P)B_2$ Compounds**

### **7.1. Introduction**

In the previous chapters, the effect of the Si/P ratio and doping with different 3d metals (V and Cr) on the structural and magnetocaloric properties of  $Mn_5(Si,P)B_2$  compounds has been discussed. Different 3d metals in the  $M_5XB_2$  ( $M = Fe, Mn, Co, V, Cr$  and  $X = Si, P, S$ ) system result in different magnetic properties of these compounds [1-5]. The  $Fe_5(Si,P)B_2$  compounds in this system [6-11], have been explored most extensively and in-depth. In comparison with the  $Mn_5(Si,P)B_2$  compounds, the  $Fe_5(Si,P)B_2$  compounds always have a higher saturation magnetization and a higher Curie temperature. Wäppling *et al.* reported that the Curie temperature of  $Fe_5SiB_2$  and  $Fe_5PB_2$  was 784 and 628 K [6], respectively. These values are significantly higher than the values of 406 and 305 K obtained in Chapter 4 in this study for  $Mn_5SiB_2$  and  $Mn_5PB_2$ , respectively. McGuire *et al.* studied the effect of Mn and Co doping on the magnetic properties of the  $Fe_5(Si,P)B_2$  compounds [1]. McGuire and Parker [1] reported a Curie temperature of 640 K for  $Fe_5PB_2$ , slightly higher than reported by Häggström [6]. The saturation magnetizations of  $Fe_5SiB_2$  and  $Fe_5PB_2$  compounds are 9.06 and 8.00  $\mu_B/f.u.$ , respectively. These values are higher than the ones for the corresponding  $Mn_5(Si,P)B_2$  compounds that were found in Chapter 4. Mn substitution of Fe reduces the saturation magnetization of the  $Fe_5SiB_2$  compound. However, the Curie temperature of the  $Fe_5PB_2$  compound increases by 10 K with the introduction of Mn. In Chapter 5, we found that Cr doping leads to a decrease in Curie temperature and saturation magnetization in the  $Mn_5(Si,P)B_2$  compounds. It therefore seems that Fe and Cr substitutions have an opposite effect on the magnetic properties of the  $Mn_5(Si,P)B_2$  system. In order to investigate this behavior in more detail, the effect of simultaneous Fe and Cr doping on the magnetocaloric properties of this system are studied in this Chapter.

## 7.2. Experimental details

Alloys of the following compositions Mn<sub>5-x</sub>Fe<sub>x</sub>PB<sub>2</sub> and Mn<sub>5-x</sub>Fe<sub>x</sub>SiB<sub>2</sub> ( $x = 0.0, 0.5$  and  $1.0$ ), Mn<sub>4</sub>Fe<sub>1-x</sub>Cr<sub>x</sub>PB<sub>2</sub> and Mn<sub>4</sub>Fe<sub>1-x</sub>Cr<sub>x</sub>SiB<sub>2</sub> ( $x = 0.0, 0.2, 0.4, 0.6, 0.8$  and  $1.0$ ) were prepared by the ball-milling technique, with the starting materials Mn (99.6%), Fe(99.4%), Cr(99.4%), MnP (96.08%), Si (99+%) and B (99.4%), placed in a stainless steel jar with a rotation speed of 350 rpm for 10 hours. For the compounds used in the neutron diffraction (ND) experiments, <sup>11</sup>B was used as a starting material instead of natural B. A SQUID magnetometer (Quantum Design MPMS) was employed for the magnetic measurements. The XRD patterns were collected at room temperature with a PANalytical X-Pert PRO using Cu-K<sub>α</sub> radiation. ND measurements were carried out on the neutron powder diffractometer PEARL at the research reactor of the TU Delft [12]. The lattice and magnetic structure refinements were carried out using the Rietveld method [13] and the Fullprof software [14]. The magnetic measurements at temperatures above 370 K were performed in a VersaLab vibrating-sample magnetometer (VSM) with an oven function.

## 7.3 Results and discussion

### 7.3.1 Fe doped Mn<sub>5</sub>(Si,P)B<sub>2</sub> compounds

#### 7.3.1.1 Structural and magnetic properties

To explore the effect of Fe doping on the structural and magnetic properties of Mn<sub>5</sub>(Si,P)B<sub>2</sub> compounds, we prepared Mn<sub>5-x</sub>Fe<sub>x</sub>SiB<sub>2</sub> and Mn<sub>5-x</sub>Fe<sub>x</sub>PB<sub>2</sub> ( $x = 0.0, 0.5$  and  $1.0$ ) compounds. The main phase of the Mn<sub>5-x</sub>Fe<sub>x</sub>SiB<sub>2</sub> and Mn<sub>5-x</sub>Fe<sub>x</sub>PB<sub>2</sub> ( $x = 0.0, 0.5$ , and  $1.0$ ) compounds is crystalized into the Cr<sub>5</sub>B<sub>3</sub> structure. The Mn<sub>5-x</sub>Fe<sub>x</sub>PB<sub>2</sub> compounds were accompanied by different amounts of the (Mn,Fe)<sub>2</sub>P impurity phase. The concentration of the impurity phase increases with the Fe content, as shown in Fig. 7.1(a). Fe doping has no effect on the formation of the main phase of Mn<sub>5-x</sub>Fe<sub>x</sub>SiB<sub>2</sub>. No extra peaks besides the main phase were observed in the room-temperature XRD patterns. In Fig. 7.1(b) the unit-cell volume  $V$  of the main phase is plotted as a function of the Fe content. The unit-cell volume of the Mn<sub>5-x</sub>Fe<sub>x</sub>SiB<sub>2</sub> and Mn<sub>5-x</sub>Fe<sub>x</sub>PB<sub>2</sub> ( $x = 0.0, 0.5$ , and  $1.0$ ) compounds decreases with the introduction of Fe. The change in unit-cell volume was  $\approx 1 \text{ \AA}^3$  for each 10% of added Fe. The estimated unit-cell volume of Fe<sub>5</sub>SiB<sub>2</sub> and Fe<sub>5</sub>PB<sub>2</sub> (where Fe completely replaces Mn) are about 318 and 311  $\text{\AA}^3$ , respectively. These values are consistent with the results of 318.45 and 311.67  $\text{\AA}^3$  reported by McGuire and Parker [1]. Fig. 7.1(c) and (d) show the saturation magnetization  $M_s(5 \text{ K})$  and the Curie temperature  $T_C$  of the Mn<sub>5-x</sub>Fe<sub>x</sub>SiB<sub>2</sub> and the Mn<sub>5-x</sub>Fe<sub>x</sub>PB<sub>2</sub> ( $x = 0.0, 0.5$ , and  $1.0$ ) compounds. The  $M_s$  and  $T_C$  values of the compounds increased with the Fe content.

## Chapter 7 Effect of Simultaneous Doping of Fe and Cr on the Magnetocaloric Properties of $Mn_5(Si,P)B_2$ Compounds

For the  $Mn_{5-x}Fe_xSiB_2$  and  $Mn_{5-x}Fe_xPB_2$  compounds  $M_S$  increases from 105.56 and 91.07  $Am^2kg^{-1}$  to 120.30 and 115.00  $Am^2kg^{-1}$ , respectively. Hedlund *et al.* [11] reported that  $M_S(300\text{ K})$  values for the  $Fe_5SiB_2$  and  $Fe_5PB_2$  compounds were 150.06 and 122.97  $Am^2kg^{-1}$ , respectively. These values are significantly higher than the ones obtained for the  $Mn_5SiB_2$  and  $Mn_5PB_2$  alloys studied in Chapter 4. In comparison with the Mn compounds, the Fe compounds always have a higher  $M_S$ . In  $(Mn,Fe)_5(Si,P)B_2$  compounds, the value of  $M_S$  depends significantly on the Mn/Fe ratio. The higher the Fe content, the higher the saturation magnetization of the compound. The Curie temperature of the compounds increases from 406 and 305 K to 506 and 412 K for  $(Mn,Fe)_5SiB_2$  and  $(Mn,Fe)_5PB_2$ , respectively. According to the literature [11], the Curie temperature of the  $Fe_5SiB_2$  and  $Fe_5PB_2$  compounds corresponds to 800 and 615 K, respectively. The Curie temperature exhibits the same trend as the saturation magnetization: for a higher Fe content a higher Curie temperature is found.

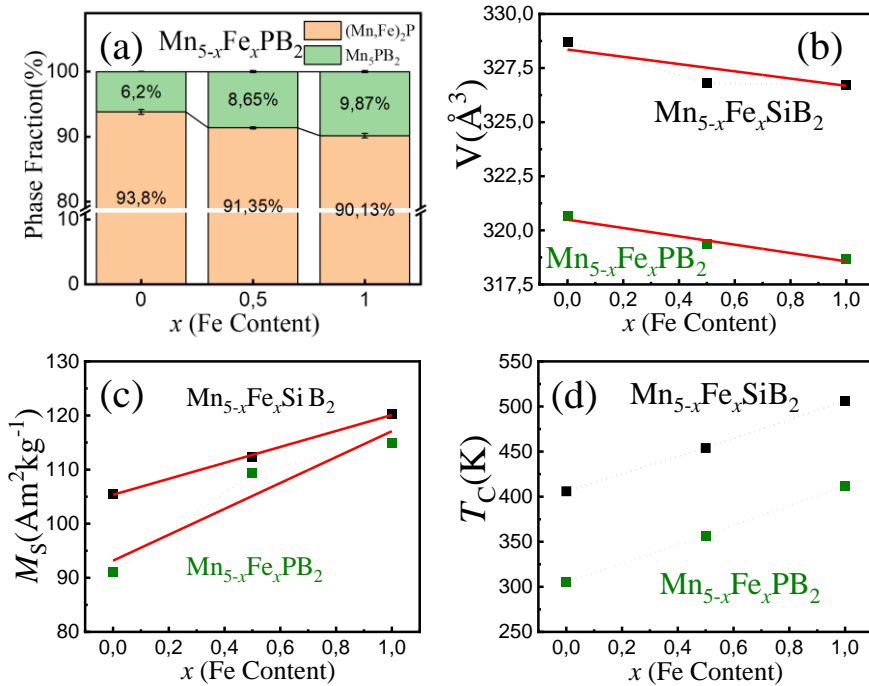


**Fig. 7.1** (a) Phase fraction of the  $Mn_{5-x}Fe_xPB_2$  ( $x = 0.0, 0.5$  and  $1.0$ ) compounds. (b) Unit-cell volume  $V$  of the  $Mn_{5-x}Fe_xSiB_2$  and  $Mn_{5-x}Fe_xPB_2$  ( $x = 0.0, 0.5$  and  $1.0$ ) compounds. Saturation magnetization (c)  $M_S$  and (d) Curie temperature  $T_C$  of  $Mn_{5-x}Fe_xSiB_2$  and  $Mn_{5-x}Fe_xPB_2$  ( $x = 0.0, 0.5$  and  $1.0$ ) compounds.

### 7.3.1.2 Mössbauer Spectroscopy and neutron diffraction

The Mössbauer spectra of the  $\text{Mn}_4\text{FePB}_2$  and  $\text{Mn}_4\text{FeSiB}_2$  compounds in the FM state are shown in Fig. 7.2. Although there are only two magnetic sites occupied by Fe in the unit cell, Fe(1) at 16l and Fe(2) at 4c, three spectral lines are needed to fit the main phase in the Mössbauer spectra. This finding is similar to that of the previously reported  $\text{Fe}_5(\text{Si,P})\text{B}_2$  Mössbauer results. Since the Fe(1) atom on the 16l site is irregularly surrounded by 3 B, 2 Si/P and 2 Fe(2), where Si/P is easily replaced by B, the resulting Fe(1) line splits into Fe(1)a and Fe(1)b [4, 6, 7]. The fitted parameters for the  $\text{Mn}_4\text{FePB}_2$  and  $\text{Mn}_4\text{FeSiB}_2$  compounds are listed in Table 7.1. When the Fe atoms randomly occupies 16l and 4c sites in the unit cell, the contribution of the Fe(1) and Fe(2) atoms to the spectra should be close to 4:1. Observing the spectral contribution of the Fe(1) and Fe(2) atoms in the spectra, it is found that the Fe(1)/Fe(2) contribution ratio for  $\text{Mn}_4\text{FePB}_2$  and  $\text{Mn}_4\text{FeSiB}_2$  is 4:2.5 and 4:1.5, respectively. This means that the Fe atoms prefer to occupy the 4c site, rather than the 16l site. This preference in occupancy is more pronounced for the  $\text{Mn}_4\text{FePB}_2$  compound. The total magnetic moment of  $\text{Mn}_4\text{FePB}_2$  and  $\text{Mn}_4\text{FeSiB}_2$  calculated using the proportionality factor of  $14.2 \text{ T}/\mu_{\text{B}}$  suggested in the literature [15] are 6.86 and  $7.43 \mu_{\text{B}}/\text{atom}$ , respectively. These values are slightly higher than the 6.76 and  $7.01 \mu_{\text{B}}/\text{atom}$  measured by SQUID. Additionally, beside the main phase contribution, both compounds have a PM state contribution for Fe(3). The XRD patterns did however not show any corresponding PM peaks.

The neutron diffraction results show that the Fe doped compounds have the same lattice and magnetic structure as the parent compounds. The main phase crystallizes into  $\text{Cr}_5\text{B}_3$ -type structure for Fe-doped compounds, in which Fe and Mn share the 16l and 4c sites in the unit cell, and the magnetic moments are oriented within the *a-b* plane. The occupancy of Fe on 16l and 4c sites obtained by neutron diffraction refinements of the  $\text{Mn}_{4.5}\text{Fe}_{0.5}\text{P}^{11}\text{B}_2$  and  $\text{Mn}_{4.5}\text{Fe}_{0.5}\text{Si}^{11}\text{B}_2$  compounds is shown in Fig. 7.3(a). Fe preferentially occupies the 4c site significantly more than the 16l. This trend is more evident in the  $\text{Mn}_{4.5}\text{Fe}_{0.5}\text{P}^{11}\text{B}_2$  compound, consistent with the Mössbauer results. Fig. 7.3(b) and (c) show the effect of Fe doping on the magnetic moments on the 16l and 4c sites. In the  $\text{Mn}_{4.5}\text{Fe}_{0.5}\text{Si}^{11}\text{B}_2$  compound the magnetic moments on both sites increase with the Fe content. However, the magnetic moment on the 4c site in the  $\text{Mn}_{4.5}\text{Fe}_{0.5}\text{P}^{11}\text{B}_2$  compound decreases with the Fe content. This may be related to the preferred occupation of Fe at the 4c site in the  $\text{Mn}_{4.5}\text{Fe}_{0.5}\text{P}^{11}\text{B}_2$  compound. The total magnetic moment of the  $\text{Mn}_{4.5}\text{Fe}_{0.5}\text{P}^{11}\text{B}_2$  and  $\text{Mn}_{4.5}\text{Fe}_{0.5}\text{Si}^{11}\text{B}_2$  compounds obtained by neutron diffraction fitting is 6.41 and  $7.57 \mu_{\text{B}}/\text{atom}$ , respectively.

## Chapter 7 Effect of Simultaneous Doping of Fe and Cr on the Magnetocaloric Properties of $\text{Mn}_5(\text{Si,P})\text{B}_2$ Compounds

Table 7.1 Fitted Mössbauer parameters of the  $\text{Mn}_4\text{FePB}_2$  and  $\text{Mn}_4\text{FeSiB}_2$  compounds in the FM state. The magnetic moment was calculated by using the proportionality factor of  $14.2 \text{ T}/\mu_{\text{B}}$  suggested in the literature [51]. Experimental uncertainties: Isomer shift: I.S.  $\pm 0.02 \text{ mms}^{-1}$ ; Line width:  $\Gamma \pm 0.03 \text{ mms}^{-1}$ ; Hyperfine field:  $\pm 0.1 \text{ T}$ ; Spectral contribution:  $\pm 3\%$ .

Sample	$T$ (K)	IS ( $\text{mm s}^{-1}$ )	QS ( $\text{mm s}^{-1}$ )	Hyperfin e field (T)	Magnetic moment ( $\mu_{\text{B}}/\text{atom}$ )	$\Gamma$ ( $\text{mm s}^{-1}$ )	Phase	Spectral contribution (%)
$\text{Mn}_4\text{FePB}_2$	120	0.37	0.04	16.8	1.18	0.37	Fe(1) a	20
		0.32	-0.05	19.8	1.39	0.47	Fe(1) b	35
		0.09	0.79	22.8	1.61	0.45	Fe(2)	34
		0.28	---	---	---	0.27	Fe(3) a	11
$\text{Mn}_4\text{FeSiB}_2$	120	0.25	0.02	18.9	1.33	0.37	Fe(1) a	32
		0.26	0.00	20.9	1.47	0.43	Fe(1) b	37
		0.09	-0.17	25.7	1.81	0.39	Fe(2)	26
		0.25	1.09	---	---	0.21	Fe(3) a	3
		0.12	---	---	---	0.43	Fe(3) b	2

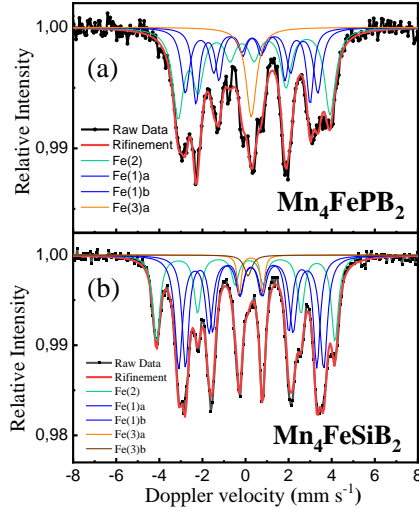


**Fig. 7.2** Mössbauer spectra of (a) the  $\text{Mn}_4\text{FePB}_2$  and (b) the  $\text{Mn}_4\text{FeSiB}_2$  compounds at 120 K. The black line represents the experimental spectrum, the patterns from Fe(1)a and Fe(1)b are in blue, Fe(2) in green, the paramagnetic pattern of Fe(3) in light and dark brown, and the summed fit in red.

## Chapter 7 Effect of Simultaneous Doping of Fe and Cr on the Magnetocaloric Properties of $\text{Mn}_5(\text{Si,P})\text{B}_2$ Compounds

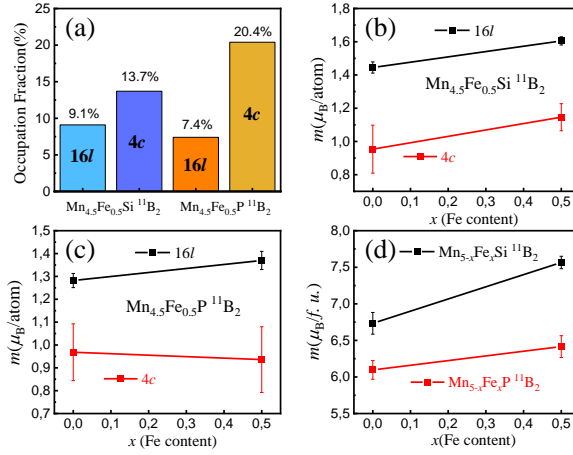


**Fig. 7.3** (a) Occupation fraction of the  $\text{Mn}_{4.5}\text{Fe}_{0.5}\text{P}^{11}\text{B}_2$  and  $\text{Mn}_{4.5}\text{Fe}_{0.5}\text{Si}^{11}\text{B}_2$  compounds obtained by ND refinements. Magnetic moment for the 16l and 4c sites for the (b)  $\text{Mn}_{4.5}\text{Fe}_{0.5}\text{Si}^{11}\text{B}_2$  and (c)  $\text{Mn}_{4.5}\text{Fe}_{0.5}\text{P}^{11}\text{B}_2$  compounds. (d) Total magnetic moment of the  $\text{Mn}_{4.5}\text{Fe}_{0.5}\text{P}^{11}\text{B}_2$  and  $\text{Mn}_{4.5}\text{Fe}_{0.5}\text{Si}^{11}\text{B}_2$  compounds obtained by ND refinements.

### 7.3.2 (Fe, Cr) doped $\text{Mn}_5(\text{Si,P})\text{B}_2$ compounds

#### 7.3.2.1 The crystalline structures and phase analysis

The main phase of the  $\text{Mn}_4\text{Fe}_{1-x}\text{Cr}_x\text{PB}_2$  and  $\text{Mn}_4\text{Fe}_{1-x}\text{Cr}_x\text{SiB}_2$  ( $x = 0.0, 0.2, 0.4, 0.6, 0.8$  and  $1.0$ ) compounds was found to crystallize into the same structure as the mother compounds, the  $\text{Cr}_5\text{B}_3$ -type structure. Fig. 7.4 (a) (b) and (c) show the dependence of the lattice parameters  $a$  and  $c$  and the unit-cell volume  $V$  of the  $\text{Mn}_4\text{Fe}_{1-x}\text{Cr}_x\text{PB}_2$  and  $\text{Mn}_4\text{Fe}_{1-x}\text{Cr}_x\text{SiB}_2$  compounds on the Fe/Cr ratio. The lattice parameters  $a$  and  $c$  and the unit-cell volume  $V$  of the compounds increase with the Cr content, which shows the same trend as the Cr doping found in Chapter 5. As shown in Fig. 7.4 (d) the  $(\text{Mn,Fe})_2\text{P}$  impurity phase in the  $\text{Mn}_4\text{Fe}_{1-x}\text{Cr}_x\text{PB}_2$  compounds increases with the Fe concentration. It shows the same trend as presented by Fe doping mentioned above in this Chapter. The formation of the  $(\text{Mn,Fe})_2\text{P}$  phase is quite sensitive to the Fe concentration in the  $\text{Mn}_4\text{Fe}_{1-x}\text{Cr}_x\text{PB}_2$  compounds. Fig. 7.5 shows the dependence of the unit-cell volume of the  $(\text{Mn,Fe})_2\text{P}$  phase on the Fe/Cr ratio in the  $\text{Mn}_4\text{Fe}_{1-x}\text{Cr}_x\text{PB}_2$  compounds. The unit-cell volume of the  $(\text{Mn,Fe})_2\text{P}$  phase was found to decrease with the Fe concentration. In the  $\text{X}_2\text{P}$  ( $\text{X} = \text{Fe, Mn, Cr, and Co}$ ) system, the unit-cell volume of  $\text{Fe}_2\text{P}$  is smaller than that of  $\text{Mn}_2\text{P}$  [16]. Accordingly, the Fe content in the  $(\text{Mn,Fe})_2\text{P}$  phase is expected to increase with the Fe concentration in the  $\text{Mn}_4\text{Fe}_{1-x}\text{Cr}_x\text{PB}_2$  compounds.

*Chapter 7 Effect of Simultaneous Doping of Fe and Cr on the  
Magnetocaloric Properties of  $\text{Mn}_5(\text{Si,P})\text{B}_2$  Compounds*

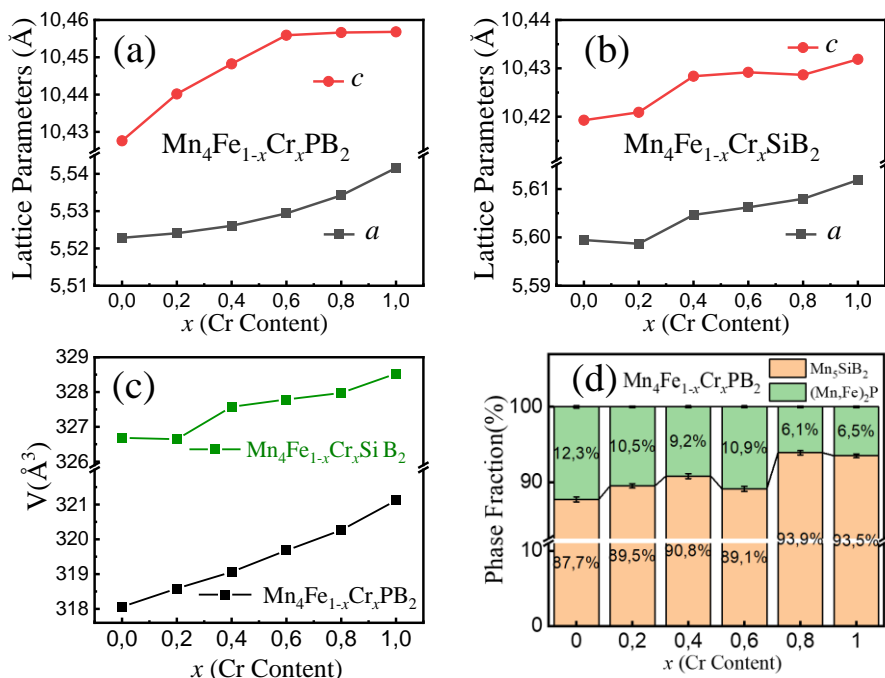


**Fig. 7.4** Lattice parameters  $a$  and  $c$  for (a) the  $\text{Mn}_4\text{Fe}_{1-x}\text{Cr}_x\text{PB}_2$  and (b) the  $\text{Mn}_4\text{Fe}_{1-x}\text{Cr}_x\text{SiB}_2$  ( $x = 0.0, 0.2, 0.4, 0.6, 0.8$  and  $1.0$ ) compounds obtained by XRD at room temperature. (c) Unit-cell volume as a function of Cr content for the  $\text{Mn}_4\text{Fe}_{1-x}\text{Cr}_x\text{PB}_2$  and  $\text{Mn}_4\text{Fe}_{1-x}\text{Cr}_x\text{SiB}_2$  ( $x = 0.0, 0.2, 0.4, 0.6, 0.8$  and  $1.0$ ) compounds. (d) Phase composition of the  $\text{Mn}_4\text{Fe}_{1-x}\text{Cr}_x\text{PB}_2$  compounds.

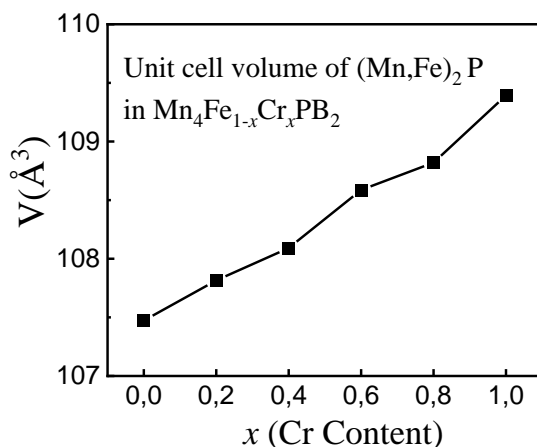
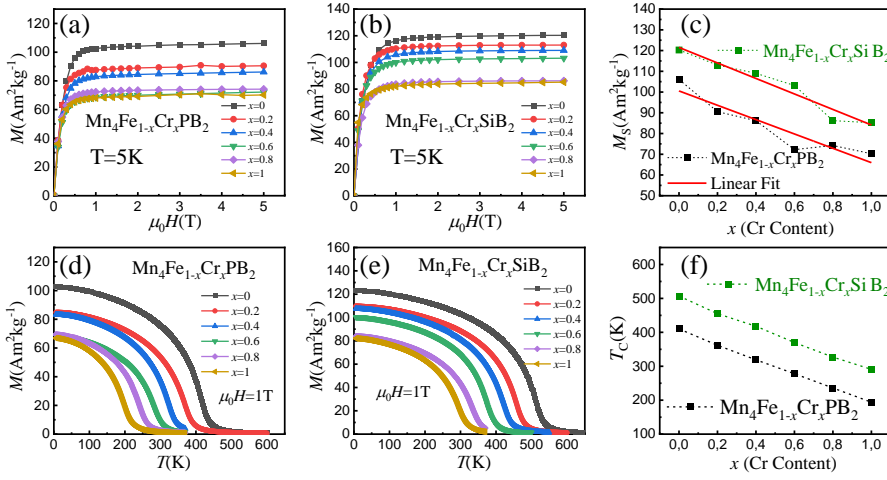


**Fig. 7.5** Unit-cell volume of the  $(\text{Mn,Fe})_2\text{P}$  phase as a function of Cr content in the  $\text{Mn}_4\text{Fe}_{1-x}\text{Cr}_x\text{PB}_2$  compounds.

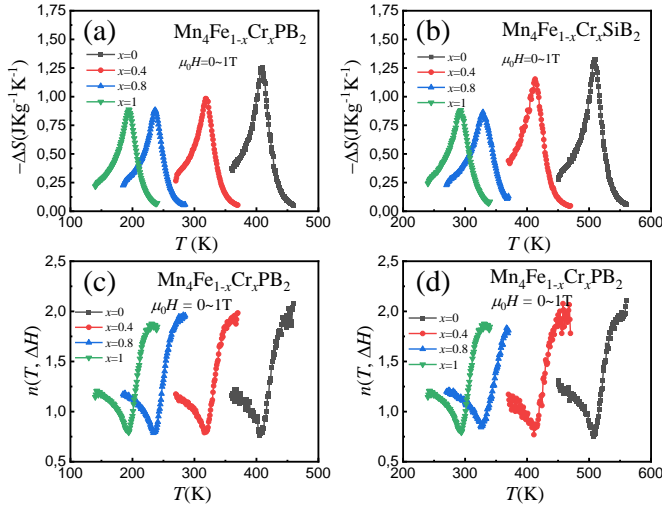
### 7.3.2.2 Magnetocaloric effect

Fig. 7.6 (a) and (b) show the field-dependent magnetization of  $Mn_4Fe_{1-x}Cr_xPB_2$  and  $Mn_4Fe_{1-x}Cr_xSiB_2$  ( $x = 0.0, 0.2, 0.4, 0.6, 0.8$  and  $1.0$ ) compounds at 5 K. The magnetization curves of the compounds exhibit ferromagnetic characteristics, and the saturation magnetization  $M_S$  decreases with the Cr content. Fig. 7.6 (c) shows the dependence of  $M_S$  on the Fe/Cr ratio for the compounds. The reduction in magnetization caused by the introduction of 10 at.% Cr for  $Mn_4Fe_{1-x}Cr_xPB_2$  and  $Mn_4Fe_{1-x}Cr_xSiB_2$  is  $18.7$  and  $17.3 \text{ Am}^2\text{kg}^{-1}$ , respectively. This is larger than the values of  $11.6$  and  $11.3 \text{ Am}^2\text{kg}^{-1}$  in the  $Mn_{5-x}Cr_xPB_2$  and  $Mn_{5-x}Cr_xSiB_2$  compounds studied in Chapter 5. The value of  $M_S$  in the  $Mn_4Fe_{1-x}Cr_xPB_2$  and  $Mn_4Fe_{1-x}Cr_xSiB_2$  compounds is more sensitive to Cr-content than in the  $Mn_{5-x}Cr_xPB_2$  and  $Mn_{5-x}Cr_xSiB_2$  compounds. In Fig. 7.6 (d) and (e) the temperature dependence of the magnetization of the  $Mn_4Fe_{1-x}Cr_xPB_2$  and  $Mn_4Fe_{1-x}Cr_xSiB_2$  compounds in an applied field of 1 T is shown. Fig. 7.6 (f) shows  $T_C$  of these compounds as a function of Cr content. Not only the  $M_S$  decreases with Cr content, but also  $T_C$ . The  $T_C$  of the  $Mn_4Fe_{1-x}Cr_xPB_2$  and  $Mn_4Fe_{1-x}Cr_xSiB_2$  compounds decreased from  $507$  and  $410 \text{ K}$  ( $x = 0.0$ ) to  $291$  and  $194 \text{ K}$  ( $x = 1.0$ ), respectively. The dependence of  $T_C$  on the Cr content is almost the same for the  $Mn_4Fe_{1-x}Cr_xPB_2$  and  $Mn_4Fe_{1-x}Cr_xSiB_2$  compounds,  $dT_C/dx \approx 21.5 \text{ K/at.\% Cr}$ . The isothermal magnetic entropy change  $|\Delta S_M|$  of the  $Mn_4Fe_{1-x}Cr_xPB_2$  and  $Mn_4Fe_{1-x}Cr_xSiB_2$  ( $x = 0.0, 0.4, 0.8$  and  $1.0$ ) compounds in a  $0 - 1 \text{ T}$  applied magnetic field change are shown in Fig. 7.7 (a) and (b). The introduction of Cr reduces the maximum isothermal magnetic entropy change  $|\Delta S_{M, \max}|$  of the compounds. The value of  $|\Delta S_{M, \max}|$  for the  $Mn_4Fe_{1-x}Cr_xPB_2$  and  $Mn_4Fe_{1-x}Cr_xSiB_2$  compounds decreases from  $1.25$  and  $1.33 \text{ Jkg}^{-1}\text{K}^{-1}$  ( $x = 0.0$ ) to  $0.88$  and  $0.89 \text{ Jkg}^{-1}\text{K}^{-1}$  ( $x = 1.0$ ), respectively. Fig. 7.7 (c) and (d) shows the calculated field exponent for the magnetic entropy change  $n$  of the compounds. The  $n$  value of the compounds gradually approaches 2 above the  $T_C$  without a divergence. Theoretically, the minimum value for a system with a SOPT corresponds to  $n_{\min} = 2/3$ . Systems with a FOPT or a CP both show a minimum value that is below  $2/3$ . The  $n$  value of the compounds is found to reach its minimum value at  $T_C$ . All compounds exhibit  $n_{\min}$  values that are slightly larger than  $2/3$ , indicating that the phase transition of the compounds belongs to a SOPT [17-20].

## Chapter 7 Effect of Simultaneous Doping of Fe and Cr on the Magnetocaloric Properties of $\text{Mn}_5(\text{Si,P})\text{B}_2$ Compounds



**Fig. 7.6** Field-dependent magnetization of (a) the  $\text{Mn}_4\text{Fe}_{1-x}\text{Cr}_x\text{PB}_2$  and (b) the  $\text{Mn}_4\text{Fe}_{1-x}\text{Cr}_x\text{SiB}_2$  ( $x = 0.0, 0.2, 0.4, 0.6, 0.8$  and  $1.0$ ) compounds at  $5\text{ K}$ . (c) Saturation magnetization as a function of the Cr content for the  $\text{Mn}_4\text{Fe}_{1-x}\text{Cr}_x\text{PB}_2$  and  $\text{Mn}_4\text{Fe}_{1-x}\text{Cr}_x\text{SiB}_2$  ( $x = 0.0, 0.2, 0.4, 0.6, 0.8$  and  $1.0$ ) compounds. Temperature-dependent magnetization of (d) the  $\text{Mn}_4\text{Fe}_{1-x}\text{Cr}_x\text{PB}_2$  and (e) the  $\text{Mn}_4\text{Fe}_{1-x}\text{Cr}_x\text{SiB}_2$  ( $x = 0.0, 0.2, 0.4, 0.6, 0.8$  and  $1.0$ ) compounds in a field of  $1\text{ T}$ . (f)  $T_C$  as a function of the Cr content for the  $\text{Mn}_4\text{Fe}_{1-x}\text{Cr}_x\text{PB}_2$  and  $\text{Mn}_4\text{Fe}_{1-x}\text{Cr}_x\text{SiB}_2$  ( $x = 0.0, 0.2, 0.4, 0.6, 0.8$  and  $1.0$ ) compounds.



**Fig. 7.7** Temperature-dependent isothermal magnetic entropy change  $|\Delta S_M|$  for (a) the  $\text{Mn}_4\text{Fe}_{1-x}\text{Cr}_x\text{PB}_2$  and (b) the  $\text{Mn}_4\text{Fe}_{1-x}\text{Cr}_x\text{SiB}_2$  ( $x = 0.0, 0.2, 0.4, 0.6, 0.8$  and  $1.0$ ) compounds in a field change of  $1\text{ T}$ . Field exponent of the magnetic entropy change  $n = \frac{d \ln(|\Delta S_M|)}{d \ln(H)}$  for (c) the  $\text{Mn}_4\text{Fe}_{1-x}\text{Cr}_x\text{PB}_2$  and (d) the  $\text{Mn}_4\text{Fe}_{1-x}\text{Cr}_x\text{SiB}_2$  ( $x = 0.0, 0.2, 0.4, 0.6, 0.8$  and  $1.0$ ) compounds.

### 7.3.2.3 Neutron diffraction study

Fig. 7.8 shows the neutron diffraction pattern and refinement of the  $\text{Mn}_4\text{Fe}_{0.5}\text{Cr}_{0.5}\text{Si}^{11}\text{B}_2$  compound in the PM and FM state. In the FM state, the compound has the same magnetic contribution to the pattern as observed for the mother compound  $\text{Mn}_5\text{Si}^{11}\text{B}_2$ , with a major contribution observable at the (123) and (204) peaks. This indicates that the  $\text{Mn}_4\text{Fe}_{0.5}\text{Cr}_{0.5}\text{Si}^{11}\text{B}_2$  compound has the same magnetic structure as the mother compound  $\text{Mn}_5\text{Si}^{11}\text{B}_2$ , i.e. the magnetic moments on the 16l and 4c sites are aligned in the *a-b* plane. The occupancy of Fe and Cr in the unit cell of the  $\text{Mn}_4\text{Fe}_{1-x}\text{Cr}_x\text{Si}^{11}\text{B}_2$  and  $\text{Mn}_4\text{Fe}_{1-x}\text{Cr}_x\text{P}^{11}\text{B}_2$  compounds obtained by ND refinement is shown in Fig. 7.9. Nominally, we doped 10% of Fe in our compound, and if Fe randomly occupies the 16l and 4c sites, the occupation should be close to 10% for both sites. In the  $\text{Mn}_4\text{Fe}_{0.5}\text{Cr}_{0.5}\text{Si}^{11}\text{B}_2$  compound the occupation of Fe on the 16l and 4c sites corresponds to 10.0% and 14.4%, respectively, which indicates a slight preference for the 4c site. This preference in occupancy is more obvious in the  $\text{Mn}_4\text{Fe}_{0.5}\text{Cr}_{0.5}\text{P}^{11}\text{B}_2$  compound, where the occupation is as high as 21.2% for the 4c site and 9.6% for the 16l site. This observation is consistent with the results observed in the  $\text{Mn}_{5-x}\text{Fe}_x(\text{Si},\text{P})^{11}\text{B}_2$  compounds in this Chapter. It is interesting to note that Cr exhibits the opposite preference in occupancy as Fe, as Cr prefers to occupy the 16l site. In the  $\text{Mn}_4\text{Fe}_{0.5}\text{Cr}_{0.5}\text{Si}^{11}\text{B}_2$  compound the occupation of Cr on the 16l and 4c sites is 12.2% and 7.8%, respectively. This preference for Cr on the 16l site is more visible in the  $\text{Mn}_4\text{Fe}_{0.5}\text{Cr}_{0.5}\text{P}^{11}\text{B}_2$  compound, where only 1% of the 4c site is occupied by Cr. Fig. 7.10 shows the total magnetic moment obtained from the refinement of the neutron diffraction data for the  $\text{Mn}_{5-x}\text{Fe}_x(\text{Si},\text{P})^{11}\text{B}_2$  and  $\text{Mn}_4\text{Fe}_{1-x}\text{Cr}_x(\text{Si},\text{P})^{11}\text{B}_2$  compounds. As mentioned in Chapter 5, Cr decreases the total magnetic moment (per formula unit) of the  $\text{Mn}_{5-x}\text{Cr}_x(\text{Si},\text{P})^{11}\text{B}_2$  compounds, while the introduction of Fe increases the total magnetic moment of the  $\text{Mn}_{5-x}\text{Fe}_x(\text{Si},\text{P})^{11}\text{B}_2$  compounds (see section 7.3.1). As the total magnetic moment of the  $\text{Mn}_4\text{Fe}_{0.5}\text{Cr}_{0.5}\text{Si}^{11}\text{B}_2$  and  $\text{Mn}_4\text{Fe}_{0.5}\text{Cr}_{0.5}\text{P}^{11}\text{B}_2$  compounds is lower than that of the mother compounds, the effect of Cr on the total magnetic moment is greater than that of Fe.

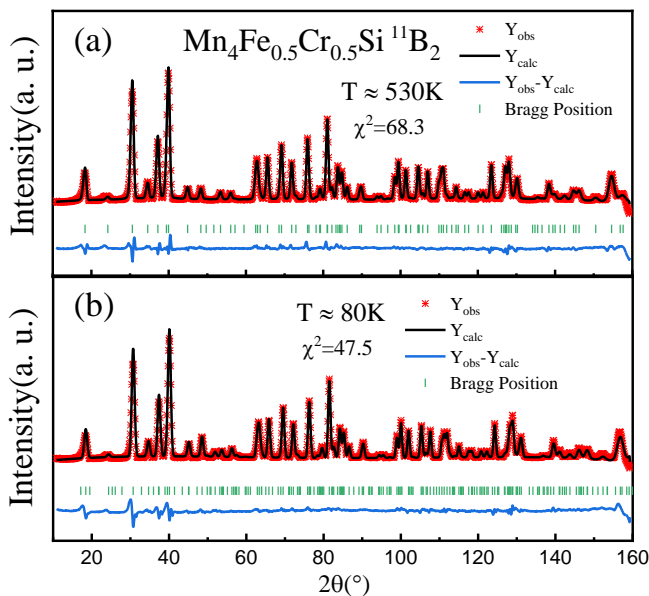


**Fig. 7.8** Neutron powder diffraction measurements and refinements for the  $\text{Mn}_4\text{Fe}_{0.5}\text{Cr}_{0.5}\text{Si}^{11}\text{B}_2$  compound in (a) the paramagnetic and (b) the ferromagnetic state.

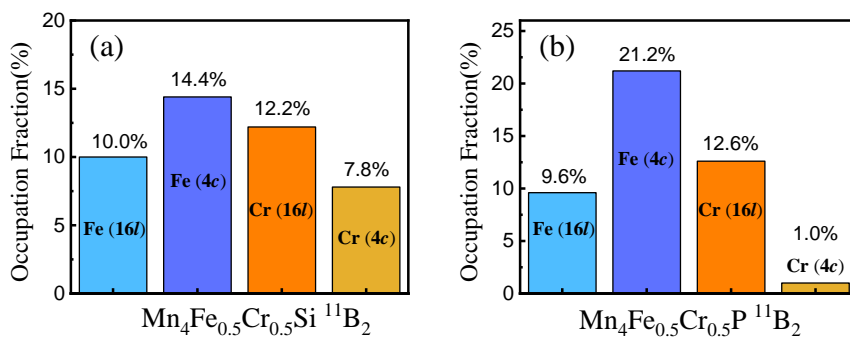


**Fig. 7.9** Occupation of Fe and Cr on the two magnetic sites 16l and 4c for (a) the  $\text{Mn}_4\text{Fe}_{0.5}\text{Cr}_{0.5}\text{Si}^{11}\text{B}_2$  and (b) the  $\text{Mn}_4\text{Fe}_{0.5}\text{Cr}_{0.5}\text{P}^{11}\text{B}_2$  compounds.

## Chapter 7 Effect of Simultaneous Doping of Fe and Cr on the Magnetocaloric Properties of $\text{Mn}_5(\text{Si,P})\text{B}_2$ Compounds

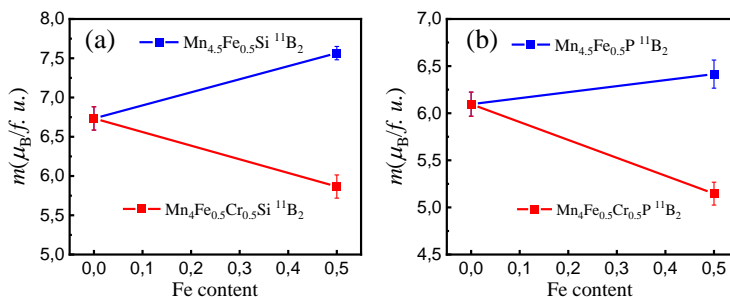


**Fig. 7.10** Total magnetic moment obtained from a refinement of the neutron diffraction data for (a) the  $\text{Mn}_{4.5}\text{Fe}_{0.5}\text{Si}_{11}\text{B}_2$  and  $\text{Mn}_4\text{Fe}_{0.5}\text{Cr}_{0.5}\text{Si}_{11}\text{B}_2$  compounds and for (b) the  $\text{Mn}_{4.5}\text{Fe}_{0.5}\text{P}_{11}\text{B}_2$  and  $\text{Mn}_4\text{Fe}_{0.5}\text{Cr}_{0.5}\text{P}_{11}\text{B}_2$  compounds.

### 7.4 Conclusions

In summary, Fe doping and simultaneous doping of Fe and Cr, has no significant effect on the main phase structure of the  $\text{Mn}_4(\text{Fe,Cr})(\text{Si,P})\text{B}_2$  compounds. The P-containing compounds are always accompanied by a certain amount of  $(\text{Mn,Fe})_2\text{P}$  impurity phase. The main phase of the Si-containing compounds is relatively stable, with no impurity phases. Fe increases both  $M_S$  and  $T_C$  of the  $\text{Mn}_{5-x}\text{Fe}_x(\text{Si,P})\text{B}_2$  compounds. For the  $\text{Mn}_{5-x}\text{Fe}_x\text{SiB}_2$  and  $\text{Mn}_{5-x}\text{Fe}_x\text{PB}_2$  compounds  $M_S$  increases from 105.6 and 91.1  $\text{Am}^2\text{kg}^{-1}$  ( $x = 0.0$ ) to 120.3 and 115.0  $\text{Am}^2\text{kg}^{-1}$  ( $x = 1.0$ ) and  $T_C$  increases from 406 and 305 K ( $x = 0.0$ ) to 506 and 412 K ( $x = 1.0$ ), respectively. The  $M_S$  and  $T_C$  values of the  $\text{Mn}_4\text{Fe}_{1-x}\text{Cr}_x(\text{Si,P})\text{B}_2$  compounds are sensitive to the Fe/Cr ratio. A higher concentration of Cr leads to a lower  $M_S$  and  $T_C$ . The  $T_C$  value of the  $\text{Mn}_4\text{Fe}_{1-x}\text{Cr}_x(\text{Si,P})\text{B}_2$  ( $x = 0.0, 0.2, 0.4, 0.6, 0.8$  and  $1.0$ ) compounds can be tuned continuously in the temperature range from 194 to 507 K by varying the Fe/Cr ratio. The  $|\Delta S_{M, \max}|$  value of the  $\text{Mn}_4\text{Fe}_{1-x}\text{Cr}_x(\text{Si,P})\text{B}_2$  compounds decreases with the Cr content. All the  $\text{Mn}_4\text{Fe}_{1-x}\text{Cr}_x(\text{Si,P})\text{B}_2$  compounds demonstrate a SOPT. The Mössbauer results show that Fe prefers to occupy the 4c site in the unit cell. The refinement of the ND results confirm this occupancy preference. In contrast to Fe, Cr prefers to occupy the 16l site. This preference for Cr is most pronounced in the  $\text{Mn}_4\text{Fe}_{1-x}\text{Cr}_x\text{P}_{11}\text{B}_2$  compounds. The refinement of the ND data shows that the  $\text{Mn}_{5-x}\text{Fe}_x(\text{Si,P})\text{B}_2$  and  $\text{Mn}_4\text{Fe}_{1-x}\text{Cr}_x(\text{Si,P})\text{B}_2$  compounds have the same magnetic structure as the mother compounds  $\text{Mn}_5(\text{Si,P})\text{B}_2$  and that the magnetic moments are aligned within the  $a$ - $b$  plane. The total magnetic moment of the compounds decreases with the Cr content, which is consistent with the SQUID magnetization measurements. The effect of Cr on the total magnetic moment in the  $\text{Mn}_4\text{Fe}_{1-x}\text{Cr}_x(\text{Si,P})\text{B}_2$  compounds is more pronounced than that of Fe.

## *Chapter 7 Effect of Simultaneous Doping of Fe and Cr on the Magnetocaloric Properties of $Mn_5(Si,P)B_2$ Compounds*

### References

- [1] M.A. McGuire and D.S. Parker, Magnetic and structural properties of ferromagnetic  $Fe_5PB_2$  and  $Fe_5SiB_2$  and effects of Co and Mn substitutions, *J. Appl. Phys.* 118 (2015) 163903.
- [2] M. Werwiński, Magnetic properties of  $Fe_5SiB_2$  and its alloys with P, S, and Co, *Phys. Rev. B* 93 (2016) 174412.
- [3] M. Werwiński, Magnetocrystalline anisotropy of  $Fe_5PB_2$  and its alloys with Co and 5d elements: A combined first-principles and experimental study, *Phys. Rev. B* 98 (2018) 214431.
- [4] J. Cedervall, E. Nonnet, D. Hedlund, L. Häggström, T. Ericsson, M. Werwiński, A. Edström, J. Rusz, P. Svedlindh, K. Gunnarsson, M. Sahlberg, Influence of Cobalt Substitution on the Magnetic Properties of  $Fe_5PB_2$ , *Inorg. Chem.* 57 (2018) 777.
- [5] J. Thakur, P. Rani, M. Tomar, V. Gupta, H.S. Saini, M.K. Kashyap, Tailoring in-plane magnetocrystalline anisotropy of  $Fe_5SiB_2$  with Cr-substitution, *AIP Conference Proceedings* 2115 (2019) 030506.
- [6] L. Häggström, R. Wäppling, T. Ericsson, Mössbauer and X-Ray Studies of  $Fe_5PB_2$ , *J. Solid State Chem.* 13 (1976) 84.
- [7] R. Wäppling, T. Ericsson, L. Häggström, Y. Andersson, Magnetic Properties of  $Fe_5SiB_2$  and related compounds, *J. Physique Colloques C6* (1976) 591.
- [8] T. Ericsson, L. Häggström, R. Wäppling, Spin Rotation in  $Fe_5SiB_2$ , *Phys. Scr.* 17 (1978) 83-86.
- [9] J. Cedervall, S. Kontos, T.C.Hansen, O. Balmes, F.J. Martinez-Casado, Z. Matej, P. Beran, P. Svedlindh, K. Gunnarsson, M. Sahlberg, Magnetostructural transition in  $Fe_5SiB_2$  observed with neutron diffraction, *J. Solid State Chem.* 235 (2016) 113.
- [10] T.N. Lamichhane, V. Taufour, S.Thimmaiah, D.S.Parker, S. L. Bud'ko, P.C. Canfield, A study of the physical properties of single crystalline  $Fe_5B_2P$ , *J. Magn. Magn. Mater.* 401 (2016) 525.
- [11] D. Hedlund, J. Cedervall, A. Edström, M. Werwiński, S. Kontos, O. Eriksson, J. Rusz, P. Svedlindh, M. Sahlberg, K. Gunnarsson, Magnetic properties of the  $Fe_5SiB_2$ - $Fe_5PB_2$  system, *Phys. Rev. B* 96 (2017) 094433.
- [12] L. van Eijck, L.D. Cussen, G.J. Sykora, E.M. Schooneveld, N.J. Rhodes, A.A. van Well, C. Pappas, Design and performance of a novel neutron powder diffractometer: PEARL at TU Delft, *J. Appl. Cryst.* 49 (2016) 1398.
- [13] H.M. Rietveld, A profile refinement method for nuclear and magnetic structures. *J. Appl. Cryst.* 2 (1969) 65.
- [14] J. Rodriguez-Carvajal, Recent advances in magnetic-structure determination by neutron powder diffraction, *Physica B* 192 (1993) 55.
- [15] O. Eriksson, A. Svane, Isomer shifts and hyperfine fields in iron compounds, *J. Phys.: Condens. Matter* 1 (1989) 1589.

*Chapter 7 Effect of Simultaneous Doping of Fe and Cr on the  
Magnetocaloric Properties of  $Mn_5(Si,P)B_2$  Compounds*

- [16] C.T. Zhou, J.D. Xing, B. Xiao, J. Feng, X.J. Xie, Y.H. Chen, First principles study on the structural properties and electronic structure of  $X_2B$  ( $X = Cr, Mn, Fe, Co, Ni, Mo$  and  $W$ ) compounds, *Comput. Mater. Sci.* 44 (2009) 1056.
- [17] J.Y. Law, V. Franco, L.M. Moreno-Ramírez, A. Conde, D.Y. Karpenkov, I. Radulov, K.P. Skokov, O. Gutfleisch, A quantitative criterion for determining the order of magnetic phase transitions using the magnetocaloric effect, *Nature Comm.* 9 (2018) 2680.
- [18] C.P. Bean and D.S. Rodbell, Magnetic disorder as a first-order phase transformation, *Phys. Rev.* 126 (1962) 104.
- [19] N.H. van Dijk, Landau model evaluation of the magnetic entropy change in magnetocaloric materials, *J. Magn. Magn. Mater.* 529 (2021) 167871.
- [20] L.D. Landau, On the theory of phase transitions. I., *Zh. Eksp. Teor. Fiz.* 7 (1937) 19.

## Summary

The  $M_5XB_2$  ( $M = \text{Fe, Mn, V, Cr}$  and  $X = \text{Si, P}$ ) materials system was previously studied for permanent magnet applications. However, some of the compounds in this materials system exhibit considerable room-temperature magnetocaloric effects. This thesis presents a study of the crystal structure, magnetic structure and the magnetocaloric effect in  $M_5XB_2$  compounds.

All the  $M_5(\text{Si,P})B_2$  ( $M = \text{Mn, Fe, V, Cr}$ ) compounds studied in this thesis crystallize in the tetragonal  $\text{Cr}_5\text{B}_3$ -type structure ( $I4/mcm$  symmetry). The  $3d$  metal atoms  $M$  ( $M = \text{Mn, Fe, V, Cr}$ ) occupy the  $16l$  and  $4c$  sites, Si/P share the  $4a$  site, and B occupies the  $8h$  site.  $M_5\text{PB}_2$  compounds are accompanied by different amounts of the  $(\text{Mn,Fe})_2\text{P}$  impurity phase. Fe increases the amount of  $(\text{Mn,Fe})_2\text{P}$  impurity phase. For the  $M_5\text{SiB}_2$  compounds, V doping introduces a new  $\text{Mn}_2\text{B}$  impurity phase, while other  $M_5\text{SiB}_2$  compounds are quite stable without any impurity phase. Lattice parameters  $a$  and  $c$  and the unit-cell volume  $V$  of the  $M_5(\text{Si,P})B_2$  compounds decrease with the P and Fe content and increase with the Cr and V content. As a result of a significant magneto-elastic coupling in the ferromagnetic state,  $\text{Mn}_5\text{SiB}_2$  exhibits a negative thermal expansion between 360 and 400 K. It is found that Fe prefers to occupy the  $4c$  site, while Cr prefers to occupy the  $16l$  site in the unit cell. This preference in occupancy is more pronounced in the  $M_5\text{PB}_2$  ( $M = \text{Mn, Fe, Cr}$ ) compounds.

In the  $M_5(\text{Si,P})B_2$  compounds a ferromagnetic ordering was observed below the transition temperature, without a spin reorientation at lower temperatures. The saturation magnetization and the Curie temperature of the compounds strongly dependent on the Si/P ratio and on the different  $3d$  metal concentrations in the  $M_5(\text{Si,P})B_2$  ( $M = \text{Mn, Fe, V, Cr}$ ) system. When the P, Cr and V content increases, the saturation magnetization and the Curie temperature of the compounds decrease. The introduction of Fe increases the saturation magnetization and the Curie temperature of the compounds. The saturation magnetization of the compounds studied in this thesis varies from 70.54 to 120.30  $\text{Am}^2\text{kg}^{-1}$  depending on composition, while the Curie temperature can be adjusted continuously from 194 to 507 K. For a temperature change of 30 K (around the transition) in a field of 1 T the  $\text{Mn}_5\text{PB}_2$  and  $\text{Mn}_5\text{Si}_{0.5}\text{P}_{0.5}\text{B}_2$  compounds present a change in magnetization of  $\Delta M$  of 28.1 and 31.1  $\text{Am}^2\text{kg}^{-1}$ , respectively. The  $\Delta M$  values of these two compounds are comparable to those for Heusler alloys.

The phase transition of the compounds corresponds to a typical SOPT. A discontinuous step in the specific heat capacity without latent heat is observed at the transition temperature. The heating and cooling  $M$ - $T$  curves of the compounds coincide without

thermal hysteresis. The field exponent for the magnetic entropy change  $n$  shows no increase beyond a value of 2 near the transition temperatures and all compounds exhibit a minimum value  $n_{\min}$  that is slightly larger than  $2/3$ . The maximum isothermal magnetic entropy change  $|\Delta S_{M, \max}|$  decreases with the P, Cr, V content.

All the  $M_5(\text{Si,P})^{11}\text{B}_2$  ( $M = \text{Mn, Fe, V, Cr}$ ) compounds have the same magnetic structure, a ferromagnetic ordering with propagation vector  $\mathbf{k} = (0,0,0)$  and two different magnetic sites ( $16l$  and  $4c$ ) in the unit cell. The magnetic moments on the  $16l$  and  $4c$  sites are oriented within the  $a$ - $b$  plane. Although the Si/P ratio and different  $3d$  metal concentrations do not change the magnetic structure of the compounds, they do have a varying influence on the magnetic moment on the two magnetic sites and the total magnetic moment per formula unit. Fe increases the total magnetic moment of the compounds, while P, Cr and V result in a decrease.

Although the compounds are not competitive for magnetic cooling due to their lower value for  $|\Delta S_M|$ , the considerable  $\Delta M$ , without latent heat and without thermal hysteresis, in combination with the continuously adjustable  $T_C$  in the temperature range above room temperature (for example, compounds  $\text{Mn}_5\text{Si}_{1-x}\text{P}_x\text{B}_2$  ( $x=0.5-0.8$ ) have  $T_C$  between 315 to 350 K, with  $\Delta M/\Delta Q = 1.44, 1.54$  and  $1.44 \text{ Am}^2/\text{kJ}$  respectively), makes them promising candidate materials for magnetocaloric energy harvesting applications.

## Samenvatting

Het  $M_5XB_2$  ( $M = \text{Fe, Mn, V, Cr}$  en  $X = \text{Si, P}$ ) materiaalsysteem was eerder onderzocht voor toepassingen als permanente magneten. Echter, enkele van de verbindingen in dit materiaalsysteem vertonen aanzienlijke magnetocalorische effecten bij kamertemperatuur. Dit proefschrift beschrijft een studie naar de kristalstructuur, de magnetische structuur en het magnetocalorische effect in  $M_5XB_2$  verbindingen.

Alle in dit proefschrift bestudeerde  $M_5(\text{Si,P})B_2$  ( $M = \text{Mn, Fe, V, Cr}$ ) verbindingen vertonen een tetragonale  $\text{Cr}_5\text{B}_3$ -type structuur ( $I4/mcm$  symmetrie). De  $3d$  metaalatonen  $M$  ( $M = \text{Mn, Fe, V, Cr}$ ) bezetten de  $16l$  en  $4c$  posities, Si/P deelt de  $4a$  positie en B bezet de  $8h$  positie.  $M_5\text{PB}_2$  verbindingen worden vergezeld door verschillende hoeveelheden van de  $(\text{Mn,Fe})_2\text{P}$  onzuiverheidsfase. Fe verhoogt de hoeveelheid van de  $(\text{Mn,Fe})_2\text{P}$  onzuiverheidsfase. Voor de  $M_5\text{SiB}_2$  verbindingen introduceert V doping een nieuwe  $\text{Mn}_2\text{B}$  onzuiverheidsfase, terwijl de andere  $M_5\text{SiB}_2$  verbindingen vrij stabiel zijn zonder onzuiverheidsfasen. De roosterparameters  $a$  en  $c$  en het volume van de eenheidscel  $V$  van de  $M_5(\text{Si,P})B_2$  verbindingen nemen af met de toegevoegde hoeveelheid P en Fe en nemen toe met de toegevoegde hoeveelheid Cr en V. Vanwege de aanwezigheid van een aanzienlijke magneto-elastische koppeling in de ferromagnetische toestand vertoont  $\text{Mn}_5\text{SiB}_2$  een negatieve thermische uitzetting tussen 360 en 400 K. Er is gevonden dat Fe een voorkeur heeft om de  $4c$  positie te bezetten, terwijl Cr een voorkeur heeft om de  $16l$  positie te bezetten binnen de eenheidscel. Deze voorkeur in bezetting is meer uitgesproken in de  $M_5\text{PB}_2$  ( $M = \text{Mn, Fe, Cr}$ ) verbindingen.

Voor de  $M_5XB_2$  verbindingen was een ferromagnetische ordening waargenomen onder de overgangstemperatuur zonder een spin-reoriëntatie bij lagere temperaturen. De verzadigingsmagnetisatie en de Curie temperatuur van de verbindingen hangt sterk af van de Si/P verhouding en van de verschillende concentraties van  $3d$  metalen in het  $M_5(\text{Si,P})B_2$  ( $M = \text{Mn, Fe, V, Cr}$ ) system. Wanneer de hoeveelheid P, Cr en V toeneemt, dan nemen de verzadigingsmagnetisatie en de Curie temperatuur van deze verbindingen af. De introductie van Fe leidt tot een toename van de verzadigingsmagnetisatie en van de Curie temperatuur van de verbindingen. De verzadigingsmagnetisatie van de in dit proefschrift bestudeerde verbindingen varieert afhankelijk van de samenstelling van 70.54 tot 120.30  $\text{Am}^2\text{kg}^{-1}$ , terwijl de Curie temperatuur continu kan worden ingesteld in het temperatuurgebied van 194 tot 507 K. Voor een temperatuursverandering van 30 K (rond de overgang) in een veld van 1 T vertonen de  $\text{Mn}_5\text{PB}_2$  en  $\text{Mn}_5\text{Si}_{0.5}\text{P}_{0.5}\text{B}_2$  verbindingen een verandering in magnetisatie  $\Delta M$  van respectievelijk 28.1 en 31.1  $\text{Am}^2\text{kg}^{-1}$ . De waarden van  $\Delta M$  voor deze twee verbindingen zijn vergelijkbaar met die voor Heusler legeringen.

De faseovergang van de verbindingen komt overeen met een karakteristieke SOPT. Een discontinue stap in de soortelijke warmtecapaciteit zonder latent warmte is waargenomen bij de overgangstemperatuur. De  $M$ - $T$  curves voor opwarmen en afkoelen van de legeringen vallen samen zonder hysteresis. De veldexponent voor de magnetische  $n$  laat zien dat er geen toename is tot waarden boven de 2 rond de overgangstemperatuur en dat alle verbindingen een minimum waarde  $n_{\min}$  vertonen die iets groter zijn dan  $2/3$ . De maximale isotherme magnetische entropieverandering  $|\Delta S_{M, \max}|$  neemt af met de hoeveelheid P, Cr en V.

Alle  $M_5(\text{Si,P})^{11}\text{B}_2$  ( $M = \text{Mn, Fe, V, Cr}$ ) verbindingen vertonen dezelfde magnetische structuur, een ferromagnetische ordening met een propagatie-vector  $\mathbf{k} = (0,0,0)$  en twee magnetische posities (16l and 4c) in de eenheidscel. De magnetische momenten op de 16l en 4c posities zijn gericht in het  $a$ - $b$  vlak. Hoewel de Si/P verhouding en de verschillende 3d metaal-concentraties geen invloed hebben op de magnetische structuur van de verbindingen, hebben ze wel van invloed op het magnetische moment op de twee magnetische posities en op het totale magnetische moment per formule-eenheid. Fe verhoogt het totale magnetische moment van de verbindingen, terwijl P, Cr en V leiden tot een afname.

Hoewel deze verbindingen niet concurrerend zijn voor magnetische koeling vanwege de lagere waarden voor  $|\Delta S_M|$ , maken de aanzienlijke waarde van  $\Delta M$ , zonder latente warmte en zonder hysteresis, in combinatie met de continu instelbare waarde van  $T_C$  in het temperatuurgebied boven kamertemperatuur ze wel veelbelovende kandidaat-materialen voor magnetocalorische energieconversie toepassingen.

## Outlook

The investigation of the novel room-temperature magnetocaloric material system  $M_5XB_2$  ( $M = \text{Fe, Mn, V, Cr, and X = Si, P}$ ) suggests that it may not have significant advantages in the field of magnetic refrigeration, however, it offers great potential in the field of energy harvesting. Through my doping work, I expect to provide new possibilities and directions for improvements in the performance of this material system. Here are some perspectives on future research and applications:

**Optimize Doping Strategies:** Further try other feasible alternative elements, study the electronic structure and magnetic properties of the material, and optimize the room temperature magnetocaloric effect to obtain better magnetocaloric properties.

**Preparation methods:** Due to limitations of experimental conditions, some of my doping work did not achieve the expected results. For instance, Co, Ni, C, and Sn doping did not yield samples with desirable single-phase. Subsequent research endeavors could explore alternative preparation methods to address this challenge and enhance the material's phase properties.

**Engineered Energy Harvesting Applications:** Given the potential applications of this material system in the field of energy harvesting, future research could focus on engineering designs for effective applications in practical energy conversion devices. This may include developing new energy harvesting devices or optimizing existing energy conversion technologies.

Overall, the prospects of this new room-temperature magnetocaloric material system in the field of energy harvesting provide a broad space for future research, and my doping work provides a useful basis for further optimizing material properties and applications. These prospects will help guide future research directions and promote the practical application and development of this material system.



## Appendix

**Table 1** transition temperature  $T_C$ , saturation magnetization  $M_S$ , lattice parameters  $a$  and  $c$ , unit-cell volume  $V$ , density  $d$ ,  $\Delta M$  and maximum magnetic entropy change  $\Delta S_M$  for the compounds studied in thesis. The  $M_S$  from SQUID magnetometer measurements at 5 K and  $T_C$  from SQUID magnetometer measurements in an applied field of 0.01 T, lattice parameters, unit-cell volume and density were obtained by room-temperature XRD,  $\Delta M$  is the difference in magnetization for a temperature span of  $\Delta T = T_{\text{hot}} - T_{\text{cold}} = 30$  K, and  $\Delta S_M$  was calculated by  $M$ - $T$  data in 0-1 T.

	$x$	$M_S$ (Am <sup>2</sup> kg <sup>-1</sup> )	$T_C$ (K)	$a$ (Å)	$c$ (Å)	$V$ (Å <sup>3</sup> )	$d$ (kgm <sup>-3</sup> )	$\Delta M$ (Am <sup>2</sup> kg <sup>-1</sup> )	$\Delta S_M$ (Jkg <sup>-1</sup> K <sup>-1</sup> )
Mn <sub>5</sub> Si <sub>1-x</sub> P <sub>x</sub> B <sub>2</sub>	0	105.56	406	5.61032(4)	10.44349(9)	328.716(5)	6.570	31.3	1.90
	0.1	101.54	398	5.60345(5)	10.44529(11)	327.968(5)	6.670	31.8	---
	0.2	105.17	386	5.59878(4)	10.44915(9)	327.543(4)	6.670	29.8	---
	0.3	102.17	374	5.59174(4)	10.45302(8)	326.840(4)	6.617	30.1	---
	0.4	101.16	359	5.58316(4)	10.45688(9)	325.959(4)	6.611	31.2	---
	0.5	97.33	346	5.57184(4)	10.45612(11)	324.614(5)	6.663	31.1	1.33
	0.6	100.43	339	5.56262(5)	10.45959(11)	323.648(5)	6.772	32.4	---
	0.7	97.75	329	5.55612(4)	10.46460(9)	323.047(4)	6.713	29.4	---
	0.8	99.25	318	5.54635(4)	10.46912(8)	322.051(4)	6.736	32.1	---
	0.9	94.12	309	5.53888(4)	10.47478(9)	321.358(4)	6.707	28.9	---
	1	91.07	305	5.53276(6)	10.47474(12)	320.647(6)	6.869	28.1	1.35
Mn <sub>5-x</sub> Cr <sub>x</sub> SiB <sub>2</sub>	0.1	104.59	396	5.60825(2)	10.43196(6)	328.111(3)	6.543	30.15	1.76
	0.2	99.20	374	5.60647(4)	10.42993(9)	327.839(4)	6.554	31.69	---
	0.3	97.31	363	5.60594(4)	10.42817(9)	327.722(4)	6.557	29.57	1.46
	0.4	93.21	356	5.60399(4)	10.42395(8)	327.361(4)	6.564	26.00	---
	0.5	92.96	345	5.60415(3)	10.42335(6)	327.361(3)	6.564	26.97	1.27
	1	85.20	291	5.61175(3)	10.43169(5)	328.512(3)	6.636	21.25	0.88

	$x$	$M_S$ (Am <sup>2</sup> kg <sup>-1</sup> )	$T_C$ (K)	$a$ (Å)	$c$ (Å)	$V$ (Å <sup>3</sup> )	$d$ (kgm <sup>-3</sup> )	$\Delta M$ (Am <sup>2</sup> kg <sup>-1</sup> )	$\Delta S_M$ (Jkg <sup>-1</sup> K <sup>-1</sup> )
Mn <sub>5-x</sub> Cr <sub>x</sub> PB <sub>2</sub>	0.1	87.16	291	5.53081(1)	10.46306(7)	320.064(2)	6.767	27.18	1.30
	0.2	91.60	281	5.53142(3)	10.46296(3)	320.131(3)	6.766	28.60	---
	0.3	86.34	273	5.53184(3)	10.46312(6)	320.185(3)	6.803	26.18	1.45
	0.4	81.04	261	5.53319(3)	10.46381(7)	320.362(3)	6.573	24.85	---
	0.5	74.21	255	5.53363(3)	10.46201(6)	320.357(3)	6.574	21.02	1.11
	1	70.62	194	5.54156(3)	10.45684(7)	321.118(3)	6.740	20.12	0.89
Mn <sub>5-x</sub> V <sub>x</sub> SiB <sub>2</sub>	0.1	106.76	392	5.60448(3)	10.43108(4)	327.642(3)	6.613	32.68	---
	0.2	104.83	388	5.60780(1)	10.43895(3)	328.278(2)	6.503	30.36	---
	0.3	97.60	376	5.61205(1)	10.44797(3)	329.060(1)	6.422	28.64	1.65
	0.4	92.59	368	5.61287(1)	10.45153(4)	329.268(2)	6.509	26.32	---
	0.5	80.73	367	5.61153(2)	10.4493(7)	329.041(3)	6.519	20.86	0.98
Mn <sub>5-x</sub> V <sub>x</sub> PB <sub>2</sub>	0.1	97.29	298	5.53327(1)	10.46967(5)	320.551(3)	6.714	31.00	---
	0.2	93.41	289	5.53766(2)	10.47855(6)	321.332(3)	6.671	29.48	---
	0.3	91.41	283	5.54142(3)	10.4852(6)	321.972(3)	6.702	27.50	1.32
	0.4	88.65	276	5.54627(3)	10.49316(6)	322.782(3)	6.691	26.41	---
	0.5	83.73	271	5.55123(3)	10.50342(6)	323.675(3)	6.754	24.15	1.10
	1	70.54	223	5.58574(4)	10.56129(13)	329.518(5)	6.775	18.25	0.82
Mn <sub>5-x</sub> Fe <sub>x</sub> SiB <sub>2</sub>	0.5	112.3	454	5.59958(4)	10.42231(5)	326.794(5)	6.570	---	---
	1	120.3	506	5.59971(1)	10.41995(5)	326.736(2)	6.573	---	---
Mn <sub>5-x</sub> Fe <sub>x</sub> PB <sub>2</sub>	0.5	109.33	357	5.52773(4)	10.45280(9)	319.394(4)	6.783	---	---
	1	115.00	412	5.52497(4)	10.43965(11)	318.674(5)	6.794	---	---
Mn <sub>4</sub> Fe <sub>1-x</sub> Cr <sub>x</sub> SiB <sub>2</sub>	0.2	113.01	455	5.60123(2)	10.42544(5)	327.085(2)	6.578	26.76	---
	0.4	109.03	418	5.60710(2)	10.43276(5)	328.002(2)	6.551	25.53	1.15
	0.6	103.18	370	5.60857(1)	10.43338(5)	328.193(2)	6.548	25.70	---
	0.8	86.22	327	5.60919(1)	10.43090(4)	328.188(2)	6.548	20.77	0.87
	1	85.20	291	5.61343(1)	10.43466(5)	328.795(2)	6.536	21.25	0.88

	$x$	$M_S$ (Am <sup>2</sup> kg <sup>-1</sup> )	$T_C$ (K)	$a$ (Å)	$c$ (Å)	$V$ (Å <sup>3</sup> )	$d$ (kgm <sup>-3</sup> )	$\Delta M$ (Am <sup>2</sup> kg <sup>-1</sup> )	$\Delta S_M$ (Jkg <sup>-1</sup> K <sup>-1</sup> )
Mn <sub>4</sub> Fe <sub>1-x</sub> Cr <sub>x</sub> PB <sub>2</sub>	0.2	90.53	362	5.52500(2)	10.44197(6)	318.480(2)	6.795	20.10	---
	0.4	86.19	319	5.52814(2)	10.45197(6)	319.415(2)	6.781	21.24	0.98
	0.6	72.23	278	5.52884(2)	10.45488(6)	319.586(2)	6.777	17.99	---
	0.8	74.23	236	5.53506(1)	10.45818(5)	320.406(2)	6.760	19.68	0.88
	1	70.22	194	5.53907(2)	10.45229(6)	320.690(2)	6.754	20.12	0.88



### **Acknowledgements**

My doctoral journey, spanning over four years, is coming to an end. As I reflect on this experience, I am filled with profound emotion. On March 16, 2019, I arrived in Delft with a longing for the unknown and a yearning for a completely different life. In stark contrast, I had great difficulty adjusting to the language and the environment in the first six months. It was not a very happy time in life during that period. Nevertheless, with the passage of time, I grew to appreciate this place and the people. One year later, the unexpected outbreak of COVID-19 disrupted all plans. I am uncertain whether encountering this epidemic during my PhD career is a stroke of luck or misfortune. Fortunately, a year later, all things gradually returned to normal, enabling me to successfully complete my doctoral work. Throughout these four years, I have received assistance from a number of individuals. I would not have been able to complete my doctoral project without their support.

Firstly, I would like to sincerely thank my supervisor Prof. **Ekkens Brück**. We met for the first time in September 2017 at the International Conference on Magnetic Refrigeration Materials in Baotou, China. I presented my master's research in the conference. It was my first time presenting in English, and I was quite nervous; Ekkens was also present. After the meeting, through Prof. Tegus' introduction, I was able to meet Ekkens. I expressed my desire to continue my studies in the FAME group, and you informed me that there were currently no PhD positions available. However, you told me that if there is a need for a PhD student, you would notify me. Honestly, I felt somewhat discouraged at that time, sensing that opportunities were scarce. However, a year later, you reached out through your secretary, informing me that there is a project required a PhD student. I was surprised to hear this news because I thought you might have forgotten about a master's student who had recommended themselves a year ago. I appreciate that you remembered my self-recommendation, as it marked the beginning of everything that followed. In 2019, I joined the FAME group, marking the beginning of my doctoral journey. Throughout these four years, our communication has consistently been both pleasant and efficient. Your responsibility and patience in addressing my questions have been commendable. Whenever experiments encountered challenges, your suggestions were instrumental in overcoming obstacles. Beyond monitoring the project's progress, you also offered valuable insights into my doctoral courses and regularly checked in on my overall progress. Thanks to your support, I had the privilege of engaging in various international academic conferences and summer schools. These experiences not only broadened my perspectives but also expanded my professional network. The valuable insights gained from working with you will undoubtedly benefit me throughout my life.

## *Acknowledgements*

I want to express my gratitude to my co-promotor, **Niels van Dijk**. Thank you for your guidance over the past four years. Discussions with you always inspire me a lot, and each time, you start from the most fundamental physical concepts, guiding me step by step through the practical issues encountered in experiments and data analysis. In my second year of the PhD, I was supplementing my knowledge in solid-state physics and quantum mechanics, I often turned to you when facing challenging and hard-to-understand problems. Your patient explanations continued until I grasped the concepts. Your solid academic expertise demonstrated in these discussions has truly impressed me. In addition to our academic interactions, chatting with you has always been enjoyable. I've heard many interesting stories about Europe and the Netherlands. The exploration trip with you and your wife, **Cécile**, in Amsterdam remains vivid in my memory. The itinerary was well-organized, fun, and thoroughly enjoyable. Thank you! It has been an honor to work with you for four years.

I sincerely thank all the wonderful colleagues in the FAME group. It's hard to imagine how I could have completed my doctoral project without your help. Special thanks to **Anton** for his support and maintaining all the instruments, ensuring the smooth progress of our experiments. Thanks to **Bert** for teaching me how to use the sealing system-a skill that has greatly benefited me and allowed me to independently manage my experiment processes. I thoroughly enjoy our pleasant chats every Friday and appreciate the activities you organized, such as windmill sightseeing, watching football matches, and your birthday parties. Gratitude to **Kees** and **Michel Steenvoorden** for training me on XRD and providing technical support. Thanks to **Robert** and **Michel Thijs** for helping me with Neutron diffraction and providing crucial support. These techniques are essential for my doctoral project. Thank you, **Iulian**, for your assistance with Mossbauer. Not only did you help with Mossbauer measurements, but our discussions also enriched my knowledge, enabling powerful analysis when combined with other experimental data. **Qi Shen**, every discussion with you sparks more ideas. **Anika**, it has been a pleasure working in the same office for four years and I always enjoyed talking to you about music and motorcycles during breaks. **Fengqi**, the attitude you have toward your work is admirable, and I am confident that you will have a successful academic career in the future. Thanks to **Ivan**, without your calculations and literature searches, I wouldn't have been able to explore new material systems. **Liu jun**, **Bowei**, **Xinmin**, **Yifan** and **Michael**, your friendliness when I first arrived in Delft helped me quickly integrate into the group. **Ilse** and **Nicole**, thank you for your support. Every conference attendance and communication with HR wouldn't have been possible without your assistance. I also want to express my gratitude to **Jan Leen Kloosterman**, **Anna Smith**, **Wim Bouwman**, **Henk Schut** and **Stephan Eijt**. **Ziying** I feel honored to have spent time with you during my academic journey.

## *Acknowledgements*

I also want to express my gratitude to all the students I have supervised. **Stijn**, you were my first student at TU Delft, and our collaboration taught me a lot. In particular, my English improved significantly during that time. **Brammert**, your work in the lab was the highest I've seen among Bachelor students. Your experimental results greatly assisted my subsequent work. Thank you for inviting Hanggai and me to your home for dinner, we thoroughly enjoyed it. **Maarten**, you always carry yourself with confidence, a trait I truly appreciate. We overcame many challenges together at work, especially your impressive performance in handling neutron diffraction data. Your proactive approach to difficulties and positive mindset are commendable. **Justin**, thank you for your contributions to the work on W-doping. I hope you have a bright future ahead.

Thank you to my master's supervisor, Prof. **Tegus**. It is you who guided me into the research field of magnetocaloric. Your teachings have not only given me academic knowledge, but also your life philosophy that will influence me for the rest of my life. Thanks to Prof. Tegus' wife, **Dagula**, for providing me with a familial warmth in a foreign land.

I want to express my gratitude to my friends. **Otton**, although we are thousands of kilometers apart and don't communicate frequently, as my best friend, every conversation with you is relaxed and enjoyable, devoid of any sense of distance. The snippets you share always make me feel that I'm not so far away from hometown. I wish your two children a healthy and happy growth, and my best wishes to you and your family. **Hanggai**, we worked in the same office for three years and lived in the same apartment for one year. We shared many enjoyable moments, discussing academic issues and sharing bits of our lives. I have fond memories of the fantastic trip to Belgium we went on last year with your girlfriend Orilige and my girlfriend Uyinga. My birthday cake you and **Orilige** gave me is still fresh in my mind. Thanks also for the numerous invitations to your home. **Yiliqi** and **Narisu**, thank you for inviting us to celebrate the Chinese New Year and New Year at your home. Narisu's culinary skills and photography talents are amazing, helping us capture many beautiful moments. **Darkhan**, **Habur** and **Ganderi**, the time spent with you is always filled with joy and laughter. Wishing you both a wonderful future. **Baljinnyam**, thank you for always being so welcoming, I miss the days when we used to watch football games together. May you and your wife have a life filled with happiness and bliss, and may your son **Tomoo** grow up to be strong and healthy.

Lastly, I want to express my gratitude to my family. To my father, **Erdenbaater**, even though you have left us, all the memories you left behind are the most precious wealth for our family. Thank you for bringing me into this world, allowing me to experience everything it has to offer. To my mother, **Garhahongor**, after our father's passing, you single-handedly raised the three of us siblings. I deeply understand how challenging it is

## *Acknowledgements*

to be a single mother. You've always been selfless, respecting every decision I make in life and providing full support. Without your dedicated efforts, the three of us siblings wouldn't have the lives we have today. My sisters, **Seqenqimeg** and **Seqengerel**, thank you for your selfless support over the years and for taking care of Mom, allowing me to pursue my dreams without worrying about her. My beloved niece, **Hairhan**, you are the first next generation in our family, and your arrival has brought endless joy. Now that you've grown up and are about to enter university, wish you a life full of happiness. My dear, **Uyinga**, thank you for coming into my life. In moments of hardship and confusion, you consistently offer unwavering support and care, filling my life with boundless warmth. As we journey through life together, I eagerly anticipate the bright future that awaits us. Your presence has brought joy, stability, and a profound sense of companionship to my life. May we continue to share our dreams, navigate challenges, and create countless cherished memories together.

Please accept my thanks to everyone who has been part of my life!

Hamutu Ojiyed

December 2023

### List of Publications

#### Publications related to the PhD study

1. **H. Ojiyed**, M. van den Berg, I. Batashev, Q. Shen, N.H. van Dijk and E. Brück, *Magnetocaloric properties of  $Mn_5(Si,P)B_2$  compounds for energy harvesting applications*, under review.
2. **H. Ojiyed**, B.E. Habing, M. van den Berg, N.H. van Dijk and E. Brück, *Effect of Cr doping on the Magnetocaloric Properties of  $Mn_5(Si,P)B_2$  Compounds*, in preparation.
3. **H. Ojiyed**, A. Kiecana, N.H. van Dijk and E. Brück, , *Effect of V doping on the Magnetocaloric Properties of  $Mn_5(Si,P)B_2$  Compounds*, in preparation.
4. **H. Ojiyed**, W. Hanggai, N.H. van Dijk and E. Brück, *Effect of Simultaneous Doping of Fe and Cr on Magnetocaloric Properties of  $Mn_5(Si,P)B_2$  Compounds*, in preparation.
5. A. Kiecana, W. Schaefer, M. Thijs, R. Dankelman, **H. Ojiyed**, I. Batashev, F. Zhang, N.H. van Dijk, E. Brück, *Competing magnetic interactions, structure and magnetocaloric effect in  $Mn_3Sn_{1-x}Zn_xC$  antiperovskite carbides*, J. Magn. Mater. 577, (2023) 170782.
6. Q. Shen, I. Batashev, F. Zhang, **H. Ojiyed**, I. Dugulan, N.H. van Dijk, E. Brück, *Exploring the negative thermal expansion and magnetocaloric effect in  $Fe_2(Hf,Ti)$  Laves phase materials*, Acta Materialia 257, (2023) 119149.
7. Q. Shen, I. Batashev, **H. Ojiyed**, F. Zhang, N.H. van Dijk, E. Brück, *Nonlinear influence of excess Mn on the magnetoelastic transition in  $(Mn,Cr)_2Sb$* , J. Alloy. Compd. 903, (2022) 164011.
8. F. Zhang, C. Taake, B. Huang, X. You, **H. Ojiyed**, Q. Shen, I. Dugulan, L. Caron, N.H. van Dijk, E. Brück, *Magnetocaloric effect in the  $(Mn,Fe)_2(P,Si)$  system: From bulk to nano*, Acta Materialia 224, (2022) 117532.
9. Q. Shen, I. Batashev, F. Zhang, **H. Ojiyed**, N.H. van Dijk, E. Brück, *The antiferromagnetic to ferrimagnetic phase transition in  $Mn_2Sb_{1-x}Bi_x$  compounds*, J. Alloy. Compd. 866 (2021) 158963

## List of Publications

### Publications related to the Master study

10. **H. Ojiyed**, L. Yingjie, O. Zhiqiang, Narsu, S. Zhiqiang, O. Hascholu, B. Tana, H. Jiaohong, O. Tegus, *Effect of Cu doping on mechanical and magnetic properties of  $Mn_{1.28}Fe_{0.67}P_{0.48}Si_{0.52}$  compound*. J. Funct. Mater. 1001-9731, (2018) 01-01139-06.
11. **H. Ojiyed**, H. Oimod, O. Tegus, *Magnetism and Mechanical Properties of  $Mn_{1.28}Fe_{0.67}P_{0.48}Si_{0.52}/Cu$  Composites*, Solid State Phenomena, 288, (2019) 104-112.

### Conference presentations

1. Visual oral presentation: “*Magnetocaloric Properties of a New Type of Magnetocaloric Materials -  $M_5XB_2$  System*” in 2022 Joint MMM-Intermag Conference, Mar 2022.
2. Visual oral presentation: “*Structural and Magnetocaloric Properties in  $Mn_5SiB_2$ - $Mn_5PB_2$  Compounds*” in 2021 AtC-AtG Magnetic Conference, Aug 2021.
3. Poster: “*structure and magnetocaloric properties in  $Mn_5(Si,P)B_2$  compounds*”, in The International Conference on Strongly Correlated Electron Systems 2022, Jul 2022.
4. Poster: “*Effect of V-doping on the Magnetic Transition of Fe-rich  $(Mn,Fe)_{1.9}(P,Si)$  Compounds*” in 65th Annual Conference on Magnetism and Magnetic Materials, Nov 2020.
5. Poster: “*Exploration in new room temperature magnetocaloric materials: structure and magnetocaloric properties in  $Mn_5(Si,P)B_2$  compounds*”, in the 2023 IEEE/ASME International Conference on Advanced Intelligent Mechatronics, Jan 2023.
6. Poster: “*Exploration in new room temperature magnetocaloric materials: structure and magnetocaloric properties in  $Mn_5(Si,P)B_2$  compounds*”, NWO Physics 2023, Apr 2023.

## Curriculum Vitae



Hamutu Ojiyed, born on 26-April-1984 in Inner Mongolia, China. From 2007 to 2011, he pursued his Bachelor studies in physics at the College of Physics and Electronic Information of Inner Mongolia Normal University.

In 2015, his academic pursuits led him to Inner Mongolia Normal University once again, where he was admitted to pursue a master's degree in condensed matter physics. Under the guidance of Prof. Tegus, he delved into the realm of magnetocaloric materials research, with a specific focus on exploring the mechanical properties of  $(\text{Mn,Fe})_2(\text{P,Si})$  alloys. This research culminated in the successful completion of his master's degree in science in 2018.

The subsequent chapter academic journey unfolded in 2019 when he commenced his PhD studies under the supervision of Prof. Ekkes Brück and Dr.ir. Niels van Dijk. This phase of his academic pursuit took him to the Fundamental Aspects of Materials and Energy group at TU Delft in the Netherlands. His PhD project was dedicated to the exploration of novel room temperature magnetocaloric materials. The culmination of his PhD research is presented in his thesis titled "Magnetocaloric Effect in  $M_5\text{XB}_2$  Family Compounds."



ISBN: 978-94-6384-522-9